Scale-up dynamics for the photocatalytic treatment of textile effluent

by

Zuqaqambe Gwele

Thesis submitted in fulfillment of the requirements for the degree
Masters of Engineering: Chemical Engineering

At the Cape Peninsula University of Technology, Engineering Faculty
under the supervision of
Prof. V.G Fester

Declaration

I, Zuqaqambe Gwele hereby declare that the work titled: *Scale-up dynamics for the photocatalytic treatment of textile effluent,* submitted to the Cape Peninsula University of Technology for Masters in Engineering has not previously been submitted to any other institution. Furthermore, it is my own original work except where acknowledgments indicate otherwise.

_____   _15 November 2018_____

[Signature]   [Date]

Abstract

Enhancing the efficiency of large scale photocatalytic systems has been a concern for decades. Engineering design and modelling for the successful application of laboratory-scale techniques to large scale is obligatory. Among the many fields of research in heterogeneous photocatalysis, photocatalytic reaction engineering can initiate improvement and application of conservative equations for the design and scale-up of photocatalytic reactors. Various reactor configurations were considered, and the geometry of choice was the annular shape. Theory supports the view that annular geometry, in the presence of constant transport flow properties, monochromatic light, and an incompressible flow, will allow a system to respect the law of conservation of mass.

The degradation of a simulated dye, methyl orange (MO), by titanium dioxide (TiO_2) with a simulated solar light (halogen lamp) in a continuous recirculating batch photoreactor (CRBPR) was studied. A response surface methodology (RSM) based on central composite design (CCD) was applied to study interaction terms and individual terms and the role they play in the photocatalytic degradation of MO. The studied terms were volume (L), TiO_2 (g), 2 (mL), and initial dye concentration (mg/L), to optimize these parameters and to obtain their mutual interaction during a photocatalytic process, a 2^4 full-factorial CCD and RSM with an alpha set to 1.5 were employed. The polynomial models obtained for the chosen responses (% degradation and reaction rate constant, k) were shown to have a good externally studentized vs normal percentage probability fit with R2 values of 0.69 and 0.77 respectively. The two responses had a common significant interaction term which was the H_2O_2 initial dye concentration term. The optimum degradation that was obtained in this study was a volume of 20 L, TiO_2 of 10 g, H_2O_2 of 200 mL and the initial dye concentration of 5 mg/L which yielded 64.6% and a reaction rate constant of 0.0020 min^{-1}. The model of percentage degradation was validated on a yield of 50% and 80% over a series of set volumes and the model validation was successful.

Acknowledgments

I wish to thank:

Dedication

To my dearest and loving parent

Nomabhaso Patricia Gwele

To my late father

Bennett Mphumelelo Gwele

"You were a man driven by success and progress, this milestone reminds me so much of you, through us your legacy lives on. Continue to rest in peace Nogubela, you're forever in our hearts."

To my siblings

Nosiphe Gloria Gwele,

Bantu Emanuel Gwele,

Vuyiseka Gwele,

Simo Gwele, and

lastly my nephew

Unakho Qhayiya Gwele

I can never thank you enough for your support and encouragement

Table of Contents

List of Figures

List of Tables

List of Symbols

Symbols	Description of symbol	Unit
Nomenclature		
C	Concentration	mg/L
D	Length of light path	cm
D_{ei}	Effective diffusivity	sq.cm/sec
D_i	Molecular diffusivity of specie	sq.cm/sec
f	Frequency	Sec^{-1}
h	Plank's constant	ergs(sec)/molecule
I	Light intensity	Einstein/(sec) sq.cm
I_a	Volumetric rate light	Einstein/(sec) sq.cm
k	Kinetic constant (1st order)	s^{-1}
k_w	Kinetic constant for wall reaction	min^{-1}
L	Length	cm
n	Order of reaction	
N_A	Avogadro's number	molecule/gram-mole
Q	volumetric flow rate	mL/min
R, r	Radial distance	cm
r_a	Reaction rate	$mol.dm^{-3}.s^{-1}$
t	Time	min
T	Temperature	^oC
V	Volume	L
V_R	Reactor volume	L
x	Length	cm
z	Length	cm
ε	Internal energy per unit mass	cal/gram

Greek letters

α	Molal absorptivity	Sq.cm/gram.mol
ε	Light absorbing chemical specie	_
λ	Wavelength	A
θ	Cylindrical coordinates , transmission coefficient	_
Ω	Local rate of reaction	gram-mole/(cc)(sec)
ϕ	Quantum efficiency	gram-mole/Einstein
μ	Attenuation coefficient	cm^{-1}
ν	Quantum radiation	_

Superscripts and subscripts

f	Exit or final conditions	_
i	Individual chemical specie	_
L	Length	cm
r	Radial direction	cm
t	Turbulent state, thermal conditions	_
w	Reactor wall	cm
x,z	x-z direction	_
[ ]	Concentration	_
-	Average	_
0	Inlet or initial conditions	_

Glossary

Terms and concepts

Batch reactor: a vessel used in process industries fitted with an agitator and integral heat control unit used for most chemical reactions within a fixed time, without adding or removing any reactants.

Catalyst: a substance that enhances the rate of a chemical reaction without itself undergoing any permanent change.

Methyl orange: model dye

Oxidant: a substance that has an ability to oxidize other substances.

Photocatalysis: the acceleration of a photoreaction in the presence of a catalyst.

Photocatalyst: a substance which can modify the rate of a chemical reaction using a light irradiation.

Photoreactor: any vessel in which a photochemical reaction takes place.

Reactor: a vessel in which a chemical reaction occurs.

Response surface methodology: in statistics RSM explores the relationship amongst several descriptive variables and one or more response variables.

Scale-up: The migration of a chemical process from lab-scale to bench, pilot or commercial scale.

Abbreviations

AOP: Advanced oxidation processes

BBD: Box-Behken Design

CCD: Central composite design

CPC: Compound parabolic collector

CRBPR: Continuous recirculating batch photoreactor

FPRC: Flow Process and Rheology Center

IDC: Initial dye concentration

IPC: Inclined plate collector

MO: Methyl orange

MTR: Multi-tube reactor

PTR: Parabolic trough reactor

RSM: Response surface methodology

S.I.T: Sample interval time

Outputs of this study

- Gwele Z, Fester V.G. and Chowdhury MR. 2016. Development of scale-up models for prototype photocatalytic reactor for treatment of textile effluent. *Proceedings of the 2016 6th International Conference on Nanoscience and Nanotechnology, Roodepoort Florida, 3rd- 6th April 2016.* Poster

- Gwele Z, Fester VG, and Chowdhury MR. 2018. Development of scale-up models for prototype photocatalytic reactor for treatment of textile effluent. *Proceedings of the 2018 7th International Conference on Nanoscience and Nanotechnology, Salt Rock Hotel, Durban South Africa, 22nd- 25th April 2018.* Oral presentation

Chapter 1 – Introduction

1.1 Background

The scientific study of photocatalysis dates back about three decades (Fujishima & Zhang, 2006). It later shifted to environmental photocatalysis and photo-induced hydrophilicity as well as the commercialisation of TiO_2-based photocatalytic products after raising immense interest in photoelectrochemical solar energy conversion (Fujishima & Zhang, 2006). In the course of recent years there has been an increasing interest in systems that employ photocatalysis (Kobayakawa et al., 1998). Through the pioneering study of Fujishima and Honda (1972) on water splitting, a way was paved for patents and manuscripts aimed at utilisation of TiO_2 for water treatment, self-cleaning of surfaces and air purification.

Previous studies have focused on optimisation of existing parameters using numerous methodologies and techniques on small scale and have successfully proven their work (Cho & Zoh, 2007; Chowdhury et al., 2015; Kanki et al., 2005; Augugliaro et al., 2002; Alrousan et al., 2012). However, Wang et al. (2013a) stated that the fundamentals which have been established in the literature, are far from being fully understood or sophisticatedly applied in practice. The review further states that the operating parameters optimized in the laboratory often suffer a mismatch in the actual scenario (Wang et al., 2013a). Although extensive research on the chemistry of photocatalysis has been done, no parallel effort in the engineering aspects of the process has been reported (Satuf et al., 2007).

Reactor modelling is essential for the application of heterogeneous photocatalysis on an industrial scale (Satuf et al., 2007). Customarily, observational philosophy for scale-up begins in the laboratory and step-by-step expands to the proposed reactor size as desired commercially

(Marugan et al., 2009). There has been photoreactors that have been built in the past, however, it is found that researchers perform scale-up and design for specified contaminants under specified conditions as it is observed in the degradation of cyanide in wastewater over a TiO_2 study by Motegh et al. (2014).

1.2 Research problem

Photocatalysis based on semiconductors has shown a rapid progress in the last couple of decades and is a promising innovation in the field of ecological remediation, particularly to purify water from toxins (Motegh et al., 2014). Despite the fact that there is research output on major parts of photocatalysis such as kinetics, scale-up techniques for photocatalytic reactors are yet to be developed (Braham & Harris, 2009).

1.3 Research question

What are the relationships and interactions between operational parameters such as reactor treatment volume, catalyst concentration, hydrogen peroxide concentration and initial dye concentration driving the degradation reaction in a continuous recirculating photocatalysis process?

1.4 Aims and objectives of the study

The aim of this study is to determine the relationship between the reactor volume, catalyst concentration, hydrogen peroxide concentration, stirring rate and treatment time. The objectives are:

- To design a continuous recirculating prototype photocatalytic reactor system

- To experimentally determine optimum quantities of catalyst and H_2O_2 in the designed continuous recirculating prototype photocatalytic reactor system volumes ranging from 5 L to 20 L.

- To determine the interactions between operational parameters driving the degradation reaction in a continuous recirculating photocatalysis process.

1.5 Significance of the study

The significance of this study is to provide knowledge of the scale-up dynamics applicable to realise the full potential of photocatalysis to pilot plant and further, to industrial scale.

1.6 Delineation

This study will only evaluate Degussa P25 as this is commercially available and is reported to be an excellent photocatalyst and is widely used in various reactor design studies such as Oyama et al. (2004), Mehos et al. (1992) and Sichel and Tello, (2007). This study will only include measurement of decolourization efficiency to establish the interactions between the operational parameters. Previous studies in literature show that decolourization efficiency and mineralisation is not necessarily equivalent and that fact is recognised in this work. However, measurement of mineralisation is excluded from this study to maintain the focus on scale up and decolourization efficiency is selected as the current performance measure used to determine the success of

operation of the scale up reactor. This study will not evaluate different types of contaminants, only methyl orange is going to be treated as it is commonly used in RSM studies, which excluded the volume parameter as part of the optimisation so that it can be complimentary to what already exist in literature.

1.7 Thesis structure

In the first chapter, the relevant background to the study is outlined. The research problem, aims, objectives, and the significance and delineations of the study are also stated. The second chapter outlines the literature relevant to the study, accompanied by the necessary scientific equations. Chapter 3 entails details of the photocatalysis prototype construction and operation procedure, including safety measures. It further provide detailed experimental work as well as materials and methods. It also explains which design is going to be employed by Design-Expert® and how the design constraints are going to be set. Chapter 4 presents the pilot runs, shows some anticipated findings and provides confidence in the functionality of the continuous system. Chapter 5 provides the actual model development of the chosen parameter. It details how the parameters interact with one another, and how this was achieved by performing a factorial trial using a central composite design. Chapter 6 consists of the conclusion and recommendations as well as future work..

Chapter 2 – Literature review

2.1 Introduction

This chapter provides a review of the literature on advanced oxidation processes, focussing on established and emerging technology. Photocatalysis fundamentals will also be reviewed in this chapter, highlighting all the driving chemical equations. The fundamentals of reaction engineering kinetics involved in photocatalysis will also be shown. The phenomenon of halogen tungsten spectra will also be reviewed as tungsten is the type of lamp that will be employed in the experiments. Statistical experimental methodology will be used in developing a model within specified ranges of factors and therefore will also be included.

2.2 Advanced oxidation processes

Advanced oxidation processes (AOPs) have over the past 40 years been the subject of broad research output. In 2008, over 4,500 journal article were published, within the short space of two years (2005 - 2007) (Ray, 1998). AOPs have been used broadly in industries such as textile dyeing for many decades, and reliable equipment exists. Processes, for example, such as gravity settling, air stripping, filtration or adsorption to activated carbon are separation processes that generate a lot of waste (Ray, 1998). However, advanced oxidation processes despite the use of various reacting systems, are altogether individualized by a similar synthetic element: production of OH$^\bullet$ radicals that will change the biological material into carbon dioxide and water (Quiroz et al., 2011).

The flexibility of AOPs is additionally complemented by the fact that they offer diverse conceivable approaches to harvest OH$^\bullet$ radicals, in this way permitting better agreement with particular treatment necessities. AOPs can offer satisfactory scientific answers for water treatment, which

are critical for helping and improving the force of different sectors in the international market, including the water advancement sector (Ray, 1998).

There are a number of benefits that can be connected with AOPs: elevated reaction rates; complete mineralisation of pollutants; and they do not focus waste for additional treatment (Quiroz et al., 2011). However, AOPs can be capital-intensive, they require abundance H_2O_2, and complex science must be custom fitted to applications (Quiroz et al., 2011).

Built on the existing works and the understanding of the wastewater treatment industry, AOPs can be branched into established and emerging technologies (Kommineni et al., 2000). Emerging technologies are those that have very limited, if any, full-scale application in drinking water treatment. (Kommineni et al., 2000) The categorised established and emerging technologies are listed in Table *2.1*:

Table 2.1: Established technologies and emerging technologies (Kommineni et al., 2000)

Established Technologies	Emerging Technologies
• Hydrogen peroxide/TiO$_2$ (H$_2$O$_2$/ TiO$_2$)	• High Energy Electron Beam Irradiation (E-beam)
• Ozone/Ultraviolet Irradiation (O$_3$/UV)	• Cavitation (Sonication & Hydrodynamic)

2.3 Photocatalysis

Catalysis is defined as a chemical reaction that occurs in the presence of a catalyst. This reaction can occur naturally without the catalyst, but a catalyst is used to reduce the activation energy of the reactants and therefore to enhance the sped of the reaction (Lazar et al., 2012). The prefix "photo" means light; for instance, in the process of photosynthesis, light is used by plants as an energy source (Lazar et al., 2012). Photocatalysis is therefore a process or a reaction that occurs due to the interaction of light and a catalyst (Lazar et al., 2012).

Titanium dioxide is completely the foremost anticipated for the fact that it incorporates rare and welcoming characteristics, such as high stability, environmental tolerance and photocatalytic stability (Bignozzi & Alexander, 2011a).

There is continuously increasing debate around modifying the reactivity of titanium dioxide-based photocatalysis to drive reactions of interest from the synthesis perspective (Lazar et al., 2012). It is generally confirmed that excitation of TiO_2 with bandgap photons results in the charge separation in the semiconductor solid. As seen in Equation *2.1* to Equation *2.5*, electrons are promoted to the conduction band [e$^-$] and holes remain in the valence band [h+] (Augugliaro et al., 2002). However, Equations 1 to 5 illustrate the intermediate reactions which are in essence a mere production of HO$^\bullet$, which then attacks the pollutants (methyl orange) (Augugliaro et al., 2002). The overall equation is illustrated in Equation *2.6*, assuming that the reaction has gone to completion (Bignozzi & Alexander, 2011a). TiO_2 has three different phases which are rutile, anatase and brookite, with band gaps of 3.02eV, 3.20eV, and 2.96eV respectively (Alrousan et al., 2012).

$$TiO_2 + hv \rightarrow TiO_2(h^+ + e^-)$$

Equation 2.1

$$H_2O + h^+ \rightarrow OH^\bullet + H^+$$

Equation 2.2

$$O_2 + e^- \rightarrow O_2{}^-$$

Equation 2.3

$$OH^\bullet + MO \rightarrow degraded\ Products$$

Equation 2.4

$$O_2{}^- + MO \rightarrow degraded\ products$$

Equation 2.5

$$C_{14}H_{14}N_3NaO_3S + H_2O_2 \xrightarrow[TiO_2]{hv} CO_2 + H_2O + NO_3{}^-$$

Equation 2.6
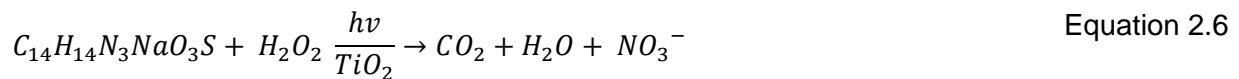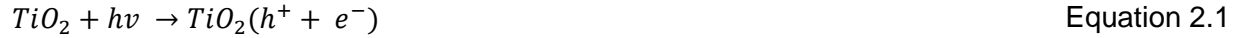
Numerous potential mechanisms are expressed by earlier studies relating to the photocatalytic decomposition of methyl orange solution (Sheikh et al., 2016). Figure *2.1* shows the plausible mechanism indicating attainable reactions within the photocatalytic degradation of azo dye. A breakdown of methyl orange structure shown in Figure *2.2* is illustrated in Figure *2.3* with all the short term by-products that are suggested by literature which eventually breakdown to $NO_3{}^-$, CO_2 and H_2O (Sheikh et al., 2016).
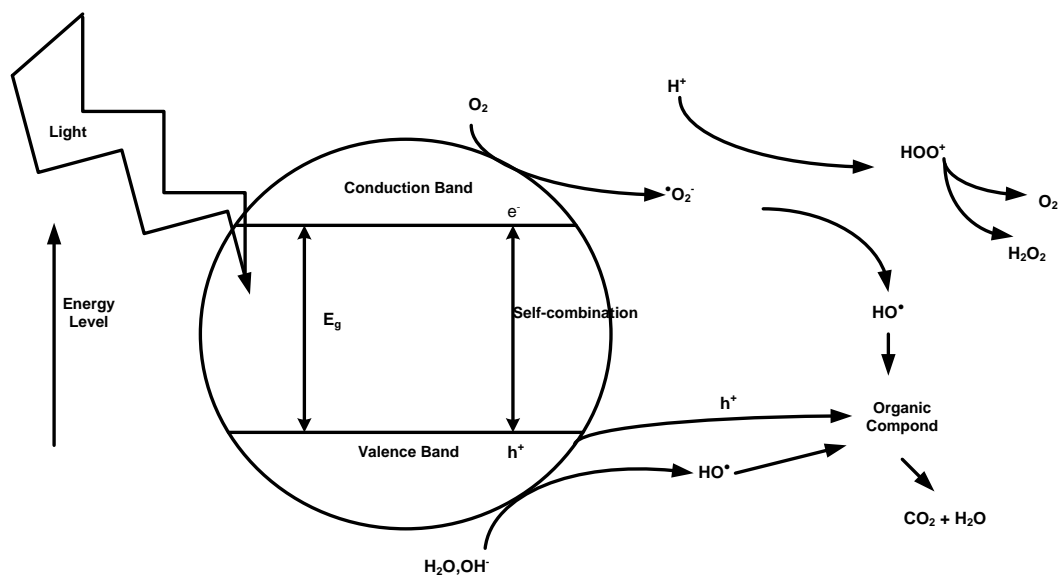
Figure 2.1: Representation of a possible mechanism for establishing electron transfer over TiO_2 band gap during photocatalysis (Wang et al., 2013)
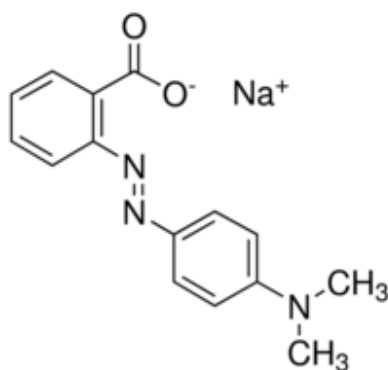
Figure 2.2: Methyl orange chemical structure (Sheikh et al., 2016)
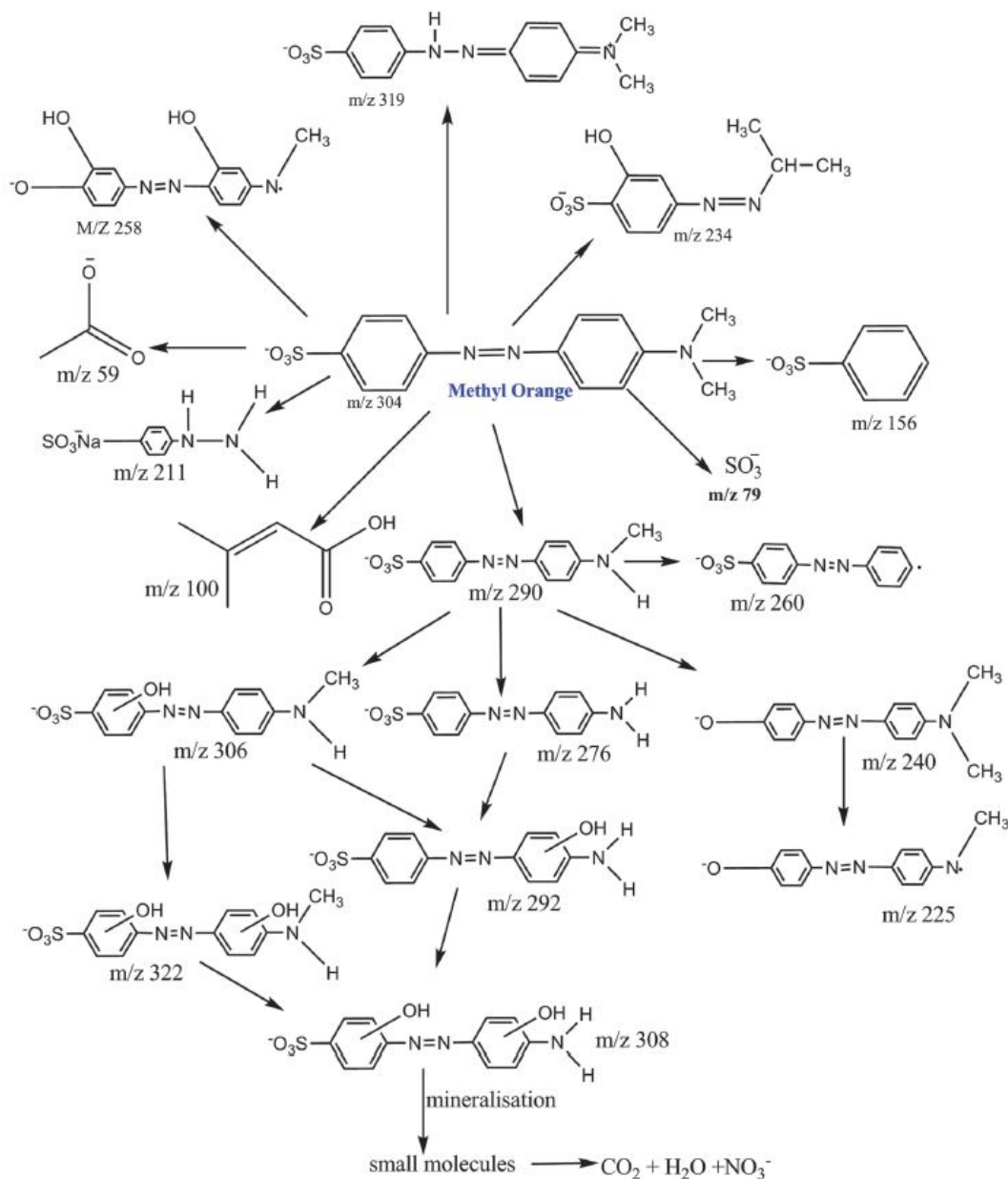
Figure 2.3: Literature-recommended photodegradation pathway and sequential events that occur throughout the photocatalytic decomposition of methyl orange (Sheikh et al., 2016)

Figure *2.3* illustrates methyl orange mineralisation as confirmed by liquid chromatography-mass spectrometry (LC-MS), which is an analytic chemistry technique that incorporates physical separation abilities of liquid chromatography (HPLC) with the analysis abilities of mass spectroscopy (MS) (Sheikh et al., 2016). The literature shows that degradation occurs in various

paths. This starts by a process cleavage of the dye double bond, followed by the addition of hydroxyl groups to rings and lastly, the cleavage of sulphonate groups from the ring (Sheikh et al., 2016). As shown on the reaction pathway in Figure *2.3*, further states that the products of methyl orange decomposition after 120 minutes have mass values (m/z) of 319, 260, 258, 234, 211, 100, 79 and 59. The intermediates formed are further split into fragments and low molecular mass intermediates which are mineralized into $NO_3{}^-$, CO_2 and H_2O (Sheikh et al., 2016).

Figure *2.3* is a generic demonstration of how various pathways in which methyl orange breaks down as adopted in the study of Sheikh et al. (2016), this representation also does not show that the demonstrated breakdown is as a result of TiO_2 and H_2O_2 nor does it show any OH$^\bullet$ radicals which is the case in the current study. This study focused on the decolourization and did not intend to investigate the kinetics of side reactions and therefore there was no need for using various testing equipment for quantification of color decomposition. This biggest challenge in photocatalysis is to scale-up and move towards industry (Braham & Harris, 2009), therefore a full mineralization study can be incorporated once the parameter interaction is fully understood and be investigated in that scale and other quantifying equipment can be utilized. It is also important to note that in the context of this study degradation means the degradation of colour and does not necessarily mean complete mineralization.

2.4 Kinetics and chemical reaction engineering

In chemical kinetics, the reactor vessel in which the reaction takes place also serves as a tool for determining unknown parameters about the reacting system; for the rate depends on various factors, such as temperature, and concentration of species (Missen et al., 1999). The advice gained from reaction kinetics is utilized to determine reactor size, thermal configuration, and the flow of components. (Fogler, 2006).

Kinetics, however, do not provide all the required information. Integrated problems like mixing (turbulent regime/transitional mixing), heat transfer, and diffusion and mass transfer become challenging. In order to increase the scale, these problems need to be addressed intensely on three different levels, which are microscopic or molecular, local macroscopic and global microscopic (Fogler, 2006).

2.4.1 Reaction rates

The rate of reaction indicates how fast species A decomposes to form a product species B in a given volume (Fogler, 2006). A chemical reaction is said to have taken place as soon as the molecules of one or more species have lost their identity and assumed a new form by a change of configuration or change in the number of atoms (Missen et al., 1999).

$$-r_A = \frac{dC_A}{dt}$$

Equation 2.7

2.4.2 Catalyst impact on reaction rates

Numerous reactions proceed at a faster rate in the presence of a catalyst (a substance that is not a reactant or product in the usual sense). The process whereby the rate is sped up by a catalyst is called catalysis (Missen et al., 1999). Mankind has been using catalysts for over 2000 years (Fogler, 2006). The making of wine, bread, and cheese were the first processes where catalysts were used in, it is reported that there was always a necessity to add small amounts of the previous batch to make the current batch (Fogler, 2006). Figure *2.4* shows that a catalyst will speed up a chemical reaction by reducing the activation energy.
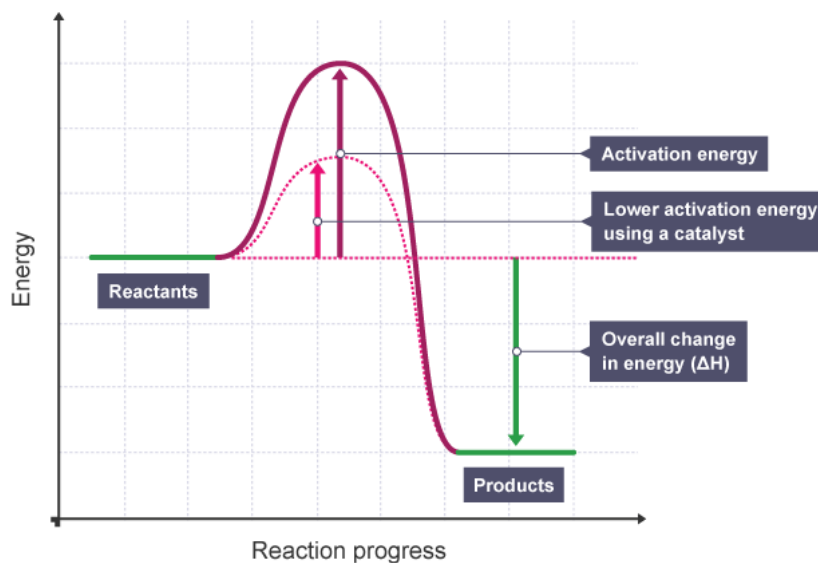
Figure 2.4: Reaction behaviour without and with a catalyst showing activation energy level and enthalpy (Hayek, 2016)

2.5 Analytical techniques

Chemicals absorb light or energy from a minimum of one region of the spectrum of electromagnetic radiation (Wielopolski, 2010). The energy at which absorption happens is dependent on the obtainable electronic, movement and vibrational energy levels of the molecule (Wielopolski, 2010). When absorption is from the ultraviolet-visible region of the spectrum, transitions happen between electronic energy levels (Allen, 2010). It is these transitions that form the basis of ultra violet-visible spectroscopy. The electromagnetic spectrum within which the IR and the UV range falls is highlighted.

The electromagnetic spectrum may be outlined in terms of wavelength or frequency. Electromagnetic radiation shows a particle-like and wave-like properties, this concept is known as particle duality, and is composed of a magnetic field and an electric field perpendicular to each other. The electric field and magnetic field oscillate in some direction (k). The distance between two troughs or crests of a wave defines a wavelength. The unit that is used in the ultraviolet-visible

range of the spectrum is a nanometre (nm) which is 10^{-9} m. Equation **2.8** shows that wavelength can be presented in terms of the Plank's constant h, and the speed of light, c.

$$E = hc/\lambda \hspace{4cm} \text{Equation 2.8}$$

Equation **2.8** shows that the energy of light is inversely proportional to the wavelength

.

2.5.1 Absorbance and transmittance

There is no direct method for measuring absorbed light, absorbed light is therefore measured indirectly by measuring the light which is not absorbed by the sample, which is the transmitted light. The Beer-Lambert law as shown in Equation **2.9** relates the absorption intensity to the incident and transmitted intensities as well as the concentration of the absorbing material.

$$Abs = log10\frac{I}{I_0} = \alpha cl \hspace{3cm} \text{Equation 2.9}$$

where: c, the concentration of absorbing substance, α is the absorption coefficient of the absorbing substance, and l, the optical path length of the cell.
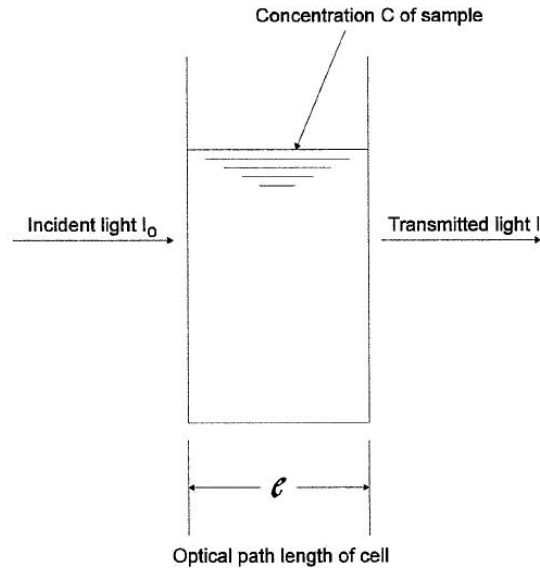
Figure 2.5: Incident light/cell/transmitted light

The Beer-Lambert law is, therefore, the source of all quantitative estimation in UV-Vis spectrometry as it relates absorption directly to concentration as shown Figure *2.5* as adopted on the operating manual of the UV-Vis machine. This is therefore how concentration in this study is quantified and a concentration-time curve can be obtained, by fixing the wavelength to λ= 464 nm

The relationship expressed in Equation *2.9* can therefore through a series of calibration standards of known concentration be directly compared to concentration and that is how the concentration/time curve is obtained.

2.6 Photoreactor design considerations

In conventional photoreactors, the magnitude of reaction is comparative to the volume of the reactor. Ignoring the effects of flow, the conversion for pseudo-homogeneous systems or homogeneous systems is dependent on geometry. However, this case doesn't hold for

35

photoreactors due to Lambert's law. The literature confirms that due to Lambert's law there are possibilities of an optimum reactor geometry and can be seen of the list (Cassano et al., 1967):

- Isothermal operations

- Monochromatic light

- No dark reaction (dead zones)

- Constant physical properties

- Steady state flow

- Flat velocity profiles and concentrations

- Efficient and uniform radiation

- First-order regarding the concentration of the same reactant and first-order rate as for light absorption by one of the reactants.

With the recorded conditions, the required reactor volume for a particular change can be assessed contrastingly for various reactor light design as illustrated in Figure *2.6* (Cassano et al., 1967):
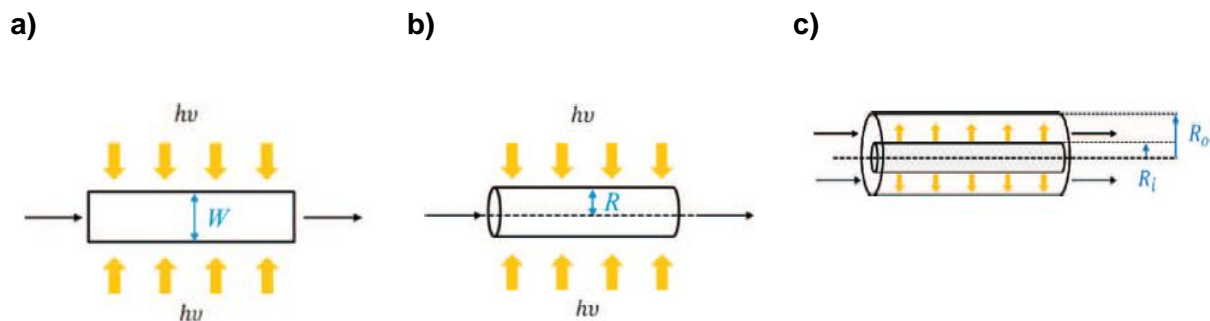
a)   **b)**   **c)**

Figure 2.6: a) Externally irradiated flat plate photoreactor; b) externally irradiated cylindrical photoreactor and c) internally irradiated annular photoreactor (Kobayakawa et al., 1998)

2.6.1 Mass conservation

The reaction rate term in mass balance is an element of creation, pressure, temperature and volumetric rate of light ingestion, I_a. In this way, a progression of differential conditions is basic intending to address assimilation of the reactants and the spectra for the emission if the light. (Cassano et al., 1967). A problem also arises due to that fact that for most photoreactions, kinetics cannot be established through overall stoichiometric connections (Cassano et al., 1967). This infers that, mostly, a mass balance containing diffusion terms is fundamental for every independent chemical species. On account of wall reactions being substantial, even with an arrangement of differential mass balances to present the spectral dispersion of the source-absorbent system and the various species, the description would not be complete (Cassano et al., 1967). Under the assumptions of monochromatic light, constant transport flow and properties, and incompressible flow, the mass balance may be expressed as follow (Cassano et al., 1967);

$$-v\nabla C_i + \left(D_i + D_i^{(t)}\right) + \nabla^2 C_i + \Omega_i = \frac{\partial C_i}{\partial t} \qquad \text{Equation 2.10}$$

Where the turbulent contributions and the molecular to the diffusivity are assumed to be additive and Ω_i is the local rate of production of species i (Cassano et al., 1967).

2.6.2 Radiation balance

Normally, there will be one radiation balance for every direction and wavelength of radiation as conveyed by Equation *2.11* :

$$\nabla . I_{m,\lambda} = -\mu_\lambda \left| I_{m,\lambda} \right| \qquad \text{Equation 2.11}$$

Where; *m* represents the direction and the attenuation coefficient, μ_λ is waveleght dependent. For unidirectional, homochromatic radiation Equation *2.11* reduces to vectorial form of Lambert's law which can be applied on any reactor geometry (Cassano et al., 1967):

$$\nabla.I = -\mu|I| \qquad\qquad \text{Equation 2.12}$$

The $\mu|I|$ product is the volumetric absorption rate, Ia; μ is appropriately divided into the light absorbed by the activated molecules, and μ_0 is the constant ground extinction coefficient corresponding to the energy dissipated without causing reaction. The extinction coefficient could be a variable if an absorbing species other than that associated with the reaction changes concentration (Cassano et al., 1967).

2.6.3 General modeling based on reactor geometry

This section addresses the derivations of photoreactor modelling equations based on their geometrical coordinates.

2.6.3.1 Parallel plate reactor shape

As shown in Figure *2.7*, the light rays are found to be perpendicular, uniform, and parallel to the reactor wall, which comprises parallel plates, and has a light path *D* and a flow length *L.* For the conditions portrayed in Figure *2.6*: a) Externally irradiated flat plate photoreactor; *b)* externally irradiated cylindrical photoreactor and c) internally irradiated annular photoreacto a) the rate of production of reactants can be expressed by (Cassano et al., 1967);

$$\Omega = -kI_aC \qquad\qquad \text{Equation 2.13}$$
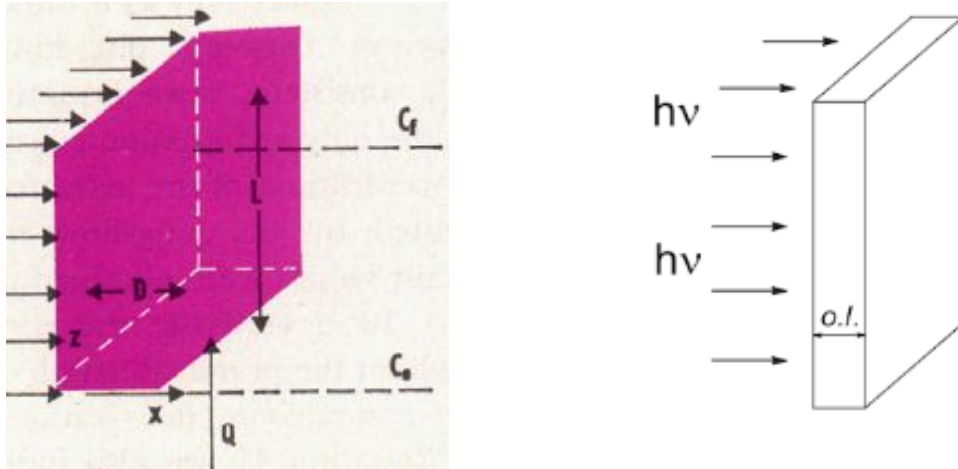
Figure 2.7: Radiation profile through a parallel plate photoreactor (Cassano et al., 1967)

Radiation equation (Equation *2.11*) can be reduced to Equation *2.14* and encompassing the boundary condition of $x = 0$, and $I = I_w$, the mass balance Equation *2.10* can be expressed as (Equation *2.15*) (Cassano et al., 1967):

$$\frac{dI}{dx} = -\alpha CI \qquad\qquad \text{Equation 2.14}$$

$$\bar{v}_z \frac{dC}{dz} = \bar{\Omega} \qquad\qquad \text{Equation 2.15}$$

where the bar describes the average values through the light path length *D*, with the boundary conditions, $z = 0$, and $C = C_0$. The expressions Equation *2.13,* Equation *2.14* and *Equation 2.15* may be solved for volume as a function of conversion. Remembering that $I_a = \mu I$, expression

Equation *2.13* may be written as Equation *2.16*, Further, integrating Equation *2.14* at boundary conditions $x = 0$, and $I = I_w$, to give I at any given distance of x and substituting results for I in Equation *2.16* gives Equation *2.17* (Cassano et al., 1967):

$$\Omega = k\alpha I C^2 \qquad\qquad \text{Equation 2.16}$$

$$\Omega = kI_w \alpha C^2 \exp(-\alpha Cx) \qquad\qquad \text{Equation 2.17}$$

Before integrating into the direction of flow z, the average rate, $\overline{\Omega}$, is found by integrating Equation *2.17* from $x = 0$ to D and results to Equation *2.18*. Furthermore, solving Equation *2.15* under the boundary conditions of $z = 0$ and $C = C_0$ yields (Cassano et al., 1967).

$$\overline{\Omega} = \frac{kI_w C}{D} \left[1 - \exp(-\alpha CD)\right] \qquad\qquad \text{Equation 2.18}$$

$$\frac{V_R kI_w}{QD} = \int_{C_f}^{C_0} \left[1 - \exp(-\alpha CD)\right]^{-1} \frac{1}{C} \, dC \qquad\qquad \text{Equation 2.19}$$

The dimensionless group on the left side of the equation is to measure the volume that is essential per unit length of the light path, $\frac{V_R}{D}$ and is a function of conversion, x, which can be expressed as (Cassano et al., 1967):

$$x = 1 - \frac{C}{C_0} = 1 - \Gamma \qquad\qquad \text{Equation 2.20}$$

Furthermore, Equation *2.19* can be expressed in terms of conversion and is the final modeling equation for the parallel plate reactor (Cassano et al., 1967):

$$\frac{V_R k I_w}{QD} = \int_{\Gamma_f}^{1} [1 - \exp(-\alpha C_0 D\Gamma)]^{-1} \frac{d\Gamma}{\Gamma}$$

Equation 2.21

2.6.3.2 Cylindrical reactor shape

With the lamp situated outside the reactor, it provides a uniform, radial, and parallel radiation. With regards to the design of the cylindrical photoreactor model equation, Equation *2.11* is expressed in cylindrical coordinates and can be presented as follows (Cassano et al., 1967);

$$\frac{1}{r}\frac{d}{dr}(rI) = \pm\mu I$$

Equation 2.22
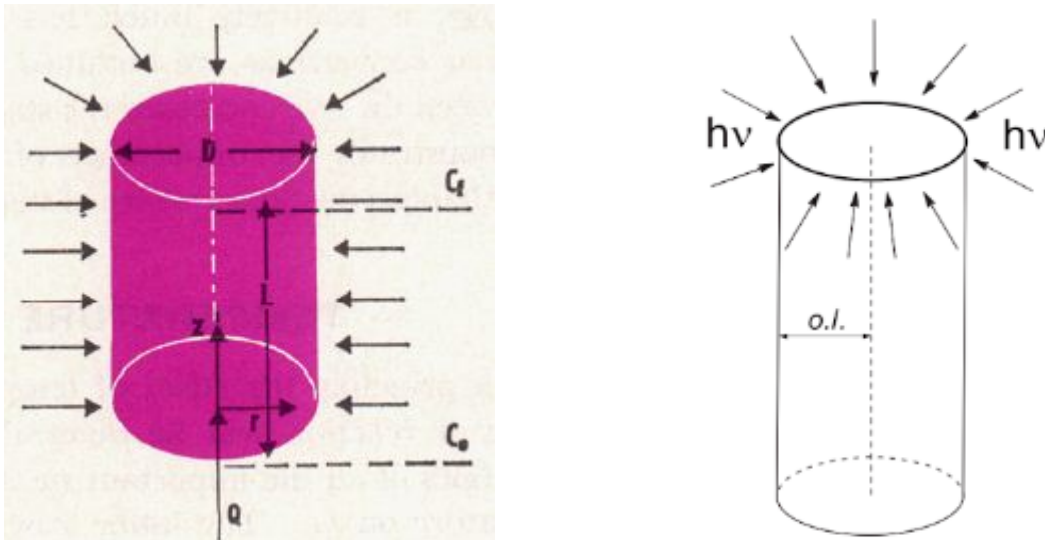
Figure 2.8: Radiation profile description through a cylindrical photoreactor (Cassano et al., 1967)

with boundary conditions of $r = R$, and $I = I_w$, and replacing μ with αC, and integrating gives (Cassano et al., 1967):

41

$$I = \frac{I_w R}{r}\{\exp[-\alpha C(R - r)] + \exp[-\alpha C(R + r)]\}$$

With the intensity equation substituted into Equation *2.16* gives the rate at any distance of r in the reactor, similar to Equation *2.17* for the plate type reactor. Proceeding as for a parallel plate reactor from Equation *2.17* to Equation *2.21*, gives the final modelling equation for a cylindrical shape type reactor:

$$\frac{V_R k I_w}{DQ} = \frac{1}{4}\int_{r_f}^{1}[1 - \exp(-\alpha C_0 D\Gamma)]^{-1}\frac{d\Gamma}{\Gamma}$$

Figure 2.9: Radiation profile through an annulus photoreactor (Cassano et al., 1967)

In this reactor configuration, radiation comes from a cylindrical lamp, from within the annulus reactor in a uniform radial and parallel beam as shown in Figure *2.9*. This reactor geometry also

uses cylindrical coordinates; however, there is a γ parameter which represent the ratio of outer to inner radius ($\gamma = \frac{R_2}{R_1}$). If the intensity is I_w at the inner radius then the final model is as follows:

$$\frac{V_R k I_w}{DQ} = \frac{1+\gamma}{4} \int_{r_f}^{1} [1 - \exp(-\alpha C_0 D)]^{-1} \frac{d\Gamma}{\Gamma}$$

Equation 2.25

2.7 Previous work on photocatalytic reactors

Photocatalytic processes are pertinent in energy production, wastewater treatment, chemical synthesis, and ozone harming substance control (Braham & Harris, 2009). The science of photocatalysis thus has a potential to address two of humankind's greatest problems, which are the consumption of non-renewable fossil fuels and global warming (Motegh et al., 2014). The most attractive aspect is that all the benefits of photocatalysis can be achieved using only solar energy as an input (Braham & Harris, 2009). A photoreactor is defined as a device that brings together and allows contact between photons, a photocatalyst and reactants, while collecting the reaction products at the same time (Levin, 2002). Braham and Harris (2009) conducted a review in which they presented a solar photoreactor design and surveyed the photocatalytic frameworks that could be most applicable in modern application.

Table **2.2** illustrates the work done previously by different research groups on significant outline and scale-up contemplations for solar photocatalytic reactors, as reviewed by Braham and Harris (2009). These designs were carefully reviewed, and the photoreactor designed by Braham and Harris (2009) took these studies into consideration. While a vast amount of work has been done on photoreactors, very little research has been done on the dynamics and the kinetics of the

reactions and the little that has been done most often neglects the volume parameter. Sannino et al. (2013) and Dijkstra et al. (2001) studied the mathematical and kinetic modeling of photocatalytic reactions respectively but did not evaluate parameters such as volume; they also did not evaluate the interactions of parameters.

Motegh et al. (2014) and Puma et al. (2007) developed photoreactors based on specified contaminants under specified conditions; the lack of understanding of the interaction of parameters can be observed in Table *2.2*.

It therefore essential that the interaction of parameters be understood in photoreactors to allow for the knowledge to be easily transferred to an industrial scale.

Table 2.2: Summary of photoreactor designs and overall performance using solar illumination for water treatment (Braham & Harris, 2009)

				Photocatalyst		Contaminants			
Reference	Reactor	Area (m^2)	Volume (l)	Type	Concentration	Type	initial conc.	Final Conc.	Time/energy
Kanki et al. (2005).	PTR	1	-	Pt-TiO$_2$ (synth)	-, supported (photodeposited)	Gaseous toluene	20ppm	4.2ppm	5.7s
(Oyama et al., 2004)	PTR (dish)	0.785	3	TiO$_2$ (P25)	6g/L, suspended	Commercial detergent	100mg/L	15mg/L	120 min
(Mehos et al., 1992)	PTR	156	15L/min	TiO$_2$ (P25)	0.9g/L, suspended	Trichloroethylene	106ppb	<0.5ppb	10min
(Sichel & Tello, 2007)	CPC	0.4	14	TiO$_2$ (P25)	20g/m^2, supported (deposited from colloid)	Escherchia coli	10^{6}CFU/mL	~10^{2}CFU/mL	90min
(Fernandez-Ibañez et al., 1999)	CPC	0.75	11	TiO$_2$ (P25)	0.05g/L, suspended	Escherichia coli	10^{4}CFU/mL	~20CFU/mL	2.6kJ/L
(Bandala et al., 2004)	PTR	0.72	10	TiO$_2$ (-)	0.5g/L, suspended	Oxalic acid	10mM	3mM	20kJ/L
	CPC	0.72	10	TiO$_2$ (-)	0.5g/L, suspended	Oxalic acid	10mM	1.5mM	28kJ/L
(Thu et al., 2005)	IPC	1.36	25	TiO$_2$ (PC 500)	-,suspended	Formetanate	50mg/L	0mg/L	20kJ/L

2.7.1 Previous photoreactor designs

For this study, designs that were developed previously were taken into consideration, and factors taken into consideration by other research groups were also incorporated into the design of the photoreactor developed in this study. A short review was conducted mainly evaluating the designs and the photoreactor designs considered for the photoreactor design in this work were produced by the following research groups, in chronological order. The design aspects of the listed studies are briefly described, because they influenced the design of the photoreactor in this study. Findings and conclusions will also be included, taking into account the fact that in the respective studies different contaminants were treated, which were also different to the methyl orange treated in this work.

2.7.1.1 Ray and Beenackers, (1998)

Through this work, Ray and Beenackers, (1998) confirmed the potential of photocatalysis to convert the organic pollutants dissolved in water into harmless substances. They further confirmed that there was no viable pilot plant that existed using this technology. Therefore it was necessary to develop such a photoreactor, though their study addressed parameters such as light distribution, the surface area of catalyst per unit area of the reactor (Ray & Beenackers, 1998)

The group designed a photoreactor (multiple tube reactor) to address the water treatment problems discussed in the literature. Their design consisted of several hollow tubes that were coated on the outside surface with a photocatalyst. Even though this dissertation will only focus on a slurry system and not an immobilized system, the reactor design and process configuration shown in Figure *2.10* were considered when the designing the photoreactor designed in this study.
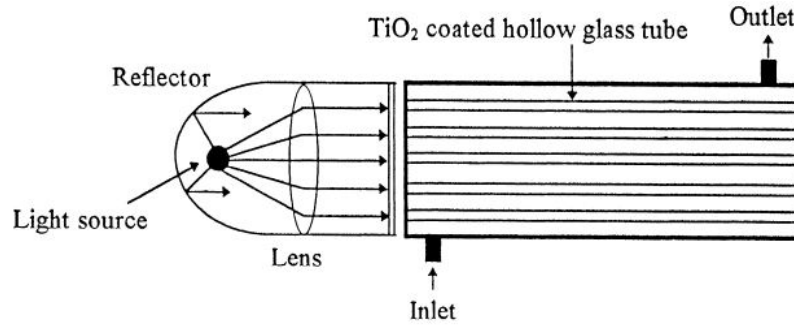
Figure 2.10: Schematic diagram of the photoreactor design (MTR) (Ray & Beenackers, 1998)
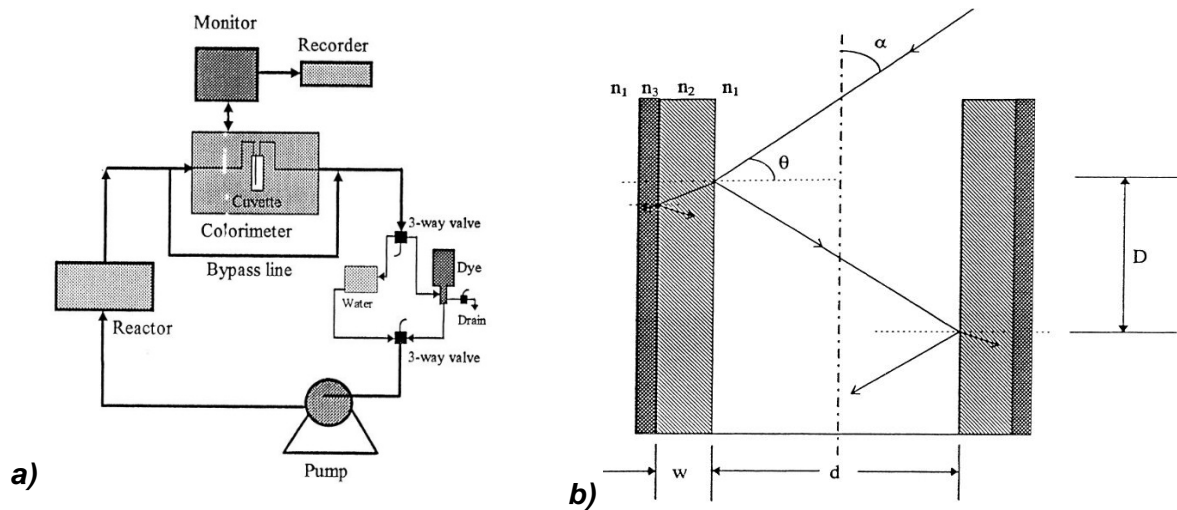
Figure 2.11: a) The process configuration of the photoreactor; b) The light distribution profile across the length of the photoreactor (n1: air; n2: glass; and n3: supported photocatalyst) (Ray & Beenackers, 1998)

The photoreactor shown in Figure *2.10* is constructed of a cylindrical vessel which is 0.056 m in diameter, in which there are 54 hollow quartz glass tubes of 0.006 m in diameter each, coated with a photocatalyst on their peripheral surfaces.

The tubes were held together by two Teflon plates on either side in which 54 holes were drilled. For efficiency and high surface area per unit volume, the tubes were organised in a triangular pitch of 0.007 m. The design of the MTR was influenced by the traditional design of a shell-and-

tube heat exchanger, where the organic pollutant/effluents flow on the shell side, with the lamps situated on the tube side. As illustrated in Figure *2.11* (b), the angles θ and α will be maintained through the entire length of the photoreactor, and this is proof of uniform light distribution.

2.7.1.2 Dijkstra et al. (2002)

According to Yue (1992), kinetic models presented in the literature very often neglected the photon flux and the amount of the photocatalyst on the degradation rate, especially for immobilized systems. Yue (1992) further stated that this resulted in the models being reactor dependent. To close this existing gap, Dijkstra et al. (2002) conducted a study in which a simple kinetic model was developed which included the influences of photon flux, the concentration variation of the model component, the oxidant, the photocatalyst quantity, and oxygen.

The reactor configuration in this study together with the process configuration was influenced by the configurations found in the study conducted by Dijkstra et al. (2002).
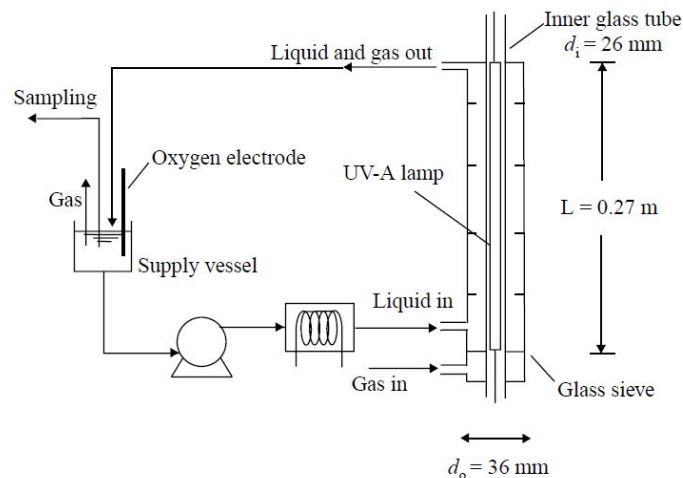
Figure 2.12: Photoreactor and process configuration of the study conducted by Dijkstra et al., (2002)

Similar to process used by Ray and Beenackers (1998) as illustrated in Figure *2.11 (a)*, yet another recirculating is observed. However, both system as designed by Ray and Beenackers, (1998) and Dijkstra et al. (2002) are heterogeneous systems as opposed to the homogenous system found in the current study. In the reactor design specification found in Dijkstra et al. (2002) there is a double wall tubular reactor made from borosilicate glass, which has a total reaction volume of 124 x10^{-6} m^3 fitted with a Philips TL29D15/09 (Cleo 15 W) UV-A lamp (Dijkstra et al., 2002). The recirculating batch system in Dijkstra et al. (2002) consisted of a holding vessel of a total volume of 650 x 10^{-6} m^3, a cooling device, a pump (verder gear pump V540.05 with Q = 25 x 10^{-5} m^3 s^{-1}) and the photoreactor (Dijkstra et al., 2002).

Although the present design is influenced by heterogeneous systems, it will not have any negative impact. Instead it will have an advantage due to mass transfer limitations being eliminated as the photocatalyst particles will be mixed well with the contaminants.

2.7.1.3 Wu et al. (2006)

Due to most studies only investigating some parameters and not all parameters, the study of Wu et al. (2006) aimed at studying the dye decomposition kinetics in a batch photocatalytic system. Through varying parameters such as initial dye concentration, UV illumination intensity, temperature, and TiO$_2$ suspension concentration, a reaction kinetic model was then established for further process design and optimisation (Wu et al., 2006).
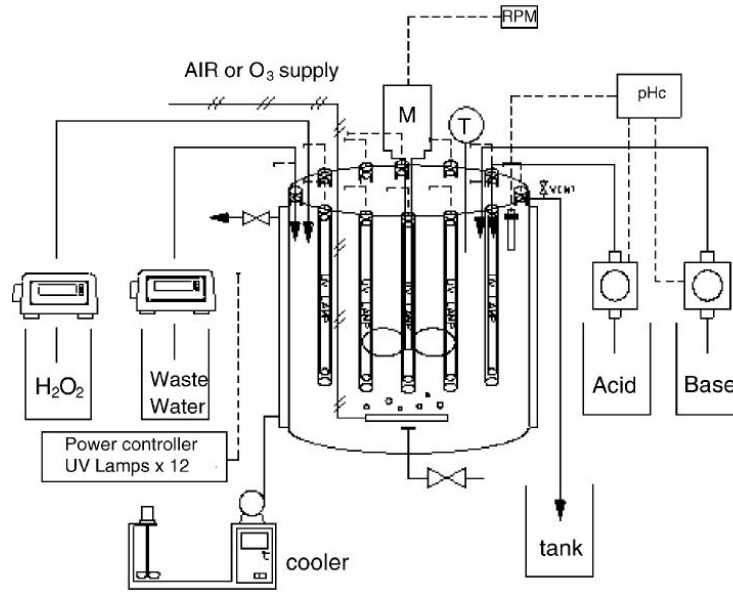
Figure 2.13: Photoreactor design and process configuration of the study conducted by Wu et al. (2006)

Different to the design and process configurations shown in Figure *2.10* and Figure *2.12*, the design by Wu et al. (2006) is a batch system. The design which is the object of current study was influenced by Wu et al. (2006).

The stainless steel photoreactor designed by Wu et al. (2006) has a cooling jacket in which the cooling water is circulated between the photoreactor and a water bath. The light source is a set of twelve 365 nm 8W lamps which are independently controlled, and the system also has a monitoring system to monitor pH history during the reaction (Wu et al., 2006).

2.7.1.4 Puma et al. (2007)

The reactor design found in the study by Puma et al. (2007) is composed of a vertical stainless steel hollow column in which a falling film of slurry-suspended TiO_2 flows along in the internal wall of the column. The falling film does not make contact with the lamp (36 W UVA blacklight, Philips

TL-D 36 W/08 SLV) since the lamp is protected by a borosilicate glass lamp shield (Puma et al., 2007). The reactor column is 1.6 m long with an inner radius of 0.108 m (Puma et al., 2007). The photoreactor is designed such that the falling fluid falling rate is 40.4 L min^{-1}, with a film thickness of 0.481 X10^{-3} m. The film Reynolds number is 725 (laminar) (Puma et al., 2007).
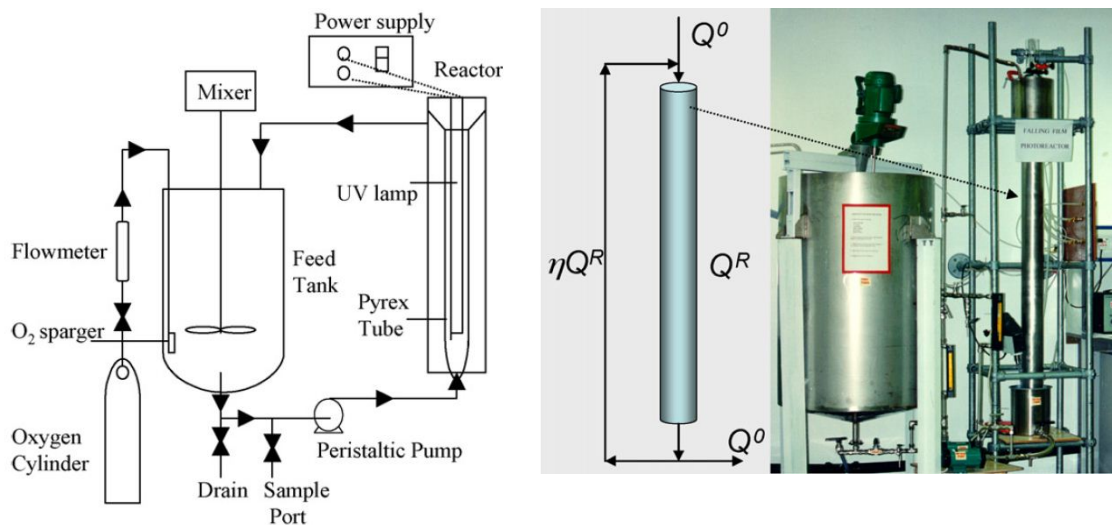
Figure 2.14: Photoreactor design and process configuration found on Li Puma et al. (2007)

2.7.1.5 Valadés-Pelayo et al. (2015)

The advancement and application of predictive and scale-up methodologies of photocatalytic reactor modeling has been an ongoing research subject in the last decade (Valadés-Pelayo et al., 2015). Recent years have seen interest in the applicability of kinetic models utilising semi-empirical radiation methods for bench- to pilot-scale reactors (Valadés-Pelayo et al., 2015). Marugan et al. (2009). and Satuf et al. (2007) reported in a methodology to scale up an annular slurry photoreactor (0.12 L) and a laboratory-scale photoreactor (flat plate) of a volume of 5209 cm^2.
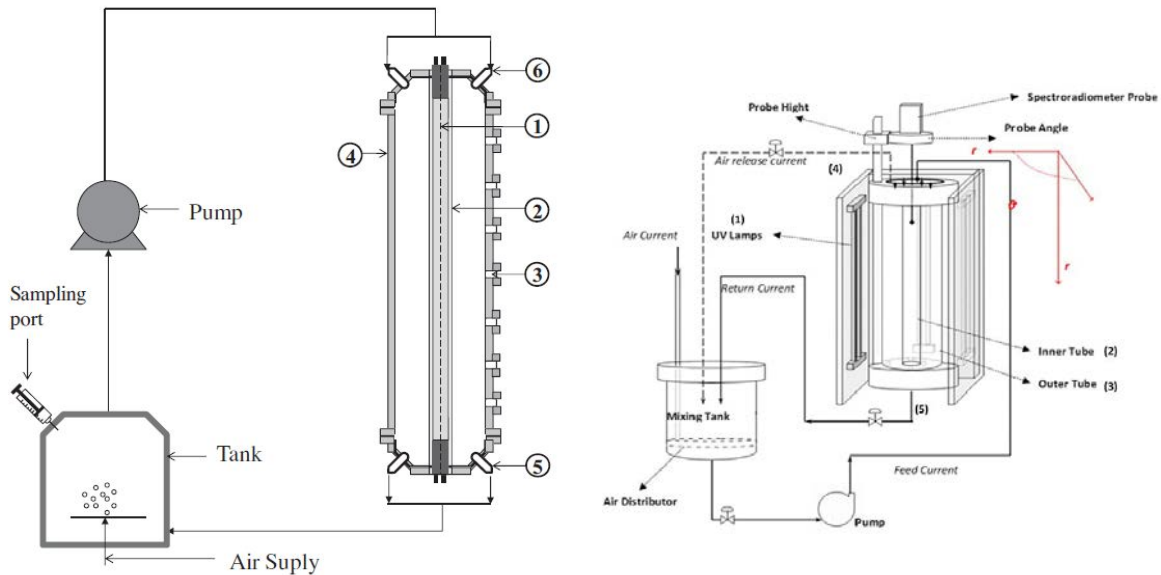
Figure 2.15: Photoreactor design and process configuration found on Valadés-Pelayo et al. (2015)

Furthermore, Valadés-Pelayo et al (2015) reported the design parameters and operating conditions of the bench-scale system as a 2.65 L annular Photo-CREC water II photoreactor, which consisted of a tank and a recirculating pump (16 L min-1) with a air supply and sampling ports respectively. As shown in Figure *2.15*, the configuration of the Photo-CREC water II photoreactor is such that the lamp (15 W black light lamp) is positioned at the central axis of the reactor, with the entire system having a total volume of about 6 L (Valadés-Pelayo et al., 2015). The bench-scale reactor also consists of an outlet and an inlet, a Pyrex glass inner tube, silica windows, and a black outer tube (Valadés-Pelayo et al., 2015).

Table *2.3* summarises previous work done on continuous and batch systems, focussing on the system size and configuration as well as the nature of the photocatalyst during the operations of the particular system.

Table 2.3: A summary of previous photoreactor designs

Reference	System configuration	Reactor type	Nature of operating catalyst	System size
Ray & Beenackers, (1998)	Continuous recirculating	Multiple tube reactor (MTR)	Immobilised	Consists of a cylindrical vessel 0.056 m in diameter, in which there are 54 hollow quartz glass tubes of 0.006 m diameter each
Dijkstra et al. (2002)	Continuous recirculating	Annular reactor	Suspended	Composed of a total reaction volume of 124 x10^{-6} m^3 and a holding vessel of 650 x 10^{-6} m^3
Wu et al. (2006)	Batch system	Vessel reactor	Suspended	Stainless steel vessel with a capacity of 15 L
Puma et al. (2007)	Continuous recirculating	Annular	Suspended	Stainless steel reactor column is 1.6 m with an inner radius of 0.108 m
Valadés-Pelayo et al. (2015).	Continuous recirculating	Annular Photo-CREC water II photoreactor	Immobilised	A 2.65 L reactor with the total volume of the system of about 6 L

2.7.2 Photoreactor design summary

Taking into account the listed research output as well as their respective reactor designs, the current project was carefully designed for optimal performance, taking into account all the key parameters such as light distribution. Although the design in this work draws a degree of influence from each photoreactor reported in the short design review, the recirculating aspect is common to all, excluding Wu et al. (2006). This allows a controlled reaction space/volume at any given time and also promotes uniform light distribution. However, the distribution of light methodology found on Wu et al. (2006) was a major influence on the design of this work despite the fact that their reactor configuration was a batch system.

The design used in this study, however, differs from the listed literature reactor designs in that it is a double jacketed photoreactor with the light and cooling area on the inside and the reaction medium being the shell area. This is due to the fact that irrespective of the light intensity under which one wishes to operate, maximum cooling can be easily achieved, whilst at the same time having a very thin reaction space.

The main focus of this design was to prioritise and take into consideration the theory provided by Lazar et al. (2012) and Linsebigler et al. (1995) which stresses the importance of light distribution on a photocatalyst in order for the reaction to occur. Furthermore, the theory is illustrated through the series of photocatalysis reaction steps demonstrated in Equation *2.1*. Equation *2.5* was also prioritised.

Furthermore, in this work the holding tank is designed with a conical bottom to eliminate settling and to promote a high exposure of the photocatalyst to the light source found in the photoreactor, as the photocatalyst spends less time in the holding tank. Another major distinction between this work and the reviewed studies is the sample port. Valadés-Pelayo et al. (2015), Puma et al. (2007), and Dijkstra et al. (2002) all sample from the bulk solution in the holding tank as shown in

Figure *2.15*, Figure *2.14*, and Figure *2.12* respectively. However, in this work, the sampling point chosen was similar to that of Ray and Beenackers (1998). It can be argued that the sample that these groups considered does not reflect the actual performance of the photoreactor, due to the fact that there is a considerable amount of dilution caused by the return of the already-treated solution. Therefore the time/concentration curve is not a true representation of the performance of the reactor, but rather reflects the dilution factor of the bulk solution caused by the returning treated solution.

2.8 Response surface methodology

RSM is a compilation of mathematical and statistical systems useful for improving, evolving and optimizing processes (Myers et al., 2009). Box and Draper (2007) stated that the statistical design of an experiment has a pivotal role in statistical experimentation. This also plays a vital role in designs, enhancement, and formulation of not only new but robust products, and the development of pre-existing products as well (Ryan, 2007). RSM assists in estimating operation variables that may be of no significance or may have a significant impact in the main response (Myers et al., 2009). According to Box and Draper (2007) RSM was originally developed to model responses of experiments and then later evolved into the modelling of experiments. Furthermore, real-world applications of RSM contain one response (dependent variable); the input variables (independent variables) are often known as freelance variables and are subject to the management of the engineer or scientist, for the purpose of the test or experiment (Myers et al., 2009).

Figure *2.16* a) Illustrates a typical representation of a theoretical response surface where in this particular example, the response is the yield in percentage and the variables are time (ε_1) and temperature (ε_2).
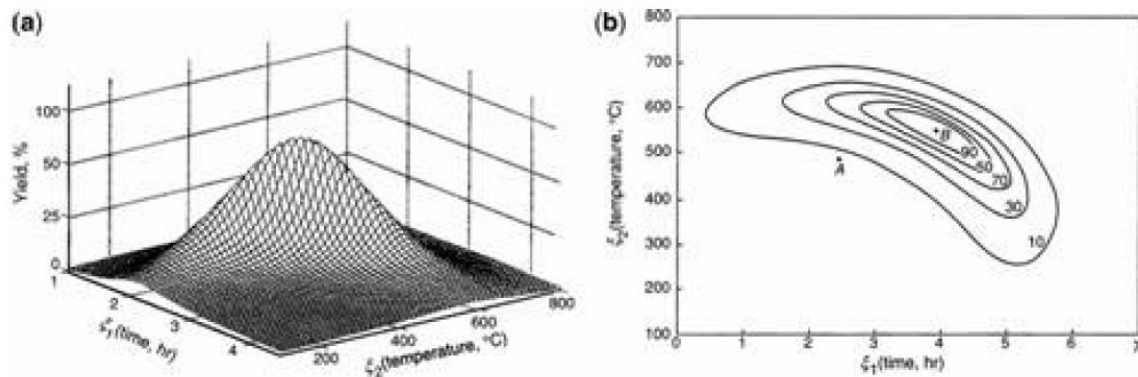
Figure 2.16: A graphical representation of a typical response surface and contour plot (Myers et al., 2009)

2.9 Design of experiments (DoE)

Box and Draper (2007) emphasised that the most vital aspect of RSM was the actual design of experiment (DoE). There are numerous strategies which assist the experimenter with the selection of the points to which the response should be evaluated; thus the corresponding experiments are designed solely for particular problems as they generally adopt a polynomial with unknown structures (Myers et al., 2009). The choice of the DoE can largely influence the accuracy of approximation of the response surface. The are a few design methodologies found on DoE software; however, this study will focus on central composite design methodology.

2.9.1 Central composite design (CCD)

Central composite designs are first-order (2^k) designs amplified by extra-axial and center points to allow an approximation of the tuning parameters' second-order model (Ryan, 2007). Myers et al. (2009) stated that a second-order model can be successfully constructed through a central composite design. Figure *2.17* illustrates a typical example of a central composite design.
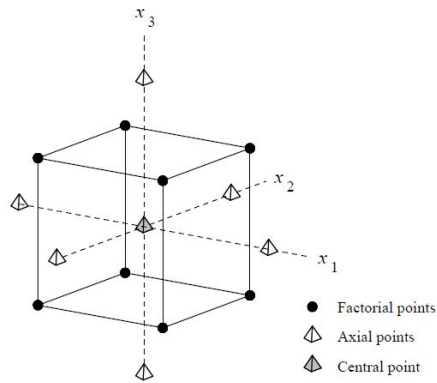
Figure 2.17: Design points of a three-variable design at 2 levels of a central composite design (Myers et al., 2009)

The design shown in Figure *2.17* encompasses 2^k factorial points, which are a central point and 2N axial points. In the construction of a second-order model, an alternative design of 3^k is adopted to reduce the number of experiments by almost half as compared to a full factorial design (there would be 15 runs on a CCD compared to 27 for a full-factorial design). However, experiments with a large number of variables may be time-consuming even in the case of CCD (Myers et al., 2009).

2.9.2 Building empirical models

This section addresses the building of empirical models, as this study aims to understand the interaction between operational parameters. It is anticipated that the models that will result from this work will be similar to those obtained in Liu and Chiou, (2005), Aleboyeh et al. (2008), Soltani et al. (2014), and Thind et al. (2017).

2.9.2.1 Linear regression models

Ryan (2007) stated that true surface responses are characteristically driven by some unknown physical mechanism. It is essentially the practical application of RSM to approximate the model

of the true surface response; furthermore, the model approximation is built on studied data of the process and is an empirical model (Myers et al., 2009).

Myers et al. (2009) explain a first-order example as a typical desire to study a relationship between the effective life of a cutting tool to the tool angle and cutting speed. The empirical model to this is described as shown in Equation *2.26*.

$$Y = \beta_0 + \beta_1 x_1 + \beta_2 x_2 + \varepsilon \qquad\qquad \text{Equation 2.26}$$

Where y, x_1 and x_2 represents the tool life, cutting speed and tool angle respectively. This is also known as a multiple linear regression model (Box & Draper, 2007). Equation *2.26* is said to be linear due to the equation being a linear function of unknown parameters β_0, β_1 and β_2. This model describes a 2-dimensional plane in x_1 and x_2 space (Khuri, 2006). The β_0 parameter fixes the intercept of the plane, β_1 and β_2 are known as partial regression coefficients, because β_1 gauges the anticipated change in **y** per unit change in x_1 when x_2 is fixed and vice versa (Khuri, 2006).

Generally, the response variable **y** may be attached to **θ** regression variables, as shown on Equation *2.27*:

$$Y = \beta_0 + \beta_1 x_1 + \beta_2 x_2 + \cdots + \beta_\omega x_\omega \ \varepsilon \qquad\qquad \text{Equation 2.27}$$

The parameters β_j, j = 0,1,2…,ω are known as regression coefficients (Khuri, 2006). The model in Equation *2.27* defines a hyperplane in the ω − dimensional space where the regression variables $\{\mathbf{x_j}\}$ (Khuri, 2006).

Models that are more complex than Equation *2.27* are often also analysed by multiple linear regression techniques, i.e. considering an inclusion of an interaction term to a first-order model into two variables, as shown in Equation *2.28*.

$$Y = \beta_0 + \beta_1 x_1 + \beta_2 x_2 + \beta_{1,2} x_1 x_2 + \varepsilon \qquad\qquad \text{Equation 2.28}$$

Where, if $\mathbf{x_1 x_2 = x_3}$ and $\boldsymbol{\beta_3 = \beta_{1,2}}$, then Equation **2.28** can be written as follows:

$$Y = \beta_0 + \beta_1 x_1 + \beta_2 x_2 + \beta_3 x_3 + \varepsilon \qquad\qquad \text{Equation 2.29}$$

Another common instant is shown in Equation **2.30**, where a 2nd – order response surface has two variables

$$Y = \beta_0 + \beta_1 x_1 + \beta_2 x_2 + \beta_{11} x_1{}^2 \beta_{22} x_2{}^2 + \beta_{12} x_1 x_2 + \varepsilon \qquad\qquad \text{Equation 2.30}$$

2.10 Evaluation of photocatalysis processes using RSM

Numerous studies have applied the methodology of surface response, for various intentions and have obtained various outcomes. Response surface methodology is also widely used in photocatalysis due to the complexity of the parameters that are involved. The breakdown mechanism or reaction pathway of photocatalytic reactions is usually very complex and comprises many side reactions, which often introduce many tedious parameters that are not easy to control. RSM therefore simplifies the experimental design process and employs a statistical analysis approach in solving the data.

The photocatalytic degradation study of reactive red 239 over 360 nm Ultraviolet light (UV) of Liu and Chiou (2005), with the aim of optimising process conditions, employed a 2^4 full-factorial CCD and response surface methodology The parameters of interest were UV intensity, TiO_2 concentration, initial pH and stirring speed (Liu & Chiou, 2005). The parameters in the current study are similar, and there is also a common parameter which is the TiO_2 concentration. All the selected parameters in this study are related to decolourisation efficiency through some linear or quadratic model (Liu & Chiou, 2005). Liu and Chiou (2005) showed that TiO_2 concentration

reveals a significant positive effect, whereas pH shows a negative effect on decolouration efficiency (Liu & Chiou, 2005). Under optimal conditions, a decolouration efficiency of 99.82% was obtained; the recorded optimal conditions were TiO_2 concentration 3.06 g/L; UV intensity, 16.08 W/m^2; initial pH, 2.64; and a stirring speed of 880 rpm (Liu & Chiou, 2005).

According to the study of Cho and Zoh (2007) regarding optimisation and modelling of the degradation of the reactive red 120 dye in a TiO_2/UV system based on RSM, the main objective was to optimise and find the best possible combination of the selected parameters to their responses which were colour removal percentage and total organic compound removal. A central composite design was also employed yielding a total number of 20 runs determined by a 2^3 full factorial trial design (also having six centre points and six axial points) (Cho & Zoh, 2007). Another similarity was that the reaction of degradation in this study follows an apparent first-order rate law. Further, the results of this work showed that the colour removal % (Y_1) was significantly affected by the synergistic effects of the linear term UV intensity (X_3) and the antagonistic effect of UV intensity (X_3^2) (Cho & Zoh, 2007). The second response, TOC removal % (Y_2), was significantly impacted by the synergistic effect of the linear terms TiO_2 (X_1) and UV intensity (X_3) (Cho & Zoh, 2007), while the quadratic effect TiO_2 (X_1^2) and UV intensity (X_3^2) had an antagonistic effect (Cho & Zoh, 2007). The predictable ridge of maximum responses and optimal concentration for Y_1 and Y_2 using canonical analysis were 100% and 67.27% respectively. It was also found that the stationary point appeared to be a saddle point for Y_1 and a maximum for Y_2 (Cho & Zoh, 2007).

Bahadir and Rauf (2008) used a response surface methodology to determine the optimum removal of toluidine blue (TB) in the presence of UV and a heterogeneous hybrid catalyst (TiO_2 impregnated with V_2O_5) (Bahadir & Rauf, 2008). The parameters of interest were TB concentration (μM), V_2O_5/TiO_2 (mg/20mL), and pH and the experimental runs were designed according to the D-optimal design. The reactor configuration used to conduct theses runs was a batch system (Bahadir & Rauf, 2008). The performance of the process was evaluated by analysing the

response of decolourisation percentage and in the optimisation process; the response can be related to the chosen factors by some linear or quadratic model (Bahadir & Rauf, 2008). The work of Soltani et al. (2014) and that of Bahadir and Rauf (2008) differ as well as the system configuration. In the study of Bahadir and Rauf (2008) it was found that the effect of the catalyst concentration and that of pH on the response (reported at 60 μM TB) was that the semi-spherical response surface gradually increased with increasing pH (5.0 - 7.0) at any catalyst concentration and would gradually decrease from pH 7.7 and above. A similar trend was observed for the catalyst concentration where the maximum value of decolourisation percentage was 78.6% at pH 7.7 and 26.5 mg/20mL catalyst; there was a decrease beyond this point (Bahadir & Rauf, 2008).

Soltani et al. (2014) developed a rectangular photoreactor immobilised with a carbon black (CB)/ZnO nanocomposite was used for the photodegradation of M.O (Soltani et al., 2014). This study was carried out with a CCD experimental design methodology with RSM, focusing on parameters such as the CB/ZnO ratio, initial pH, reaction time, and initial dye concentration (Soltani et al., 2014). An optimum decolouration efficiency of 80% was achieved under conditions of initial dye concentration, CB/ZnO, initial pH and reaction time reported to be 13 mg/L, 0.05, 5, and 95 min respectively (Soltani et al., 2014).

Thind et al.(2017) investigated a TiO_2/H_2O_2 mediated UV photocatalytic oxidation of chloropyrifos (CP) in a batch laboratory photoreactor, using a three level Box-Behken factorial design (BBD) technique combined with RSM (Thind et al., 2017). The focus parameters were TiO_2 concentration, H_2O_2 concentration and initial pH on response parameters like degradation of Chemical Oxygen Demand (COD) and degradation of CP (Thind et al., 2017). The parameter effect on response was analysed through polynomial regression models (Thind et al., 2017). This work found that the optimum process conditions yielded 74.38% and 68.29% for CP degradation and COD degradation respectively (Thind et al., 2017).

2.10.1 Summary of previous studies of photocatalysis through RSM

A summary of the factors that were considered in previous studies, and points out the uniqueness of the current study, which takes into account the treatment volume that is often neglected is provided in Table *2.4*. A review by Braham and Harris (2009) explicitly states that there is no linearity in this term and that the relationship surrounding the parameter is in fact unknown in comparison to other commonly studied parameters. Soltani et al. (2014) reported the decolourization efficiency of methyl orange over carbon black/ZnO nanocomposite. In this work Soltani et al. (2014) stated that the modification of ZnO nanoparticles with a suitable CB had a significant impact in the physicochemical properties of the pure ZnO and increased the decolourization efficiency. Subsequent to that a comparison of mineralization to decolourization efficiency was conducted showing that at 80% decolourization, 55% mineralization was realized as measured by TOC removal.

Xu et al. (2014) evaluated the discoloration of methyl orange b anatase/school composite and did not compare the discoloration to mineralization, this work only focused on optimization and reported the optimum discoloration ratio of 94.3% which could be achieved in 43 mins.

The studies presented in the summery provided in *2.10.1* (Liu & Chiou, 2005; Bahadir & Rauf, 2008; Thind et al., 2017) evaluated the decolourization efficiency and optimization without any comparison to complete mineralization.

Table 2.4: Previous photocatalysis studies carried out through RSM

		Previous studies					
		Current study	(Liu & Chiou, 2005)	(Cho & Zoh, 2007)	(Bahadir & Rauf, 2008)	(Thind et al., 2017)	Soltani et al. (2014)
Parameters	Catalyst concentration	√	√	√	√	√	√
	Oxidant concentration	√				√	
	initial pH		√		√	√	√
	Treatment volume	√					
	Stirring speed		√				
	initial dye concentration	√		√	√		√
	Reaction time						√
	Light intensity		√	√			
Other factors	No. of studied parameters	4	4	3	3	3	4
	Experimental design type	CCD	CCD	CCD	D-Optimal	BBD	CCD
	Light source type	Solar (Simulated)	Ultraviolet	Ultraviolet	Ultraviolet	Ultraviolet	Ultraviolet
	System configuration	Continuous	Batch	Continuous	Batch	Batch	Batch
	Catalysts type	TiO_2 (P25)	TiO_2 (P25)	TiO_2 (anatase)	V_2O_5/TiO_2	TiO_2 (anatase)	CB/ZnO
	Contaminant type	Methyl Orange	Reactive red 239	Reactive red 120	Toludine Blue	Chlorpyrifos	Methyl orange

2.11 Conclusion

This chapter provides an introduction to AOPs, photocatalysis and compared established against emerging AOP technologies. The mechanism of hydroxyl radical attack as recommended by literature was also considered. Photocatalysis is a process which occurs through a series of chemical reaction steps which were outlined in detail as well as the reaction kinetic engineering involved in these reaction steps. Photocatalysis is a process in which a particular reaction occurs in the presence of a light source and a catalyst; therefore, in the literature review, the impact of a catalyst on a reaction was outlined, as well as the radiation equations and profiles. The fundamentals that were employed in analysing samples using a UV-Vis spectrophotometer were addressed in this chapter. The generic mass conservation for all types of reactor geometry configuration as well as the radiation balance was outlined, focusing particularly on how the lamps were configured. A brief literature review on previous designs was conducted and it was found stated that the design aspect of heat removal that was employed in this study was influenced by the MTR design found in the study of Ray and Beenackers (1998). The recirculating process configuration was influenced by the process design found in Dijkstra et al. (2002). All the reviewed studies played a major role in the overall design of the reactor found in this study. However, the difference between this study and the studies reviewed was the evaluation methodologies, the reviewed studies focused on fundamentals such as radiative transfer equations (RTE) and kinetic rate data behavior while this study used a statistical methodology of RSM. The methodology implemented in this study involves statistical analysis by RSM, therefore the empirical models and the means of their determination were outlined. The literature reviewed in this chapter mostly evaluated the decolourization efficiency and not mineralization. However, Soltani et al. (2014) reported that there was a 25% difference between mineralization and decolourization efficiency. A brief evaluation on previous studies incorporating RSM methodology indicated that all the studies evaluated the effect of catalyst and the effect of pH was also found to be evaluated in

64

most of the studies. However, the effect of treatment volume and the effect of oxidant concentration necessary for scale up was neglected, which now forms the basis for this study.

Chapter 3 – Design, construction, and commissioning of the prototype photocatalytic reactor

3.1 Introduction

This chapter provides a list of all the equipment and chemicals that were used in the experiments. The experimental and sampling procedure are demonstrated in the order in which the experiments were conducted. The CCD design matrix and how the responses were obtained is also detailed. The material of construction, power calculations and circuit design are demonstrated in this chapter. All the aspects that were taken into consideration in the design of the continuous re-circulation batch photoreactor and therefore a detailed process design will also be reported in this chapter accompanied by block and process flow diagrams as well as a 3-D representation and a HAZOP study for loss prevention and safety considerations.

3.2 Materials

Materials used in the experiments with all their purity standards and purposes are described in this section. All the equipment with brand and model details used in this study is shown in Table *3.1*.

3.2.1 Chemicals used

All the chemicals listed were used without any pre-treatment or modification and are listed:

- **Methyl orange dye ($C_{14}H_{14}N_3NaO_3S$)** with a dye content of 85% was supplied by Sigma-Aldrich and was used in its pure form without any further pre-treatment. This was used to prepare the dye solutions of known concentrations that were treated in this study.

- **Hydrogen peroxide (H_2O_2)** 30% (w/w) was used as an oxidant for all photocatalysis experiments.

- **Titanium dioxide (TiO_2)**, Aeroxide P25, purity>99%, was used as a photocatalyst in a slurry form.

- **Ammonium hydroxide solution (NH_4OH)** was used as a base to adjust pH.

- **Hydrochloric acid solution (HCl)** was used as an acid for adjusting pH.

Table 3.1: List of equipment used

Equipment	*Brand*	*Model*
Magnetic stirrer	Lab smart	MSH-Pro+
pH meter	Crison	50 14T
Centrifuge	Sigma	2-16p
Ultrasound sonicator/homogenizer	MRC/ Heilscher	---/UP200s
UV-Vis spectrophotometer	GBC	Citra2020
Purite deionizer	O-pirite	----

3.3 Experimental and sampling procedure

A stock solution of 160 mg/L methyl orange was prepared using Milli-Q water and kept in a dark cupboard. All the experiments were conducted using this stock solution. A pre-determined volume was taken from the stock solution and diluted to the desired concentration. A known mass of TiO_2 was then added in this volume to form a slurry. After the slurry was prepared, it was homogenized for 15 minutes. The pH was adjusted by adding a base/acid to adjust it to a pH level of 4.5 to 4.8. The slurry was then transferred to the continuous recirculating batch photoreactor. After taking

the initial adsorption sample, the dark glass of the fume hood where the reactor was located was closed to avoid any additional light. This marked the beginning of a 30-minute long adsorption. At the end of 30 minutes, the desired amount of H_2O_2 was added, the pump started, and the process dye water was allowed to circulate and reach a steady state by monitoring change in the fluid height in the bulk tank. The reactor light was switched on and an initial sample of dye solution taken from the sampling point as depicted in Figure **3.5**. The sample was then transferred to a 2 mL hydrophobic micro tube and centrifuged, after which it was transferred into a UV-Vis spectrophotometer quarts cuvette for a concentration analysis.

The sample interval time was calculated based on the total volume being treated as expressed in Equation **3.1**:

$$S.I.T = \frac{V_{tot.treated}}{Q_{pump}}$$

Equation 3.1

S.I.T represents the sample interval time (min), $V_{tot.treated}$ is the total volume being treated excluding the volume of H_2O_2 (mL), and in the bulk tank and Q_{pump} is the volumetric flow rate that the pump is set to (mL/min). This allows enough time for the total volume to undergo light exposure before any sample can be taken.

3.4 Sample analysis methodology

The collected samples were analysed using a UV-Vis spectrophotometer GBC Citra2020. The UV-Vis detected the absorbance of MO when set at wavelength of 464 nm. The absorbance obtained could be related to the dimensions of the cell and the light passing through it by using the expression specified in Equation **2.9**. This expression could therefore be related to concentration by preparing a series of standards of known concentrations which were 0, 0.5, 1, 3, 5, 10, 20 and 30 mg/L. The UV-Vis then determined the absorbance corresponding to these concentrations and a straight line curve was obtained.

Two calibration curves are shown in Figure *3.1* which were obtained on different days. The R^2-values obtained for the calibration curves were 0.9996 and 0.9995. It is essential to note that due to the aging of the UV-Vis lamp, the calibration was renewed frequently. The maximum concentration for the calibration curve was 30 mg/L. This means that for reactor feeds that are above 30 mg/L, the sample needed to be diluted using the standard dilution equation as shown in Equation *3.4*:

$$C_1 V_1 = C_2 V_2$$

Equation 3.2

C_1 is the true sample concentration, C_2 is the concentration after diluting and V_1 is the volume of the sample, and V_2 is the volume of the sample plus the diluting volume.
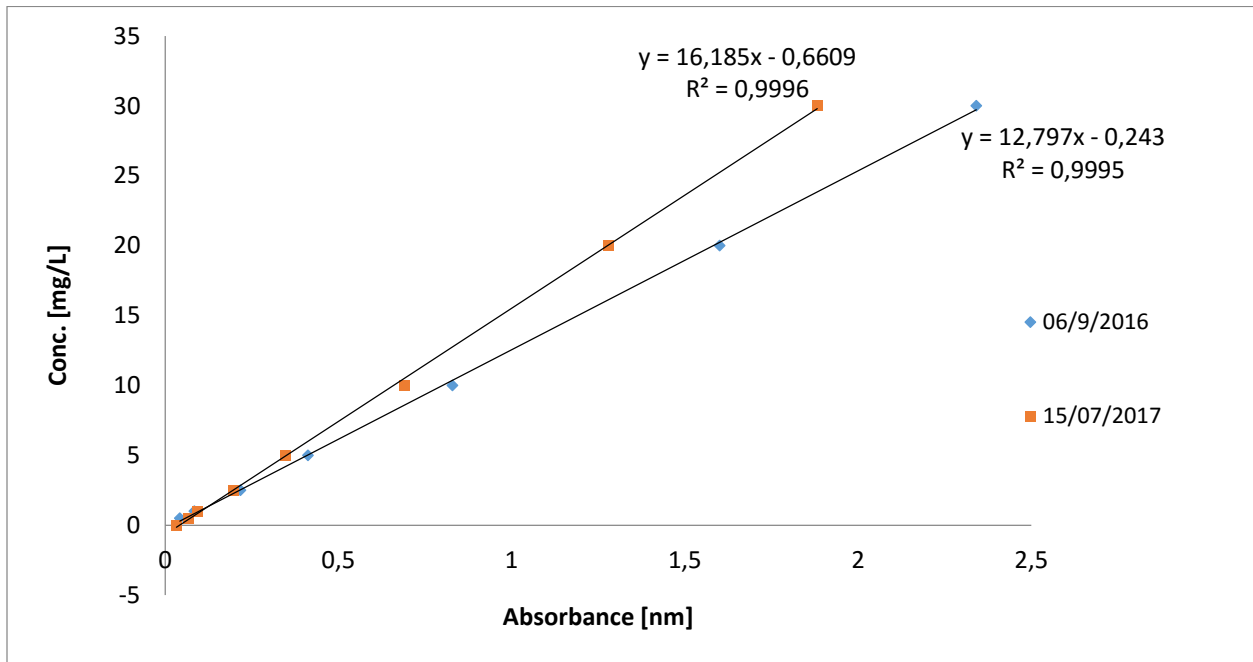
Figure 3.1: Standard calibration curves

The analysis of the results is shown step-by-step using data obtained in a demonstration run. This includes the time/concentration data, concentration/time curve, the determination of the reaction

rate constant, as well as the percentage degradation of the sample treated over a period of 60 minutes. An example of a time/concentration data is shown in Table *3.2*

Table 3.2: Typical concentration time data

Time[min]	Concentration[mg/L]	C_t/C_o	Ln[]
0	32.0	1	0
10	23.5	0.73	0.310
20	14.0	0.44	0.83
30	6.0	0.19	1.67
40	3.0	0.09	2.37
50	1.5	0.04	3.06
60	0.2	0.006	5.08
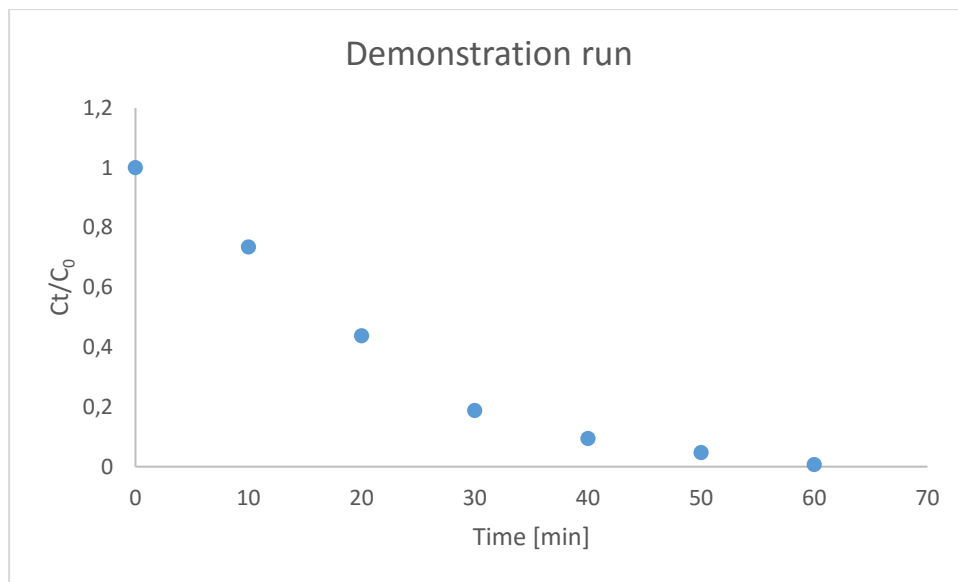
Figure 3.2: Typical concentration time curve

The total % degradation achieved for the demonstration run can be determined using Equation *3.3*

$$\% \, Degradation = \left(1 - \frac{C}{C_o}\right) \times 100$$

<div align="right">Equation 3.3</div>

where C_o and C are the representative concentrations at time 0 and time t respectively

The degradation curve in Figure **4.2** is presented as Ct/C0, versus time (t). The reaction rate constant as given in Equation **2.7** is integrated to give Equation **3.4**:

$$ln\left(\frac{C}{C_o}\right) = -k.t$$

<div align="right">Equation 3.4</div>

In order to eliminate the negative sign which represents decomposition of the reacting specie the data shown in Table **3.2** should be considered as negative values and should be plotted against time to give a straight line curve whose gradient is the reaction rate constant as shown in Figure **3.3**.
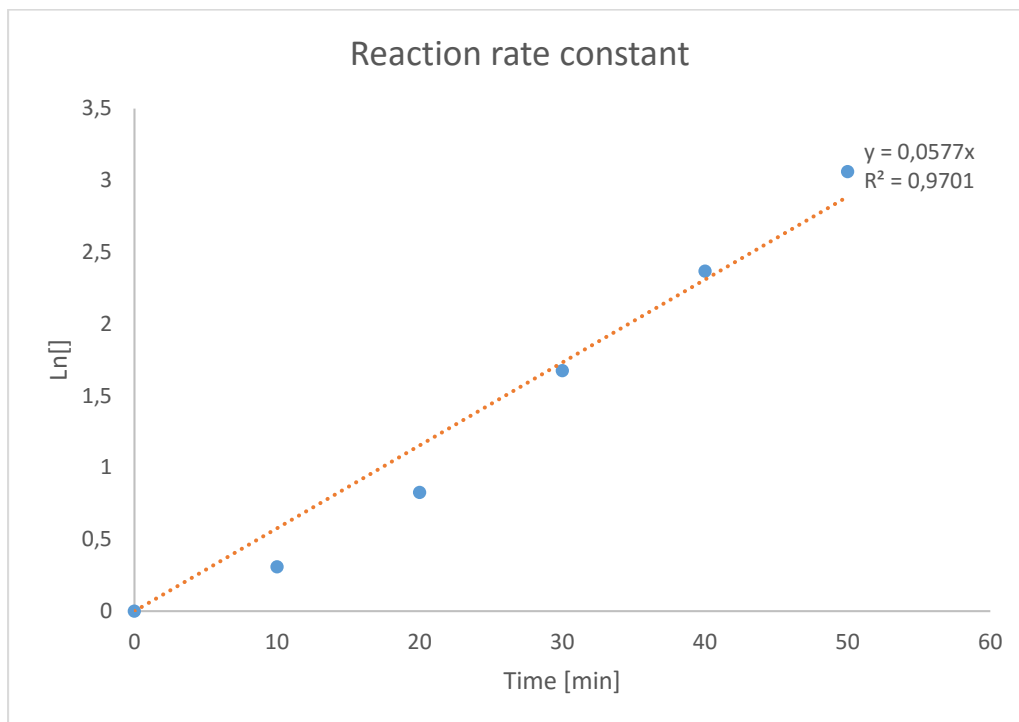
Figure 3.3: Determination of reaction rate constant

In this case the reaction rate constant is 0.0577 min^{-1}, showing that the reaction follows the first order rate law as reported in literature (Missen et al., 1999). The total percentage achieved for the demonstration run was 82% and was determined using Equation *3.3* (Bahadir & Rauf, 2008)

3.5 Experimental design and central composite design

To obtain the optimum conditions for methyl orange degradation in a continuous recirculating batch photoreactor, the experimental design as a function of the chosen main factors has to be determined, as shown in Figure *2.17*. This study was carried out using a central composite design consisting of 30 runs which were obtained by Equation *3.5* shown.

$$N = 2^k + 2k + x_o$$ Equation 3.5

where N, k and x_o represent the number of necessary experiments, the number of parameters, and the number of central points respectively (Khuri, 2006; Myers et al., 2009). Thirty runs were conducted due to the fact that there were six central points (x_o = 6), and there were four factors (k = 4), namely Volume (L), TiO_2 dosage (g), H_2O_2 dosage (mL) and initial Dye concentration (mg/L). The process parameters were coded according to the expression in Equation *3.6*:

$$x_i = \frac{x_i - x_o}{\delta X}$$ Equation 3.6

where x_o and δX are the values of x_i at the centre point and step change respectively (Montgomery, 1997).

Table *3.3* shows the original together with the coded levels of the input variable.

Table 3.3: Coded and original levels of the input variables (*A, B, C* and *D*)

Process parameters	Units	Symbol	-2(σ)	Coded values			
				-1	0	+1	+2(σ)
Volume	L	*A*	1.25	5	12.5	20	23.75
TiO$_2$ dosage	g	*B*	0	2	6	10	-
H$_2$O$_2$ dosage	mL	*C*	0	20	110	200	245
Initial dye concentration	mg/L	*D*	1.25	5	12.5	20	23.75

The CCD factorial trial allowed adequate point prediction within the selected range of operating parameters shown in Table **3.3**.

Kaneco et al. (2004), Konstantinou and Albanis (2004), Daneshvar et al. (2004) and many other authors have extensively studied the kinetics and evaluated initial conditions, however, these authors did not incorporate the volume parameter, thus inhibits the possibility of scale-up and moving closer to industrial application. Therefore further exhausting or testing the experimental work similar to these studies would be deviating from the objective which is to establish scalable models which will also bring forth the knowledge as far as dynamic parameter interactions are concerned.Findings on initial conditions obtained in a particular volume does not hold when the volume is increased to twice the size, due to the fact that there is no linearity in the scale-up of photocatalysis (Braham & Harris, 2009). This therefore draws attention to the understanding of dynamic parameter interaction around the volume parameter. CCD has been popularly employed in various photocatalytic studies and the results found in this work are not in contrast with any of the pre-existing studies. A strong motivation in employing a CCD methodology was brought about by the success that was found in the studies that used the CCD methodology as summarised in **2.10.1**,

Table 2.4 and this study considers to address dynamic parameter interaction and   scale-up

Furthermore, the design of the photoreactor in the current study emerged as a result of the need to study parameters that are neglected in literature, such as volume, catalyst loading, and peroxide dosage, and to compare the interactions of the these parameters to those that are frequently investigated in literature, such as pH, stirring rate and temperature. Traditionally these parameters have been studied through batch processes and most frequently in small volumes such as 100 mL as it can be found in Chowdhury et al. (2015) and Sheikh et al. (2016).

The batch configuration similar to the one showed in Figure *2.13* was found not to be suitable after conducting preliminary experiments because there is a direct proportionality in the distance traveled by light (path length) and change in volume. This resulted in inconsistent change in the light path length, as the volume changes made it difficult to determine the relationship of volume to TiO_2 and H_2O_2. Maskill et al. (2013) also confirm that even though batch processes are advantageous in terms of exposure time, they are often very difficult to scale-up due to light phenomena. Therefore, to eliminate this challenge, the process configuration was developed as shown in Figure *3.5*.

3.6 Continuous Process design

The following section shows the P&ID and the BFD of the process developed in this study.

3.6.1 Block and Process Flow Diagram

This section shows the design aspect and concepts behind the system and the reactor, showing the Block flow diagram of the system (as seen in Figure *3.4*), a P&ID (as seen in Figure *3.5*), 3-D

sketch-up images (as seen in Figure *3.6* and Figure *3.7*) and a schematic diagram of the photoreactor is shown in Figure *3.8*.
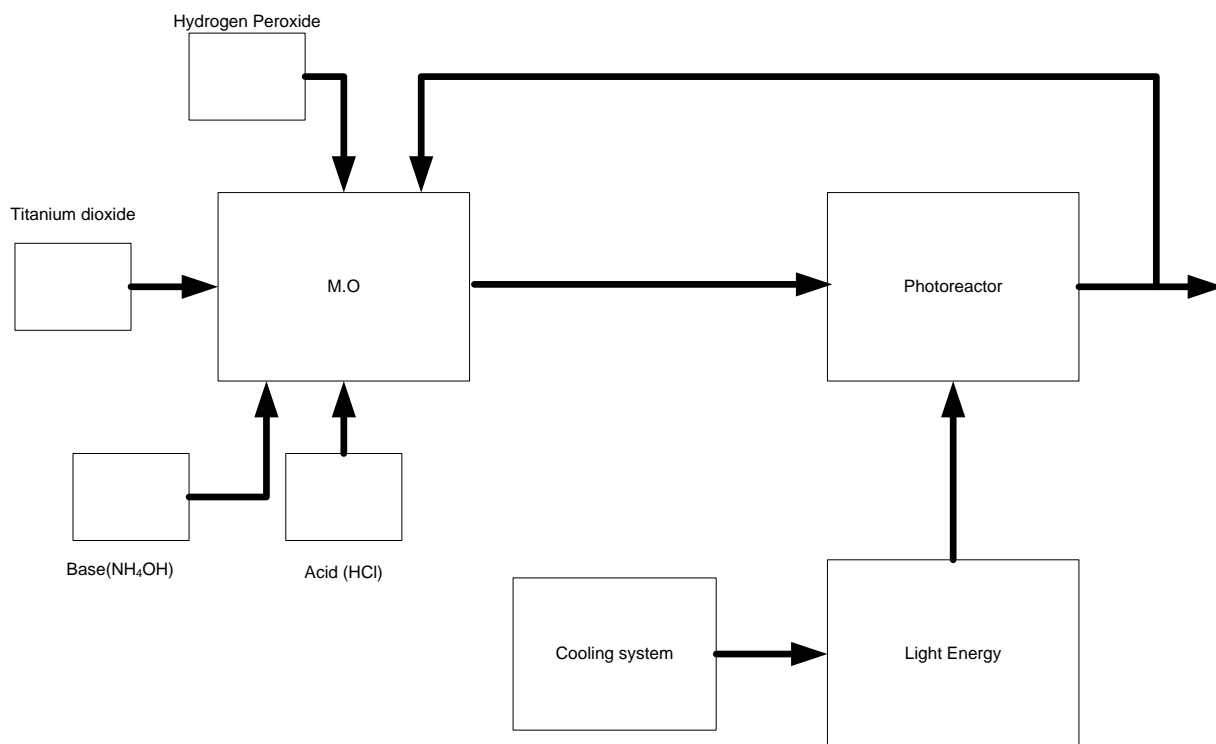
Figure 3.4: Block flow diagram of the locally developed system
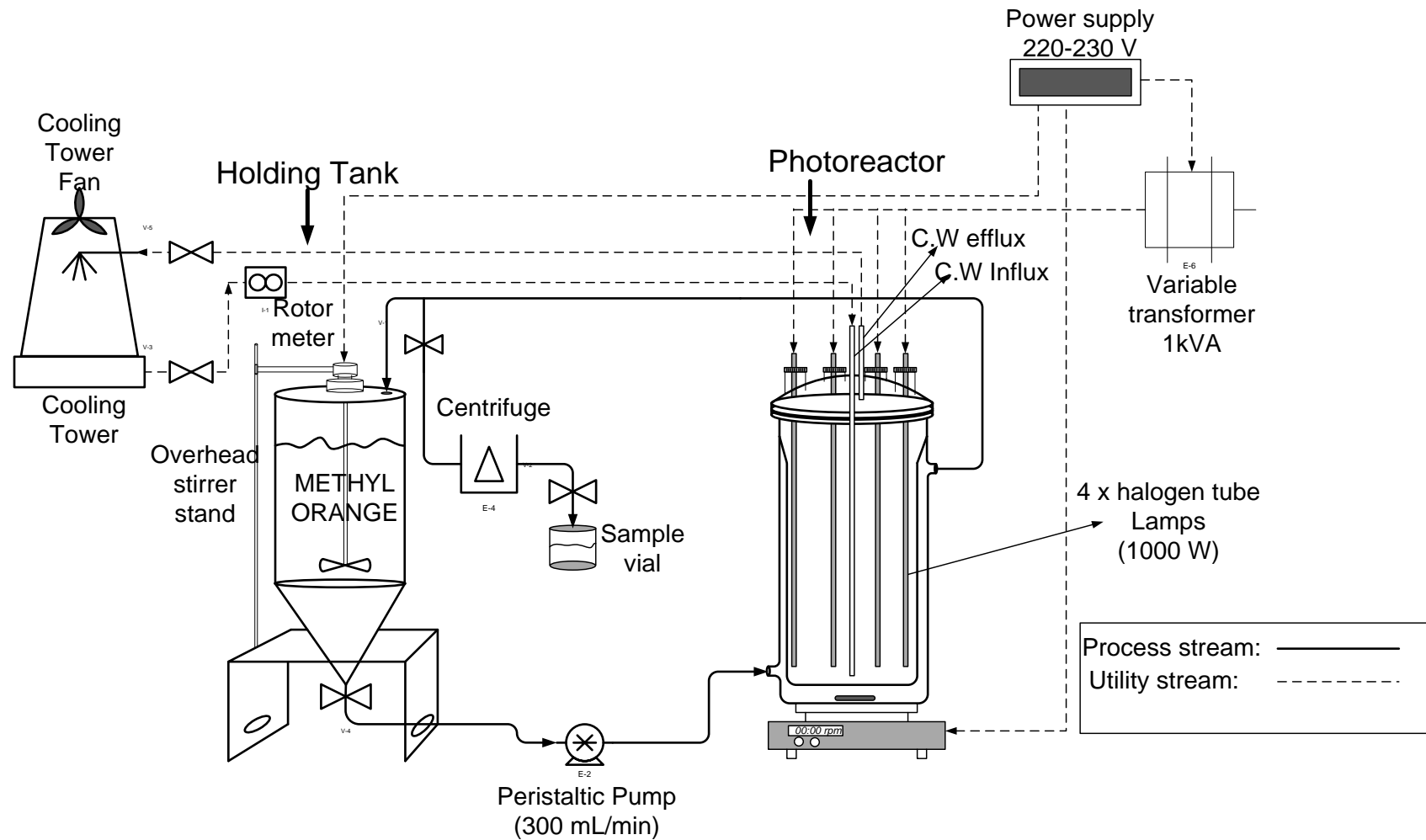
Figure 3.5: Process flow design of the photocatalysis process configuration and photoreactor design used in this study, CPUT, Cape Town, South Africa
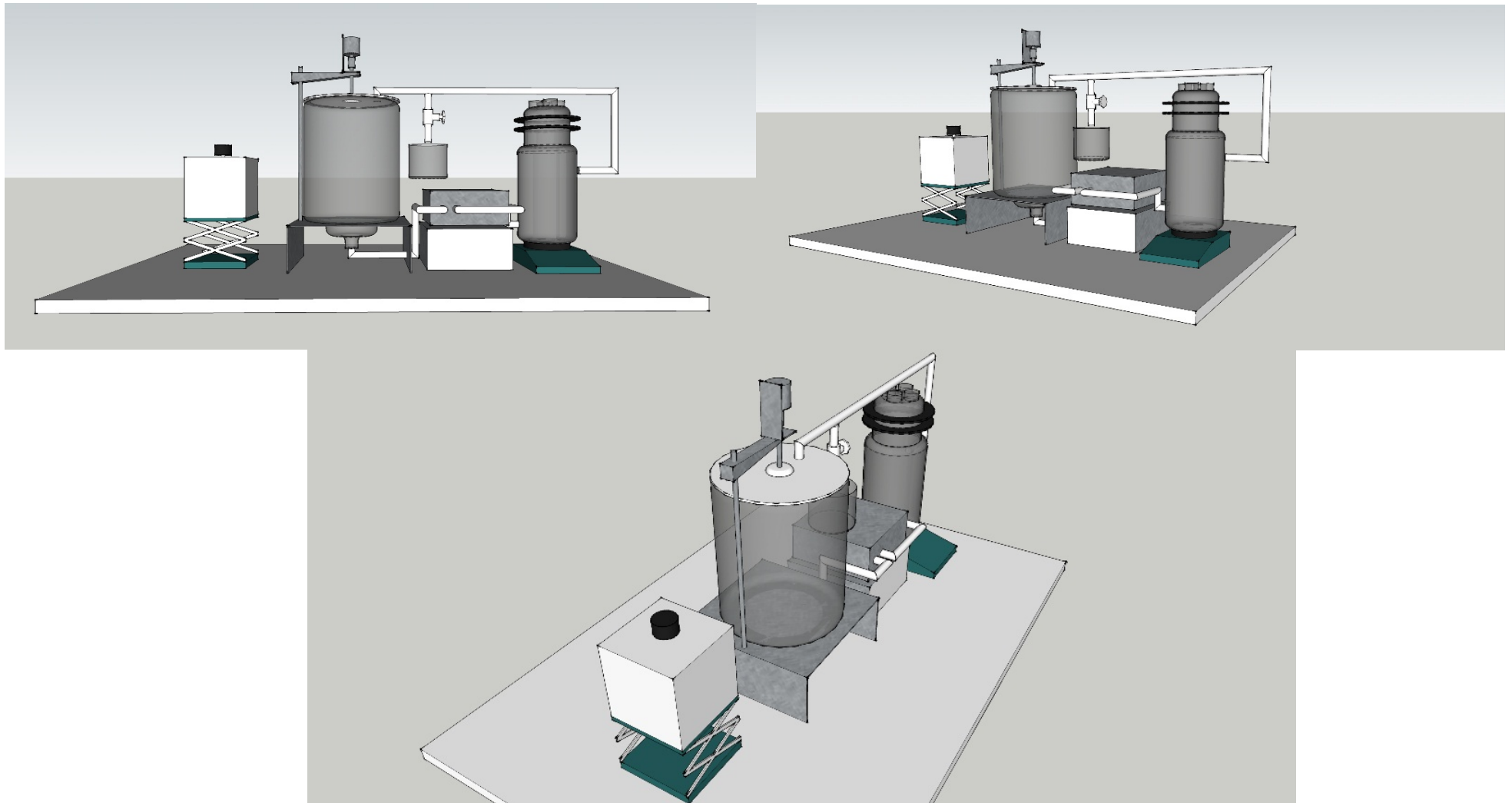
Figure 3.6: Different perspectives of a 3-D design concept for a continuous recirculating batch photocatalytic reactor
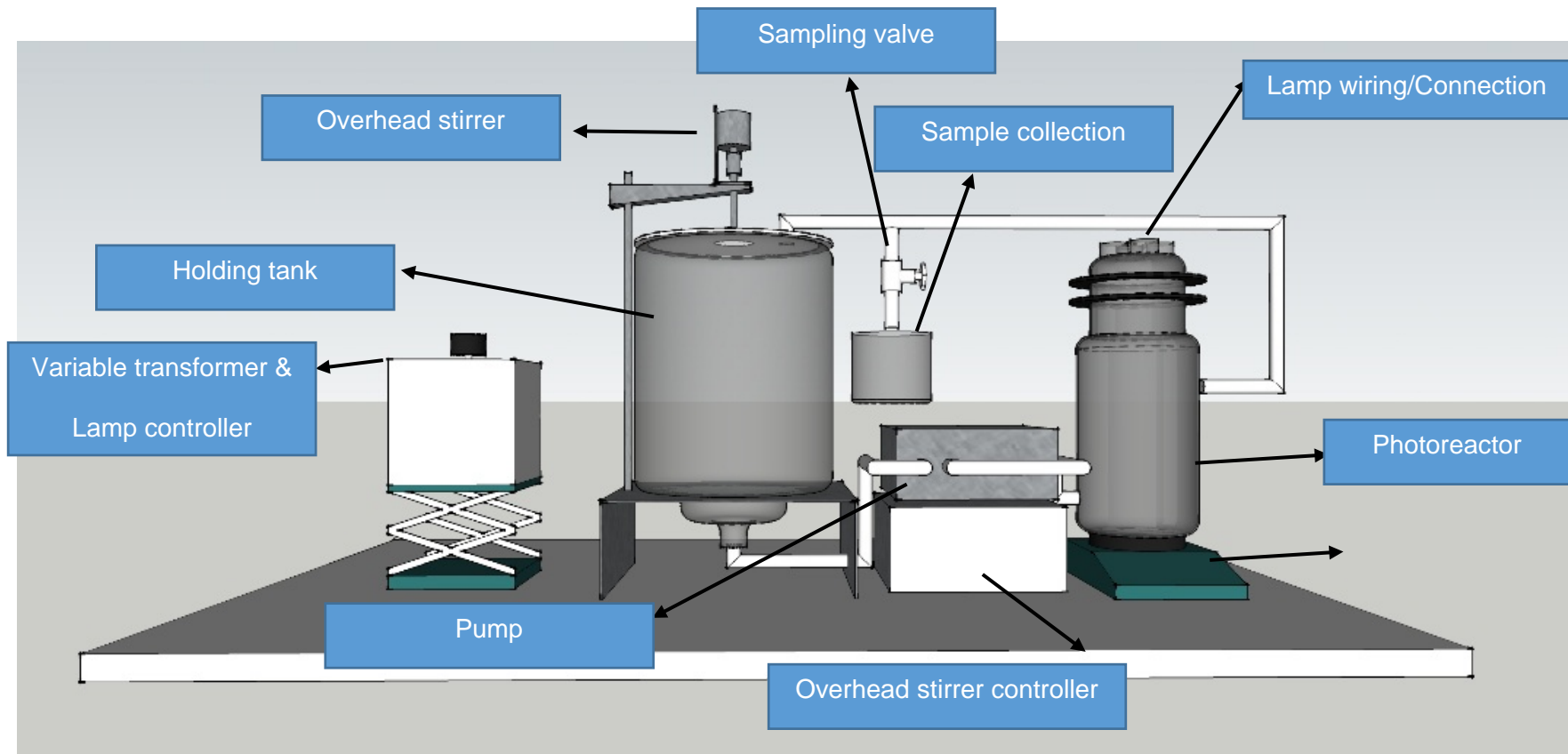
Figure 3.7: Detailed 3-D image of the design concept for the CRBPR

3.7 Locally developed annulus reactor

Figure *3.8* shows a schematic diagram of the design concept of the reactor developed in this study accompanied by legends showing a horizontal cross-section.
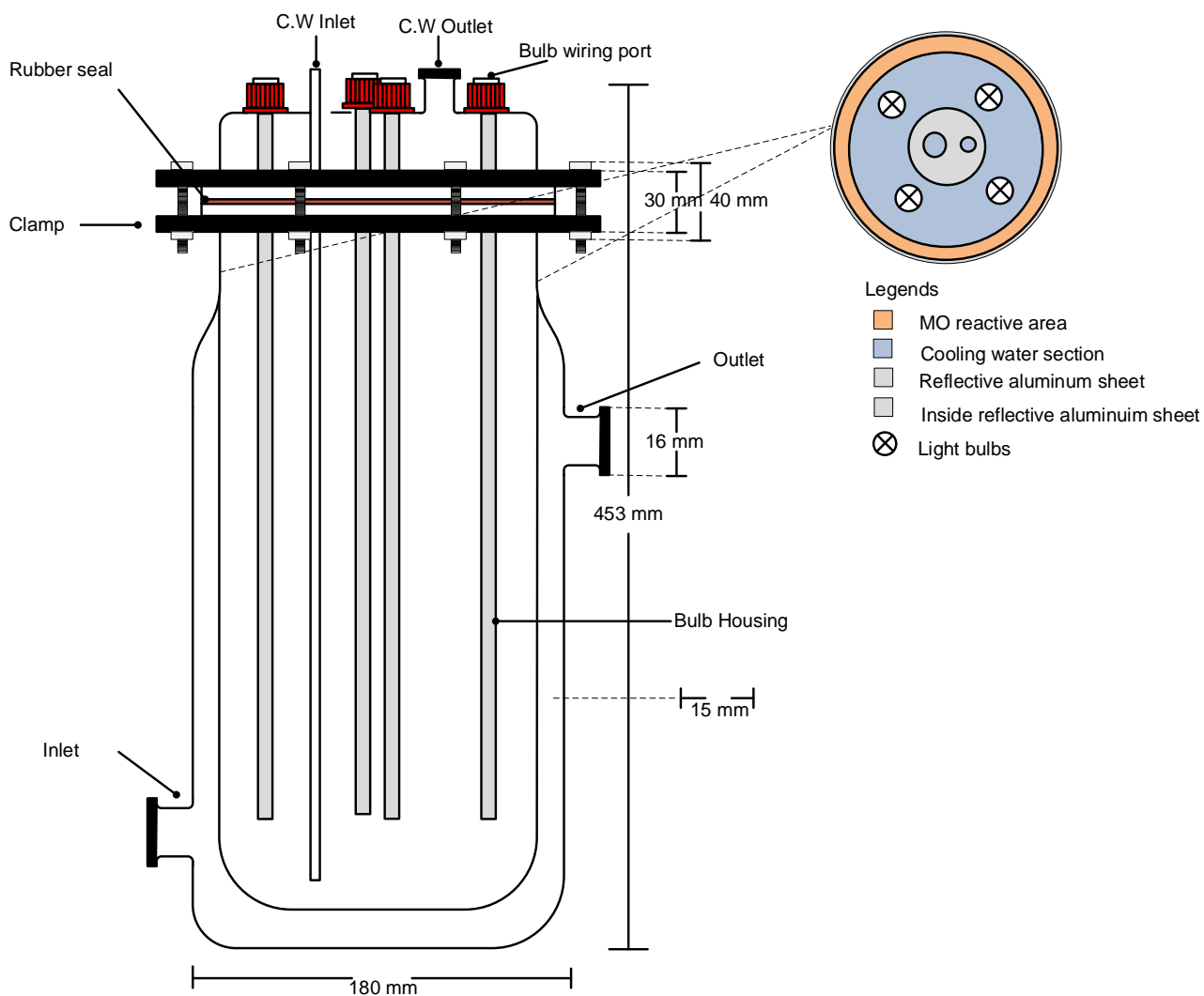
Figure 3.8: Schematic diagram of the locally developed photoreactor

The reactor developed in this study was built with Pyrex glass material. The reacting fluid was designed to pass on the shell-side (see Figure *3.8*) entering through the 16.0 mm inlet and being pumped against gravity to the top outlet of the same diameter, while the cooling water enters the top of the reactor on the bulb housing lid and flows straight to the bottom of the reactor. From there it flows slowly against gravity, finding its way to the exit, which is situated next to the inlet of the cooling water to the chiller, and back. At the exit point for the cooling water is the thermostat that monitors it, as well as the general operational temperature of the reactor. The reactor is 180 mm wide and 453 mm in height. The thickness of the inside tube is 5.0 mm and has an inner diameter of 150 mm, with an outside tube of 3.0 mm thickness. The properties of the Pyrex glass material used to build the reactor are reported in Figure *3.9* and Figure *3.9*

Property	*Value*	*Unit*
Maximum temperature	500	°C
Thermal conductivity	1.14	W/m.K
Coefficient of linear expansion	3.3	$10^{-6}/$°C
Density	2.23	g/cm^3
Young's modulus	64	Gpa
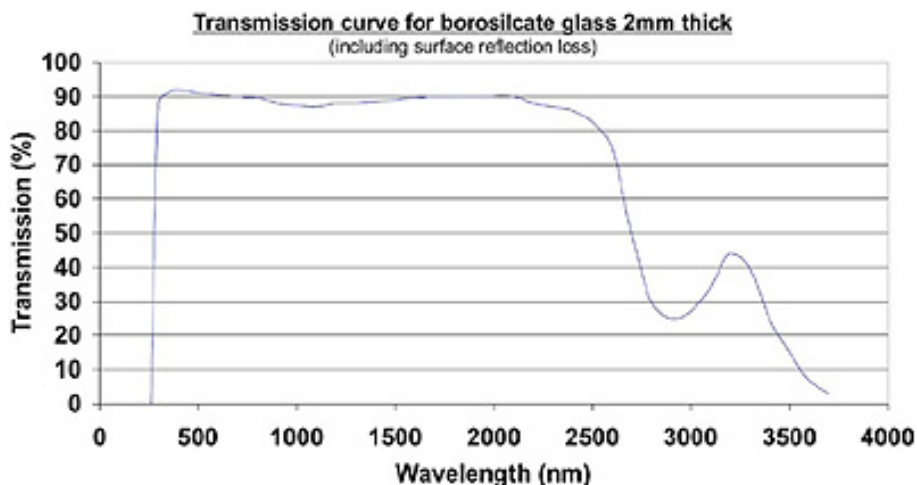
Figure 3.9: Transmittance curve for borosilicate glass (Says, 2009)

Figure *3.10* a) shows the photoreactor, b and c) the detailed clamping system combining the lamp holder and the cooling section. The reactor is opened by removing the clamping system during servicing of the lamps and general cleaning. This clamping system holds together the lid section (which also houses the lamps and assures that they do not come into direct contact with the cooling water) and the rest of the apparatus, which has the reactive shell through which the reacting fluid flows. The glass-to-glass connection has a rubber seal which was assembled using silicon glass, and the bolted clamp holds everything together. The lamps run along the entire length of the reactive space and the connecting wires are separated by ceramic beads.

Figure *3.10* d) is the assembled system in which a holding tank to the left of the image is connected to a peristaltic pump/pump controller and recirculates through the reactor back to the holding tank passing the sampling point as well as the stirrer/stirrer controller.

a)

b)

c)

d)

Figure 3.10: Photoreactor and the system, a) photoreactor without the reflective sheet, b) reactor clamping system also illustrating the lamp housing system, c) illustrates the internal reflective disc and d) the complete system illustrating the photoreactor in operation with the external reflective aluminum sheet

The system works with tungsten lamps which can reach a temperature of up to a 100 ^{0}C if not correctly monitored or controlled. It is controlled by a chiller (shown in Figure *3.11* b) that is situated outside the building, which services other systems in the CPUT Flow Process and Rheology Centre, therefore V4 shown in Figure *3.11* is used to isolate the photocatalytic system.

a)   *b)*

Figure 3.11: a) piping system that connects the chiller to various systems as well as the continuous re-circulating batch photoreactor b) chiller

The peristaltic pump used on the system has a maximum capacity of ~300mL/min and was assembled and programmed by Glass Chem in Stellenbosch, to meet the needs of the system. The overhead stirrer was also obtained from Glass Chem and is operated with a percentage setting of 0 to 100%.

a)

b)
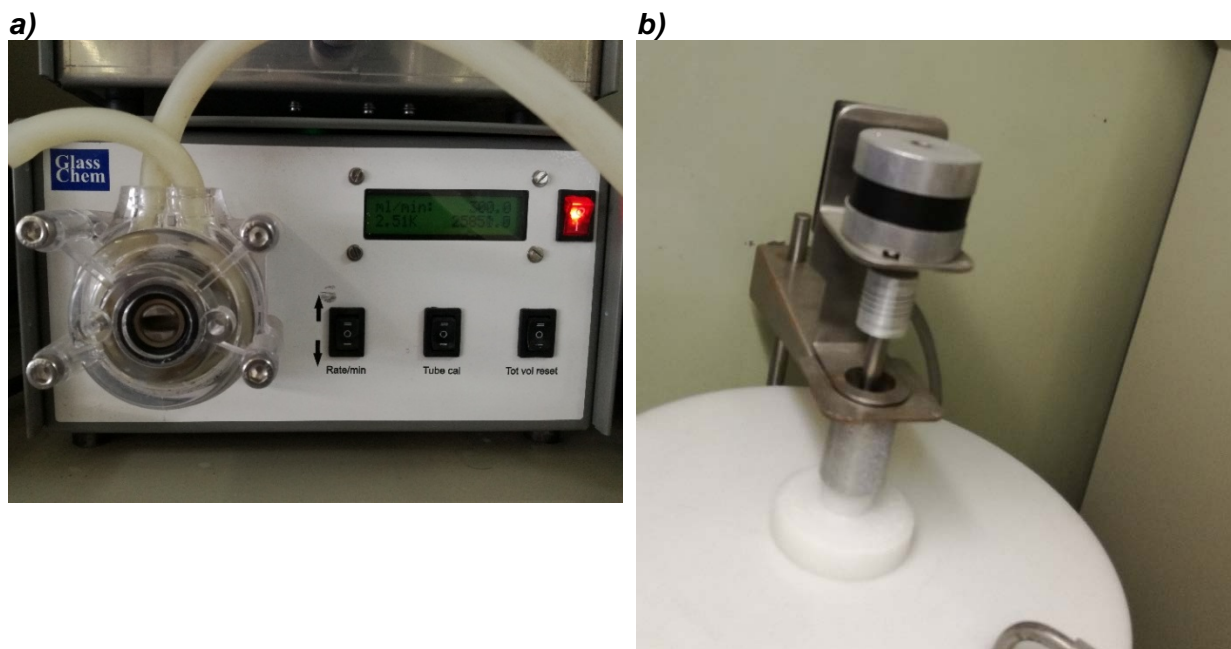
Figure 3.12: a) Peristaltic pump and b) overhead stirrer motor

3.7.1 Determining power-supply for parallel AC-Lamps

The system is built with 4 x 1000 W Halogen Haloline® R7s from Osram (Figure **3.13**) which deliver a total power output of 4000 W. However, depending on the particular experiment the operator/engineer may want to run, there is a 5 kVA variable transformer that allows this power to be reduced. For this study, all the experiments were conducted at 500 W. For safety purposes, the transformer is located outside the photoreactor system. The lamps used in the reactor were spot-welded at both ends to a pure nickel Ni200 wire; the wires were separated by ceramic beads

to prevent short-circuiting, and the lamps were inserted into four 20.0 mm tubes to prevent direct

contact with water.

Figure 3.13: Haloline 1000 w 240 v R7s

The lamp specifications are indicated in Table *3.4*

Table 3.4: Lamp specification

Product	Wattage (W)	Voltage (V)	Luminous flux (lm)	Standard	Diameter (mm)
Haloline 1000 w 240 v R7s	1000	240	22000	R7s	12.0

A schematic diagram of the circuit with four lamps is shown in Figure *3.14*
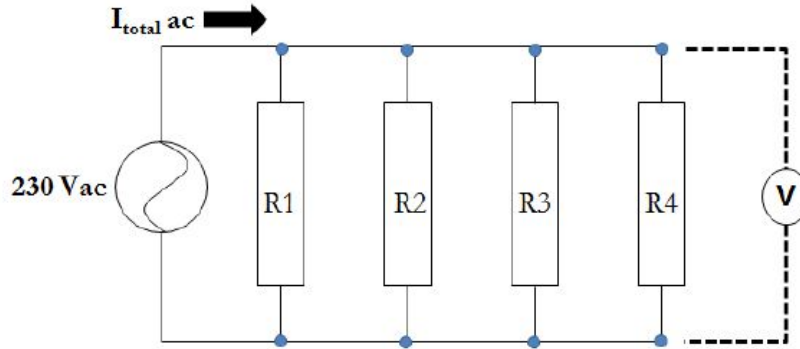
Figure 3.14: Circuit with four lamps shown as equivalent resistive components, together with a voltmeter (V) measuring voltage across the resistors

The circuit details are as follows:

- Supply at socket is 230 VAC (adjustable to suit exact value). 230 VAC is an r.m.s value = 324 V peak as a sinusoidal waveform.

- Each lamp has an equivalent DC electrical resistance calculated according to its electrical power consumption rating. This resistance was used for all calculations to estimate the power supply required.

- Based on the relationship of Power (watts, wattage) *P,* operating voltage (volts) *V,* and the equivalent resistance *R* of the lamp, the amperage (current) flowing in the system can be calculated. This current determines the minimum required power rating of the power supply unit to be used for the system.

  I. Using a 1000 W lamp at 230 Vac, the required resistance of the lamp is:

$$R = V^2/P$$

$$52.9\ \Omega = 230^2/1000$$

II. The total resistance of the *N* lamps in parallel, all with resistance *R* is:

$$\left(\frac{N}{R}\right)^{-1} = \left(\frac{4}{52.9\ \Omega}\right) = 13.2\ \Omega$$

III. Estimated total current drawn by lamps, from $V = IR$:

$$V = IR$$

$$I_{total} = \frac{V}{R}$$

$$I_{total} = \frac{230}{13.2} = \approx 17.5\ A$$

The four lamps as resistive element s therefore draw about 17.5 A as a collective. It was therefore safer to get a power source which could supply this current sufficiently, for instance a 20 A supply with adjustable voltage to change brightness (wattage).

The typical supply unit rating in $Power = VI = (20\ A) \times (230V) = 4600\ VA = 4.6\ kVA$ or higher system, hence the system used is a 5 kVA system.

Figure *3.15* shows the actual 5 kVA transformer that is used to increase and decrease the power of the lamp to the operator's specifications depending on the type of study one would conduct on the system.

Figure 3.15: 5kVA transformer

3.7.2 HAZOP

HAZOP is a prescribed hazard identification and evaluation process designed to identify hazards to process plants, to people, and the environment (Turton et al., 2012). The technique is intended to stimulate, in a methodical way, the imagination of the designers and people who operate the process to pinpoint possible hazard (Brockbank et al., 2013). HAZOP studies assume that a hazard or operating problem may occur when there is a deviation from the design or operating intention (Brockbank et al., 2013). Actions to correct found hazards can then be taken before a real incident occurs (Brockbank et al., 2013). The primary goal and true essence of performing a HAZOP study is to identify, and not to quantify or analyse, the hazards in a particular process (Brockbank et al., 2013). The product of a HAZOP is a list of alarms and recommendations for prevention of problems, not an analysis of the overall effects, occurrence, frequency and the definite solution (Turton et al., 2012). It is most cost-effective when done during plant design as it becomes cheaper to change a design rather than modify an already built plant (Turton et al., 2012).

A HAZOP study was performed on the continuous recirculating batch photoreactor system in order to identify all potential hazards and protect the operator. The HAZOP study shown in Table *3.5* was carried out based on the process fluid (peristaltic) pump and the cooling water pump recirculating the cooling water between the chiller and the reactor.

Table 3.5: Hazard analysis on the continuous recirculating batch photoreactor by HAZOP study

Cooling water pump (Centrifugal)					
Guidewords	**Deviation**	**Causes**	**Consequences**	**Safe-guards**	**Recommendations**
None	No flow	Inlet pipe blockage, airlock	Temperature spike, reactor breakage due to temperature, bulb housing tube breakage	Filter around the inlet pipe, pump should not run dry	Regular pump inspection, bleed pump
Less	Lower flow rate	Partial pipe blockage	Temperature spike, reactor breakage due to temperature, bulb housing tube breakage,	Filter around the inlet pipe	Pressure gauges on the pipe system and regular pressure testing
More	More flow	Variable speed drive failure	Tare reactor sealing gasket, reactor breakage		Inspect all valves before starting the pump
Process pump (peristaltic)					
None	No flow	Blockage from holding tank	No reaction will take place, sampling interval time will be affected	Perfect mixing in the holding tank	Regular tube pump service/ inspection

Less	Less flow	Pump programming malfunctioning	sampling interval time will be affected	Calibrate daily	Check programming frequently
More	More flow	Pump programming malfunctioning	sampling interval time will be affected	Calibrate daily	Check programming frequently

The HAZOP study was straightforward due to few unit operations in the system. The most critical part of the system is the cooling process. The cooling system is crucial due to the fact that it has two potential hazards, which are firstly, temperature spikes which would result in the reactor over-pressurizing and exploding, projecting glass fragments at the operator. Secondly, the flow rate – extremely high flow rates are also a potential hazard due to the fact that the system can only handle pressure to a certain extent. It is therefore very important for the valves to be carefully inspected during start-up and the lights should be switched off first before closing the cooling water during shutdown.

3.8 Continuous process design summary and functionality

The system comprises a 24 L holding tank made of glass. The reason for this is so that the operated an easily monitor settling in a case of stirrer failure. However, the tank is designed with a conical bottom to which the process pump is connected. The reason is that in the event of high particle dosage and a certain range of pH setting, where there might be coagulation and possible settling, the fluid can be pumped from the bottom and the particles transferred to the photoreactor so that they can participate in the reaction. The process pump is a simple peristaltic pump with a maximum speed of 300 mL/min. The flow rate is a direct function of exposure time, so the system will under operate under high flow rates, which makes this pump economic and suitable for its purpose. The reactor is also situated on a magnetic stirrer and a small magnetic stirring bead,

which prevents settling within the reactor. This is also a control variable for the parameter of stirring rate. The stirring rate in the holding tank is not considered as its sole purpose is to prevent settling. There are also aluminum reflective sheets situated on the inside in the center of the reactor and on the outside; these sheets reflect the light back-and-forth through the process fluid to ensure maximum light and to prevent loss of light. The sampling point is situated on the exit line which recirculates the process fluid to the main holding tank, because the fluid concentration needs to be quantified before mixing with the unreacted fluid.

Figure *3.16* shows the general comparison of the continuous system and batch system. These tests were conducted under the same light intensity, pH conditions, were all ran for not less than 5 hours and were of the same initial dye concentration.
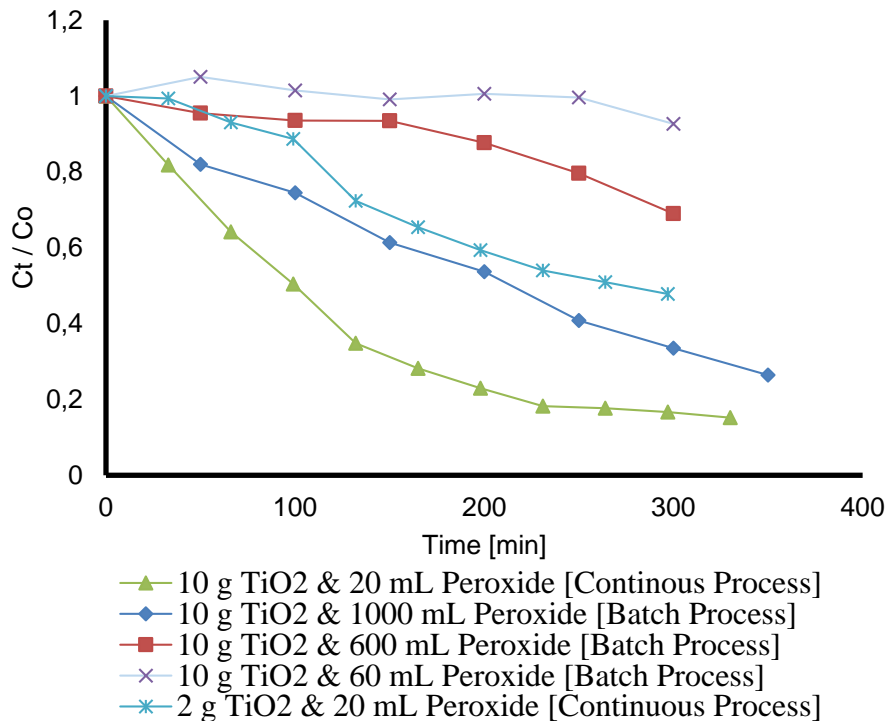
Figure 3.16: Continuous system compared with batch systems, with 5 L reaction solution, 500 W light intensity, pH (4.5-4.8), the pumping rate of 150 mL/Min (for continuous), Starring rate of 1500 rpm, 80 mg/L of MO

To supplement the empirical data shown in Figure *3.16*, it is evident that the batch process performs less efficiently compared to the continuous process. Two runs of 10 g TiO_2 dosage were carried out on a batch process with 60 mL and 600 mL dosage, showing a slight improvement. However, these results are still found to be far less efficient compared to a continuous system, with a dosage of only 2 g of TiO_2 and an H_2O_2 dosage of 20 mL. The H_2O_2 dosage was then pushed to the extremes and 1000 mL was dosed, even though it can be argued that the increase in the total volume due to such high dosage can dilute the initial dye concentration. This system still did not outperform a continuous system of the same TiO_2 dosage and 20 mL of H_2O_2 dosage.

3.9 Conclusion

A list of suitable chemicals was purchased from Sigma-Aldrich and were used without any pre-treatment or modifications. Experimental equipment was provided by the FPRC laboratory facilities and were also described according to models and make. The reactor system was custom designed and constructed as part of this study. The limits to be used in the CCD design were successfully established and presented. This chapter outlined the design considerations that were taken into account during the development of the prototype photoreactor. The proposed continuous system design was based on the short review conducted. Furthermore, another important factor is the type of material used to develop the photoreactor used in this study. Based on transmittance range, the most suitable material of choice was Pyrex glass. A HAZOP study was successfully conducted indicating that the greatest risk was the safe operation of the cooling system. The functionality of the continuous system was evaluated and it was found that one could obtain better results in a continuous system using 2 g of TiO_2 and 60 mL of H_2O_2 than 2g of TiO_2 and 1000 mL H_2O_2 in a 5 L batch reactor system.

Chapter 4 – Pilot runs

4.1 Introduction

This chapter present a series of pilot runs to validate the functionality of the continuous systems and to determine the limits required for the CCD design.

4.2 Preliminary tests on continuous recirculating batch photoreactor

The following section comprises preliminary runs that were conducted using the developed continuous recirculating batch photoreactor. The aim of these experimental runs was to evaluate the percentage degradation and degradation time at low and high values for volume initial dye concentration and to test if the limits that were chosen were going to be appropriate in addressing the objectives of this study. The combinations used were as follows: high volume – low volume, high IDC – low IDC, high H_2O_2 – low H_2O_2 and high TiO_2 – low TiO_2. The results are presented in Table *4.2* for low volumes and Table *4.3* for high volumes as well as in Figure *4.1*.

Table 4.1: Parameters and set limits for the preliminary tests conducted

Parameters	*Operating limits*	
	Low	High
Volume (L)	5	20
Initial dye concentration (mg/L)	5	20
TiO_2 (g)	2	10
H_2O_2 (mL)	20	200

Table 4.2: Low volume experiments

	Run 1	**Run 2**	**Run 3**	**Run 4**	**Run 5**	**Run 6**	**Run 7**	**Run 8**
Volume (L)	5	5	5	5	5	5	5	5
Initial dye concentration (mg/L)	5	20	5	20	5	20	5	20
TiO_2 (g)	2	2	10	10	10	10	2	2
H_2O_2 (mL)	20	20	200	200	20	20	200	200
Time (min)	200	200	200	200	264	297	264	297
% Deg	67	57	85	85	85	78	87	68
Δ IDC (Low - High)	10%		0%		7%		19%	

Table 4.3: High volume experiments

	Run 1	**Run 2**	**Run 3**	**Run 4**	**Run 5**	**Run 6**	**Run 7**	**Run 8**
Volume (L)	20	20	20	20	20	20	20	20
Initial dye concentration (mg/L)	5	20	5	20	5	20	5	20
TiO_2 (g)	2	2	10	10	10	10	2	2
H_2O_2 (mL)	20	20	200	200	20	20	200	200
Time (min)	400	400	400	400	400	400	400	400
% Degradation	24	21	59	18	32	24	39	25
Δ IDC (Low - High)	3%		41%		8%		14%	

The preliminary runs showed that volume has the highest impact compared to the other parameters as it is evident that lower volumes are easier to degrade than higher volumes at the same amount of catalyst and oxidizer concentration. The results presented in Table *4.2* and Table *4.3* show that for low volumes the percentage degradation ranged between 57% and 87%, while for high volumes it ranged between 21% and 59% and required almost double the treatment time. For low volumes the optimum percentage degradation was 87% for a 5 mg/L initial dye concentration, with 2 g TiO_2, 200 mL H_2O_2 and 264 minutes treatment time. For high volumes the optimum % degradation was 59% for 5 mg/L initial dye concentration, with 2 g TiO_2, 200 mL H_2O_2 and 264 minutes treatment time.

The initial dye concentration was found to be easier to treat when set on low levels, for both low and high volumes as one can anticipate. For low volumes the change between % degradation when the initial dye concentration was increased from 5 mg/L to 20 mg/L, it was found to be around 10%, excluding for runs 3 and 4, which showed no change, while the high volumes showed no correlations in the % degradation difference. It is important to note that the increase in the initial dye concentration had no impact on runs 3 and 4 (for low volumes) while the same increase showed a change of 41% for high volumes. This implies that an interaction between the initial dye concentration and volume could be anticipated as significant in the final model.

For low, volumes high TiO_2 dosages ranged between 78% and 85%, while lower TiO_2 yielded between 57% and 87%. On the other hand, TiO_2 dosage for high volumes showed a similar impact and ranged between 18% and 59% when set to 10 g and between 21% and 39% when set to 2 g.

The dosage of H_2O_2 dosage showed interesting results as it was the only parameter that proved to potentially challenge or diminish the effect of volume. The highest degradation that was achieved for high volumes before the H_2O_2 dosage was increased was 24%, and the increase of H_2O_2 improved the degradation to 59% which is an improvement of about 60%.

These results therefore offered a strong indication that some interesting parameter interactions could be discovered and that the developed reactor system could successfully assist in investigating the interaction of these parameters, and in learning about the scale-up dynamics.
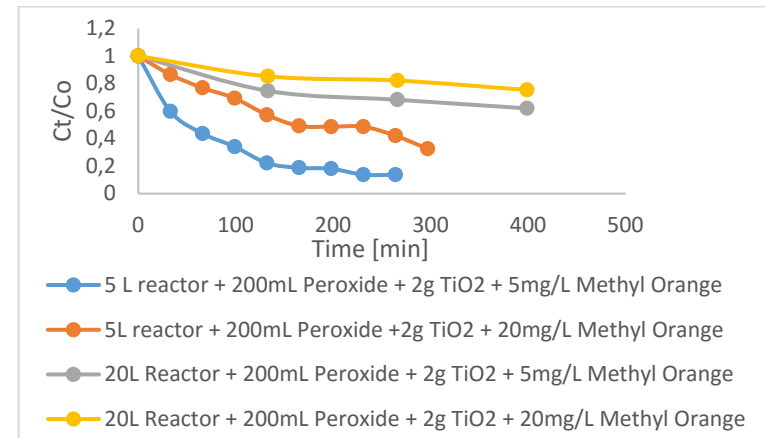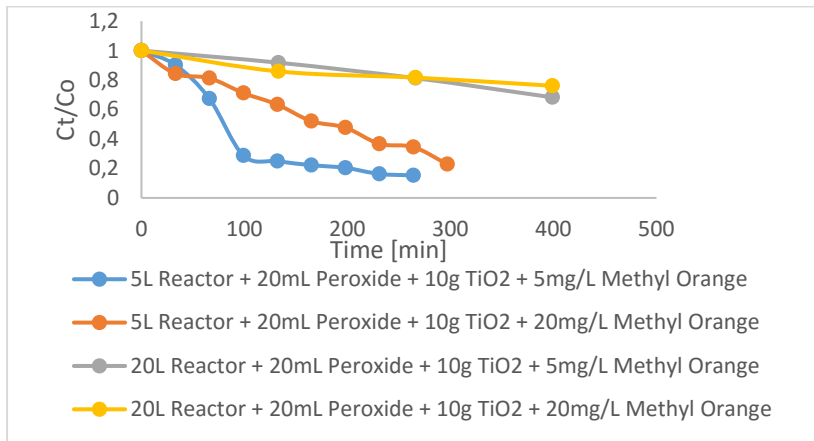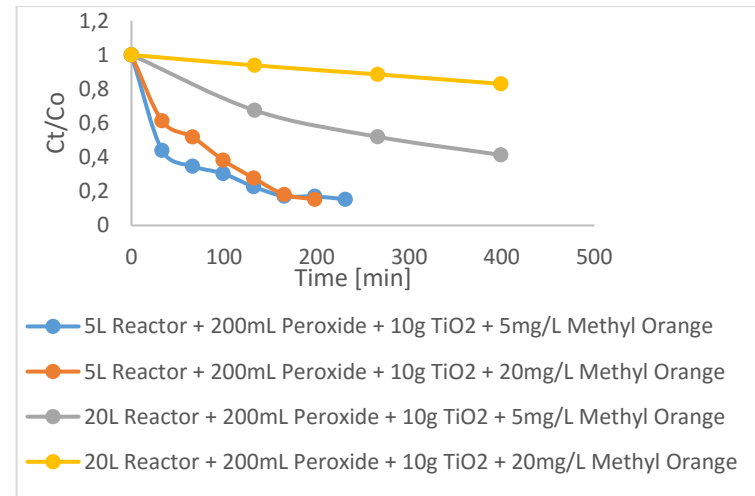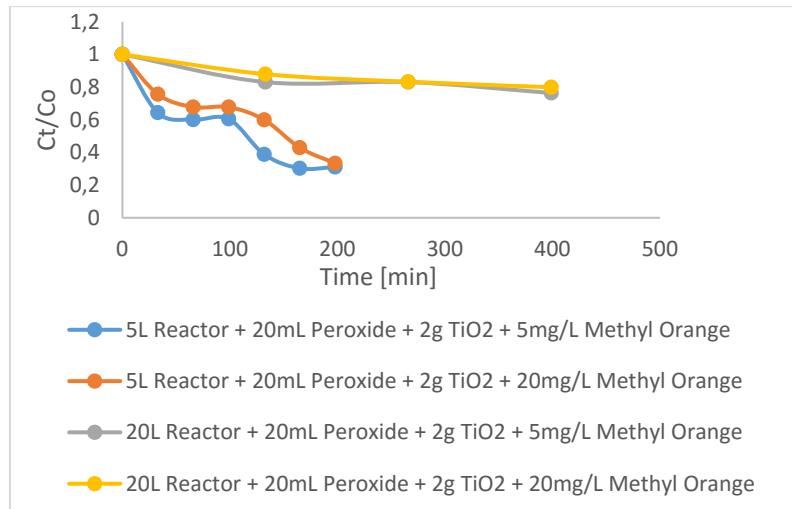
Figure 4.1: Preliminary runs performed on the continuous system, with experimental matrices of; Volume (5 – 20L), TiO_2 (2 – 10g), H_2O_2 (20 – 200mL) and IDC (5 – 20mg/L, 500 W light intensity, pH (4.5-4.8), pumping rate of 150 mL/Min (for continuous), starring rate of 1500 rpm

These results showed interesting trends regarding the effect of volume and initial dye concentration, and showed that interesting parameter interactions may exist that can only be understood by conducting a factorial trial. The developed reactor system can successfully assist in investigating these parameter interaction that is essential for understanding scale-up dynamics.

4.3 Conclusion

The results for preliminary experiments were presented. It was found that the volume had the highest impact on the treatment time. Lower dye concentrations were found to be easier to treat. H_2O_2 dosage showed interesting data as it was found that the impact of volume can be potentially diminished by the increase in H_2O_2 dosage. The preliminary tests suggested that there could be potential interaction between volume and H_2O_2. The runs were also obtained without any technical faults which also gave confidence that the continuous system was well commissioned and confirmed further suitability to conduct the study.

Chapter 5 – Effect of operating parameters on the resulting percentage degradation (%deg) and reaction rate constant (k) and scale-up dynamics

5.1 Introduction

In this chapter, the effect of initial dye concentration (IDC), TiO_2 dosage, H_2O_2 dosage and the bulk volume of the reacting model dye MO will be evaluated and discussed with respect to their resulting effects on %deg and k as obtained from the CCD experimental method.

The topics will be presented in the following order:

- Experimental responses

- Analysis of variance (ANOVA) for response %deg

- Analysis of variance (ANOVA) for response k_Freeman-Tukey

- Effect of Individual operating parameters on %deg

    - Effect of bulk volume

    - Effect of TiO_2 dosage

- Effect of operating parameter interaction on %deg

- Effect of individual operating parameters on k_ Freeman-Tukey

- Effect of operating parameter interaction on k_ Freeman-Tukey

- Optimisation and confirmation experiment

- Model validation

5.2 Experimental responses and transformations

The experimental runs that were designed through the CCD were conducted and the responses were measured and recorded with their respective runs, as are presented in Table *5.1*, the detailed time-concentration curves are provided in *Appendix 1: Time-concentration curves raw data*.

With regard to the reaction rate constant k, recorded responses were found to range from 0.0002 to 0.016, which means the max to min response ratio is equal to 80. Design-Expert® recommends that a response ratio greater than 10 requires a transformation. Due to the fact that all the responses of k were all less than 1, all the transformations found by Design-Expert® were invalid. The square root transformation recommended for $X \leq 2$ by Freeman and Tukey, (1950), known as a Freeman-Tukey transformation, is expressed as follows (Zar, 2010):

$$y = \sqrt{x} + \sqrt{x + 1}$$

Equation 5.1

The response k was therefore transformed externally on Microsoft Excel and then imported back to Design-Expert® before analysis. This means that all analysis was carried out through the transformed response which then was reverted to the true response through the following expression:

$$x = \frac{y^2 + y^{-2} - 2}{4}$$

Equation 5.2

Table 5.1: CCD variables and responses

	Actual parameters				R2		R1 (Transformed)
Run	Volume X_1	TiO$_2$ X_2	H$_2$O$_2$ X_3	IDC X_4	k	% Deg	k_Freeman-Tukey
	L	g	mL	mg/L	min^{-1}	%	
1	12.5	12	110	12.5	0.0059	89.27	1.0798
2	12.5	6	110	12.5	0.0028	61.74	1.0543
3	20	2	200	20	0.0012	24.6	1.0352
4	5	2	200	5	0.0107	86.37	1.1088
5	12.5	6	110	12.5	0.0034	62.85	1.0600
6	5	10	200	5	0.0160	84.69	1.1344
7	12.5	6	110	12.5	0.0022	32.76	1.0480
8	12.5	6	110	12.5	0.0011	57.44	1.0337
9	12.5	6	0	12.5	0.0011	37.99	1.0337
10	5	2	20	5	0.0050	55.46	1.0732
11	12.5	6	245	12.5	0.0016	57.71	1.0410
12	20	2	200	5	0.0021	72.53	1.0469
13	1.25	6	110	12.5	0.0081	85.1	1.0940
14	12.5	6	110	12.5	0.0028	65.48	1.0543
15	23.75	6	110	12.5	0.0016	48.92	1.0408
16	5	10	20	20	0.0046	77.11	1.0701
17	5	10	20	5	0.0011	84.66	1.0343
18	5	2	20	20	0.0059	66.76	1.0798
19	12.5	0	110	12.5	0.0006	15.29	1.0248
20	5	2	200	20	0.0042	64.51	1.0669
21	20	10	20	5	0.0010	31.72	1.0321
22	5	10	200	20	0.0094	84.72	1.1017
23	12.5	6	110	1.25	0.0035	61.6	1.0609

24	20	10	200	5	0.0022	58.64	1.0480
25	20	2	20	20	0.0005	20.08	1.0226
26	20	2	20	5	0.0006	23.6	1.0248
27	12.5	6	110	12.5	0.0014	35.81	1.0381
28	20	10	20	20	0.0007	23.29	1.0268
29	12.5	6	110	23.75	0.0017	19.91	1.0421
30	20	10	200	20	0.0002	17.02	1.0142

5.3 Analysis of variance

Equation **5.3** and Equation **5.5** are the final model equations which were obtained through analysis of variance (ANOVA) using a backward-stepwise model with a criterion set to a p-value and an alpha value of 0.1 (Cornell, 1990). Alternatively, the models were determined by studying the Fisher's F-test (parameters and interaction terms) and values of probability greater than F for the main model. A small probability value indicates that the model is significant ($p < 0.0001$)(Toh, 2007). Both these methods yielded similar models for both responses. The goodness of fit of the model was validated by a high R^2 coefficient. The model F-values were found to be 13.07 and 10.67 for k and %deg respectively. This implies that there is only a 0.01% chance that an F-value this large could occur due to noise.

An adequate precision greater than 4 implies that the models can be used to navigate the design space. The adequate precision obtained in this was 12. The Predicted R^2 of 0.61 was found to be in agreement with the Adjusted R^2 of 0.71, where the difference was observed to be less than 0.2. The lack-of-fit F-value was found to be 2.53. This implies that the lack of fit is not significant relative to pure error. Detailed statistical data on this section can be found in *Appendix 2: % degradation raw data*

Table 5.2: ANOVA for response k_Freeman-Tukey reduced quadratic model

Source	Sum of square	df	Mean square	F-value	P-value (Prob > F)	Remark
Model	0.018	6	0.00302	13.07	<0.0001	Significant
A	0.012	1	0.012	52.37	<0.0001	Significant
C	0.002	1	0.00201	8.69	0.0072	Significant
D	0.0006	1	0.00063	2.72	0.1130	Significant
AC	0.00085	1	0.00085	3.66	0.0684	Significant
CD	0.0015	1	0.005	6.48	0.0180	Significant
A^2	0.0011	1	0.00105	4.53	0.0442	Significant
Residual	0.0053	23	0.000231			
Lack of fit	0.005	18	0.000266	2.53	0.1539	Not Significant
Pure error		5	0.000105			
Cor	0.023	29				
R-squared = 0.77; Adjusted R-squared = 0.71; Predicted R-squared = 0.61; Adequate Precision = 12.74						

Analysis of variance for the % degradation response is presented in Table **5.3**. The results found for k and %deg were similar apart from the (**AC**) term that was found to be insignificant in this response. The term CD was found to be the common significant term for both responses.

Table 5.3: ANOVA for response (% degradation) reduced quadratic model

Source	Sum of squares	df	mean square	F-value	P-value (Prob > F)	Remark
Model	11779.3	5	2355.87	10.67	<0.0001	Significant
A	7308.45	1	7308.45	33.10	<0.0001	Significant
B	1231.82	1	1231.82	5.58	0.0266	Significant
C	955.38	1	955.82	4.33	0.0483	Significant
D	1617.85	1	1617.85	7.33	0.0123	Significant
CD	665.38	1	665.38	3.01	0.0954	Significant
Residual	5298.8	24	220.78			
Lack-of-fit		19	223.44	1.06	0.5239	Not significant
Pure error		5	210.68			
Cor total	17078.12	29				
R-squared = 0.69; Adjusted R-squared = 0.63; Predicted R-squared = 0.52; Adequate Precision = 12.74						

In both scenarios, the number of parameters is equal to that of the degrees of freedom which means that both models are solvable. Furthermore, Figure *5.1* (a) and (b) shows the externally studentized residuals against the normal % probability for the degradation of MO, and it is evident that the acquired data consistently follows a straight line trend. This demonstrates that there are no outliers or dispersed points for k and % degradation respectively. Figure *5.1* (c) and (d) depicts the residual plots which show the difference between the predicted data and the experimental data. This data is in agreement with the obtained R^2-values of 0.77 and 0.69 for k and % degradation respectively and further proves the significance of the model. This data interpretation is similar to that of Liu and Chiou (2005), for the study of the degradation of reactive 239 by UV/TiO$_2$. Detailed statistical data on this section can be found in *Appendix 3: k_Freeman-Tukey raw data*

a)
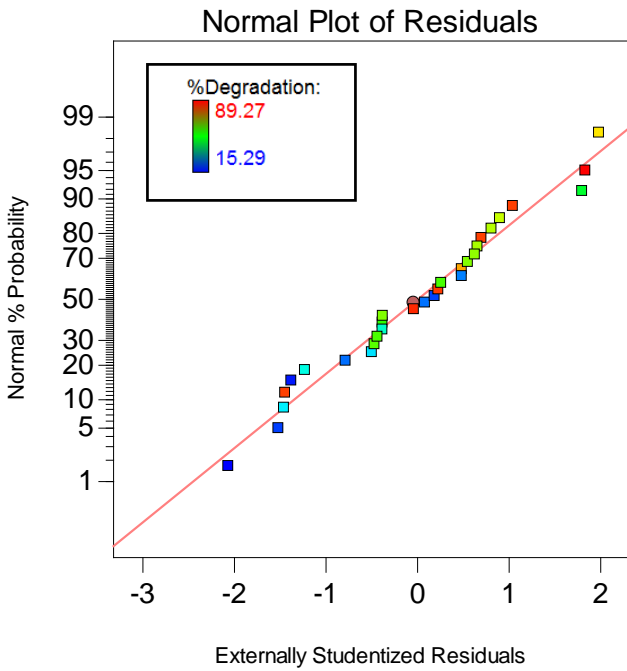
b)
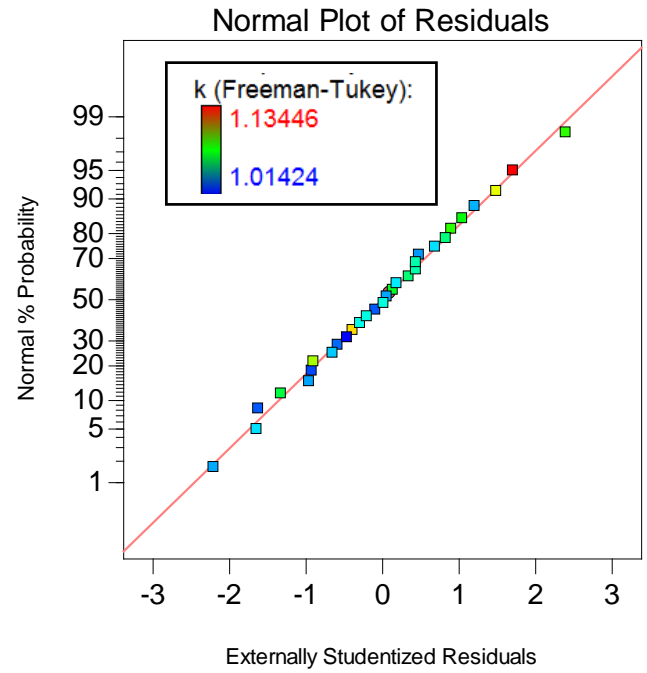
c)
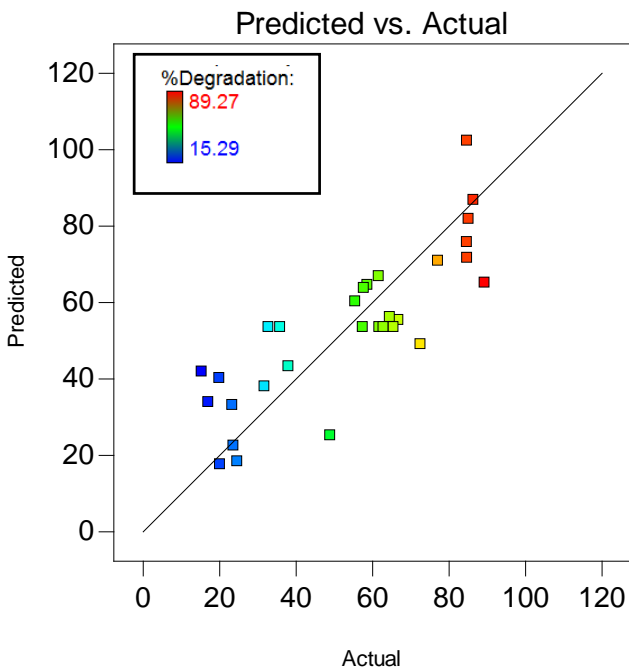
d)
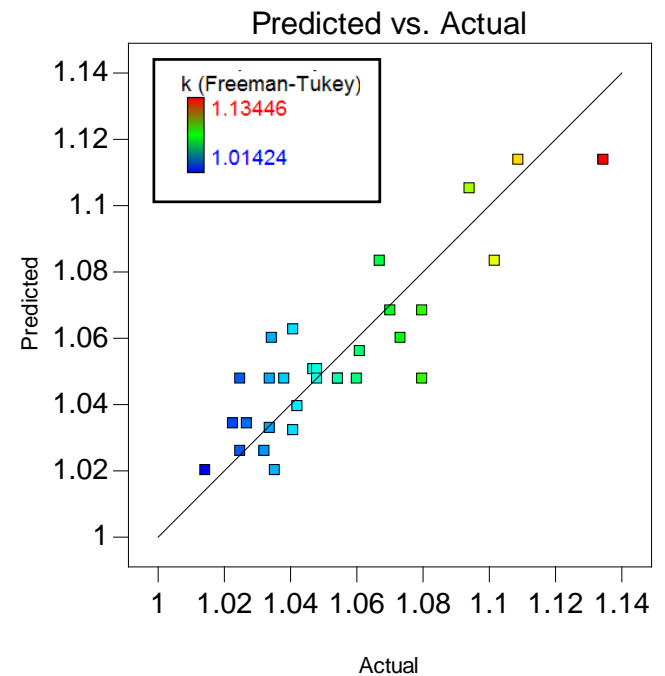
Figure 5.1: a) and b) Externally studentized residuals vs normal % probability; c) and d) Actual vs predicted responses for k and % deg respectively

5.4 Models obtained for MO degradation

According to RSM based on CCD, an experiential mutual correlation between the independent variables (4-factors) and the dependent variables (k and %deg) involved in the degradation of MO by photocatalysis was obtained using a Stat-Ease® (Design-Expert® V. 10.0.7), which can be expressed in their actual form by the following first-order and second-order polynomial coded and uncoded equations for k and %deg respectively:

Uncoded $Y_{(\% \, deg)} = 66.75 - 2.52A + 1.94B + 0.19C - 0.133D - 0.00955CD$ Equation 5.3

Coded $\%Degradation = 53.59 - 18.88 * A + 7.75 * B + 6.83 * C -$ Equation 5.4

$8.88D - 6.45 * CD$

Where;

Variable	Name	Unit
A	Volume	L
B	TiO$_2$	g
C	H$_2$O$_2$	mL
D	Initial dye concentration	mg/L

In Equation **5.3** the uncoded equation represents the actual equation that can be used to estimate the parameters, while Equation **5.4** the coded equation represents the relative ratios of the parameters amongst each other.

Uncoded $Y_{(k,Freeman-Tukey)} = 1.08 - 6.19 \times 10^{-3}A + 0.0042B + 4.24 \times$ Equation 5.5

$10^{-4}C + 8.40 \times 10^{-4}D - 1.08 \times 10^{-4}AC - 1.43 \times 10^{-5}CD +$

$1.65 \times 10^{-4}A^2$

Coded $k(Freeman - Tukey) = 1.05 - 0.24 * A + 1.05 \times 10^{-3}B + 9.9 \times$ Equation 5.6

$10^{-3} * C - 5.53 \times 10^{-3}D - 7.27 \times 10^{-3} * AC - 9.68 \times 10^{-3} * CD +$

$9.30 \times 10^3 * A^2$

5.5 Effect of volume on % degradation

The volume parameter **A** showed a Prob>F value less than 0.0001, which make this individual parameter the most significant parameter in Equation **5.3**. Figure **5.2** (a) and (b) show the % degradation as a function of volume with (a) TiO_2 set on 2 g, H_2O_2 set on 20 mL and IDC set on 5 mg/L and (b) TiO_2 set on 10 g, H_2O_2 set on 20 mL, and IDC set on 5 mg/L. The results showed that the % degradation will always decrease with the increase in volume. However, the magnitude of this decrease in % degradation is dependent on the amount of oxidizer or catalyst. For example, in Figure **5.2** (a) and (b) the increase in the TiO_2 parameter **B** improves the % degradation from a change of 60% to 25% to a change of 80% to 40% across the volume range of 5 L to 20 L. This adjustment also indicates that parameters **A** and **B** are independent of one another

a)

b)
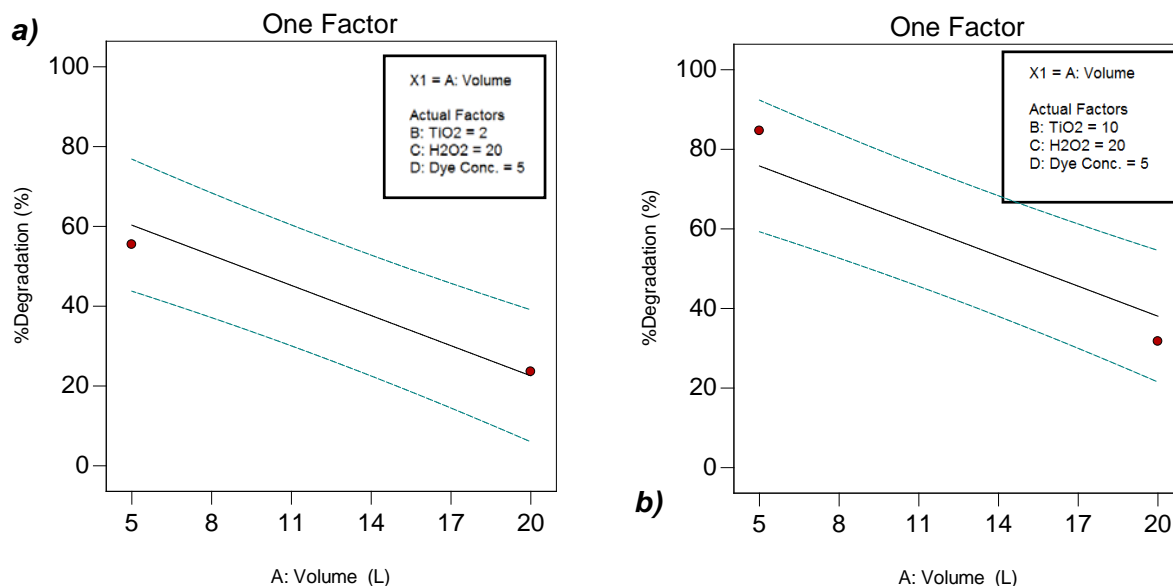
Figure 5.2: Volume parameter, a) TiO_2 set at 2 g, IDC set at 5 mg/L, H_2O_2 set at 20 mL, and b) TiO_2 set at 10 g, IDC set at 5 mg/L and H_2O_2 set at 20 mL

Figure **5.3**. (a) and (b) show the % degradation as a function of volume with (a) TiO_2 set on 10 g, H_2O_2 set on 200 mL, and IDC set on 5 mg/L; and (b) TiO_2 set on 10 g, H_2O_2 set on 200 mL, and IDC set on 20 mg/L. The adjustment made from Figure **5.2** (b) to Figure **5.3** (a) is that the H_2O_2 dosage (parameter **C**) was adjusted from 20 mL to 200 mL, which evidently improved the % degradation from a change of 80% to 40% to a change of 100% to 60% across the volume range. Similarly to the TiO_2 increase, the increase in H_2O_2 and volume were shown to be independent. The H_2O_2 effect was diminished by the increase of IDC as seen in Figure **5.3** (b), where the % degradation decreased from a change of 100% to 60% to a change of 70% to 30%.
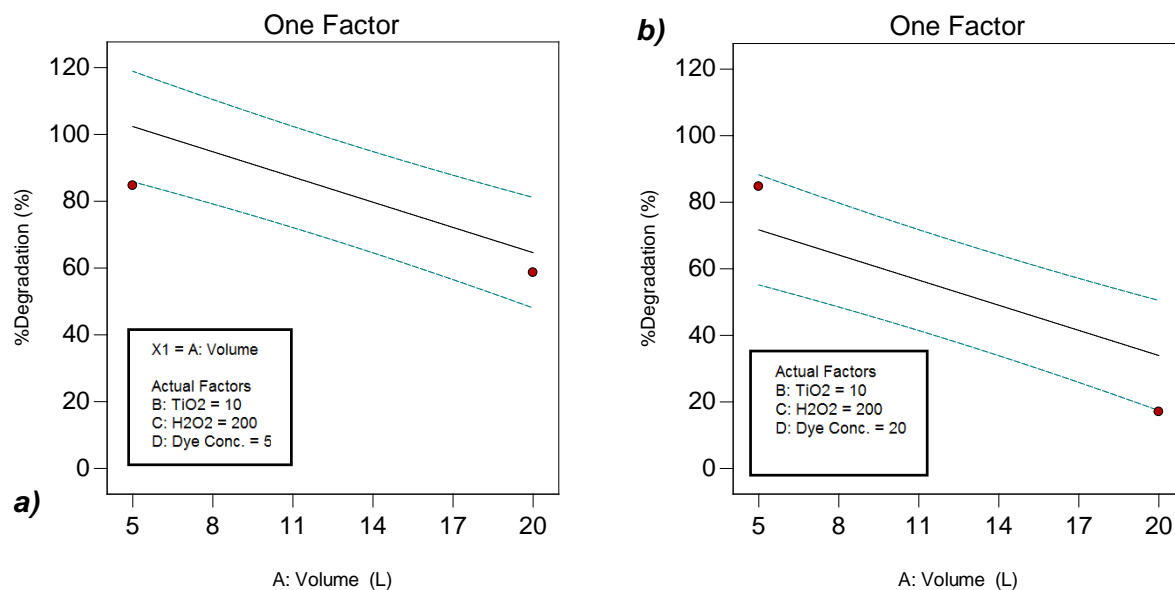
Figure 5.3: Volume parameter, a) TiO_2 set at 10 g, IDC set at 5 mg/L and H_2O_2 set at 200 mL, and b) TiO_2 set at 10 g, IDC set at 20 mg/L and H_2O_2 set at 200 mL

Previous studies have neglected the investigation of the parameter volume, which is a critical parameter to consider for scale-up. Several authors (Liu & Chiou, 2005; Cho & Zoh, 2007; Bahadir & Rauf, 2008; Thind et al., 2017; and Soltani et al., 2014) have conducted RSM studies and considered parameters such as initial pH, stirring rate, catalyst concentration, oxidant concentration and light intensity, some of which were considered in this study. However, none of them reported on the dynamics of the volume parameter. During a scale-up from Photo-CREC water II to Photo-CREC water solar simulator, Pelayo (2014) reported that there was a photocatalytic efficiency decrease of approximately 44% due the increase in volume and this is the same impact that is observed in the volume parameter in the current study.

5.6 Effect of TiO$_2$ dosage on the % degradation

The TiO$_2$ parameter was found to have a Prob>F of 0.0266 which was below 0.05 and must be included in the model Equation **5.3**. In the order of parameter significance, it can be said that the TiO$_2$ parameter is the least significant parameter. The TiO$_2$ parameter was anticipated to be significant based on the fact that a photocatalyst has a critical role on photocatalysis, and the higher the dosage of TiO$_2$, the more active sites there will be for the reaction to occur (Linsebigler et al., 1995). However, when TiO$_2$ is in excess it causes a shading effect and can negatively affect the reaction (Rajamanickam & Shanthi, 2016). Chowdhury et al. (2015) also reported that photocatalytic efficienciess decrease as as the TiO$_2$ is increased, based on experiments that were conducted in a 100 mL glass beaker.

Figure **5.5** shows the % degradation as a function of TiO$_2$ with (a) Volume set at 5 L, H$_2$O$_2$ set at 20 mL, and IDC set at 5 mg/L; (b) Volume set at 20 L, H$_2$O$_2$ set at 20 mL, and IDC set at 5 mg/L; (c) Volume set at 20 L, H$_2$O$_2$ set at 200 mL and IDC set at 5 mg/L; (d) Volume set at 20 L, H$_2$O$_2$ set at 200 mL, and IDC set at 20 mg/L.

It can be observed that the % degradation will increase with the increase in TiO$_2$ dosage. This behaviour confirms literature that states that the % degradation is dependent on the number of active sites available on the system (Bignozzi & Alexander, 2011). Figure **5.4** (a) and (b) shows a positive gradient for % degradation as a function of TiO$_2$. The % degradation change decreases from a change of 60% to 70% for low volumes to a change of 20% to 30% for high volume across the TiO$_2$ ranges from 2 g to 10 g. It is also evident that increasing H$_2$O$_2$ improves this decrease from a change of 20% to 30% to a change of 50% to 60% across the TiO$_2$ range. It is also important to note that the only thing that changes is the % degradation and not the gradient, which implies that there is no Interaction between the volume and TiO$_2$. Further, increasing the IDC will also have a negative impact in this regard, also leaving the % degradation at a change of 20% to

30%. The 40% photocatalytic efficiency drop that was encountered due to the increase of volume in Pelayo (2014) was reported to have decreased by 30% when the catalyst was increased from 40 mg/L to 120 mg/L, which is also in agreement with the TiO_2 effect that was found in this work.
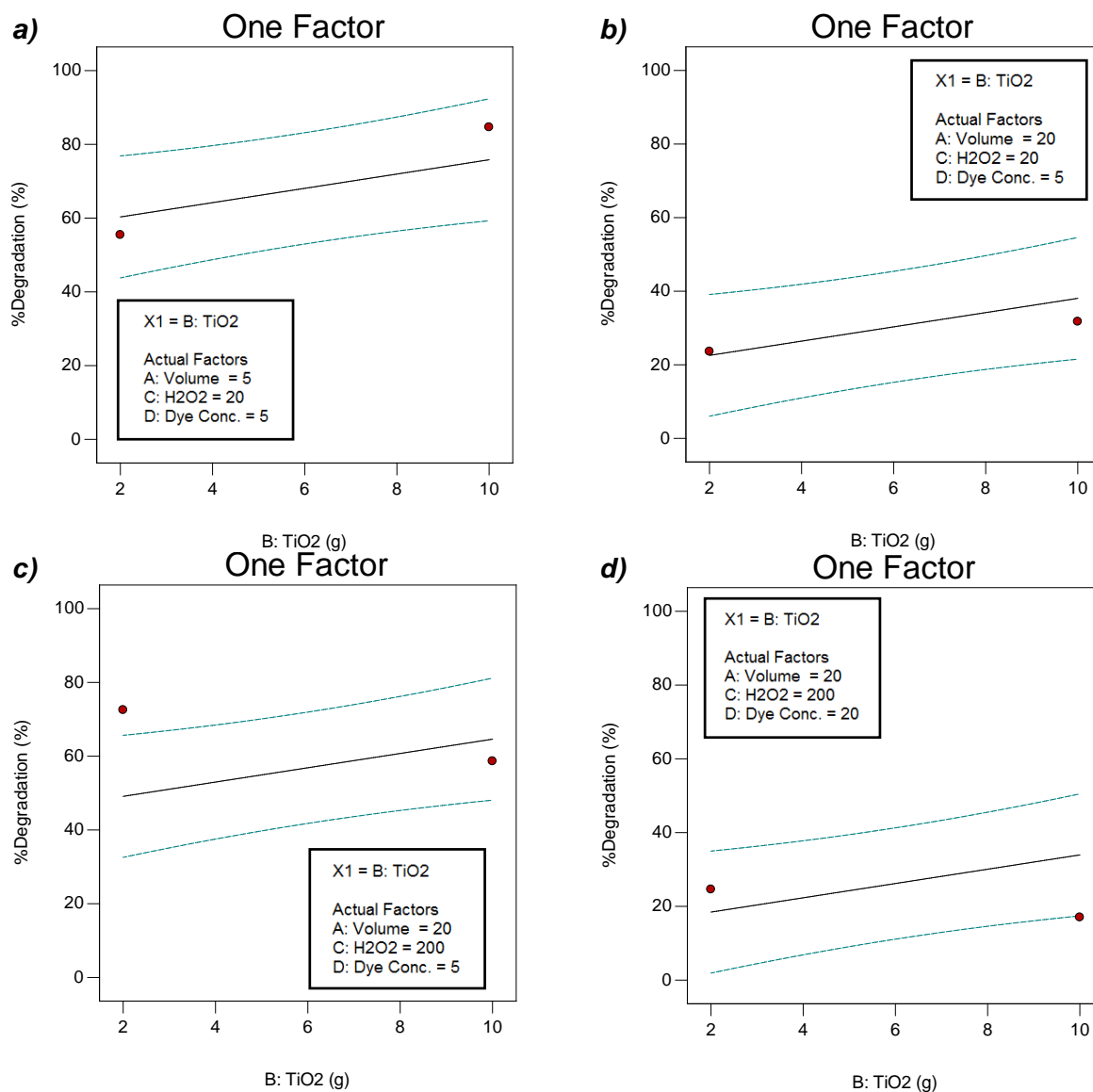
Figure 5.4: TiO_2 parameter effect on % degradation, a) volume set at 5 L, IDC set at 5 mg/L and H_2O_2 set at 20 mL, b) volume set at 20 L, IDC set at 5 mg/L and H_2O_2 set at 20 mL, c) volume set at 20 L, IDC set at 5 mg/L and H_2O_2 set at 200 mL and d) volume set at 20 L, IDC set at 20 mg/L and H_2O_2 set at 200 mL

5.7 Effect of the interaction between IDC and H_2O_2 dosage on the % degradation

The interaction between IDC and H_2O_2 dosage was shown to be significant during the analysis of variance (ANOVA). The model selection was carried out automatically using forward, backward and stepwise model selection, having an alpha value set to 0.1 and criterion set to p-values. The IDC and H_2O_2 dosage (**CD**) interaction term was found to have a P-value (Prob>F) of 0.0123. Stat-Ease® (Design-Expert® V. 10.0.7) recommends that where Prob>F less than 0.05, it suggests that the model terms are significant.

Figure **5.5** shows the contour lines in terms of percentage degraded. On the x-axis is the H_2O_2 dosage in millilitres and on the y-axis is the initial dye concentration in mg/L. The parameter settings for TiO_2 and volume are 2 g and 5 L respectively.

The results indicate that when the volume is set at 5 L and TiO_2 at 2 g, the % degradation will increase with an increase in H_2O_2 and decrease with increase in IDC, as shown in Figure **5.5**. A % degradation of more than 80% can be achieved for IDC set at a range of between 5 to 8 mg/L and a H_2O_2 dosage limit of 155 mL to 200 mL. Figure **5.5** also shows that the % degradation range visible under the set conditions ranges from 56% to 80%. Furthermore, when the volume is increased to 20 L the obtainable degradation range is 19 to 45%, as shown in Figure **5.6**; the interaction of the **CD** parameter remains inversely proportional even under these conditions, as it was for 5 L and 2 g set values of Volume and TiO_2 respectively. Further, adjusting the TiO_2 to 10 g yields a % degradation range from 34 to 59%, as one can see in Figure **5.7**. This interaction was anticipated, based on the outcomes that were obtained and discussed in the preliminary tests, and due to the fact that, as Pierre (2013) states, the amount of OH• radicals will increase with an increase in H_2O_2 dosage as they are formed though reduction of H_2O_2. Chowdhury et al. (2015), in a study of the photocatalytic activities of ultra-small β-FeOOH and TiO_2 heterojunction

structure under simulated solar irradiation, also proved empirically that the increase in H_2O_2 dosage will be effective until a plateau is reached. Chowdhury et al. (2015) in the same study reported that the increase in the IDC decreases the degradation efficiency.
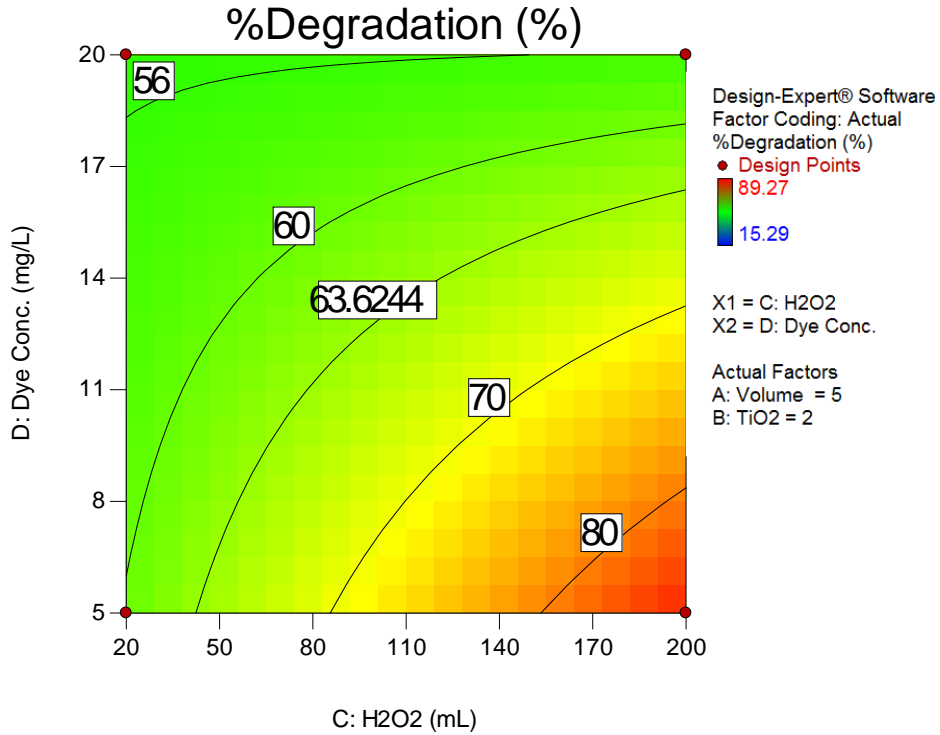
Figure 5.5: IDC and H_2O_2 interaction on % degradation with Volume and TiO_2 set at 5 L and 2 g respectively
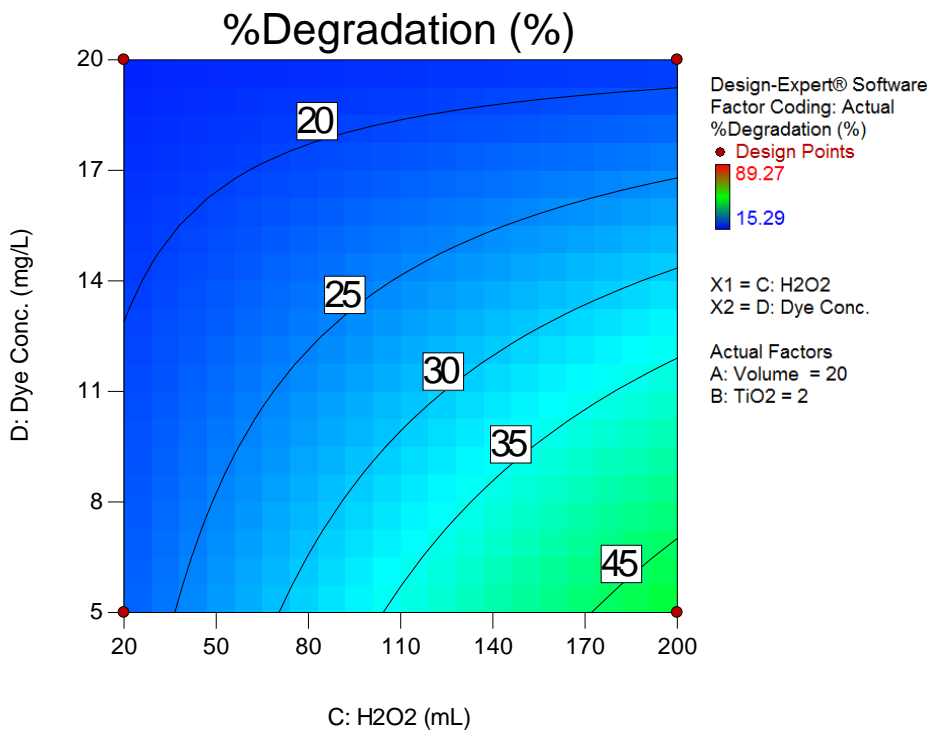
Figure 5.6: IDC and H_2O_2 interaction on the % degradation with volume and TiO_2 set at 20 L and 2 g respectively
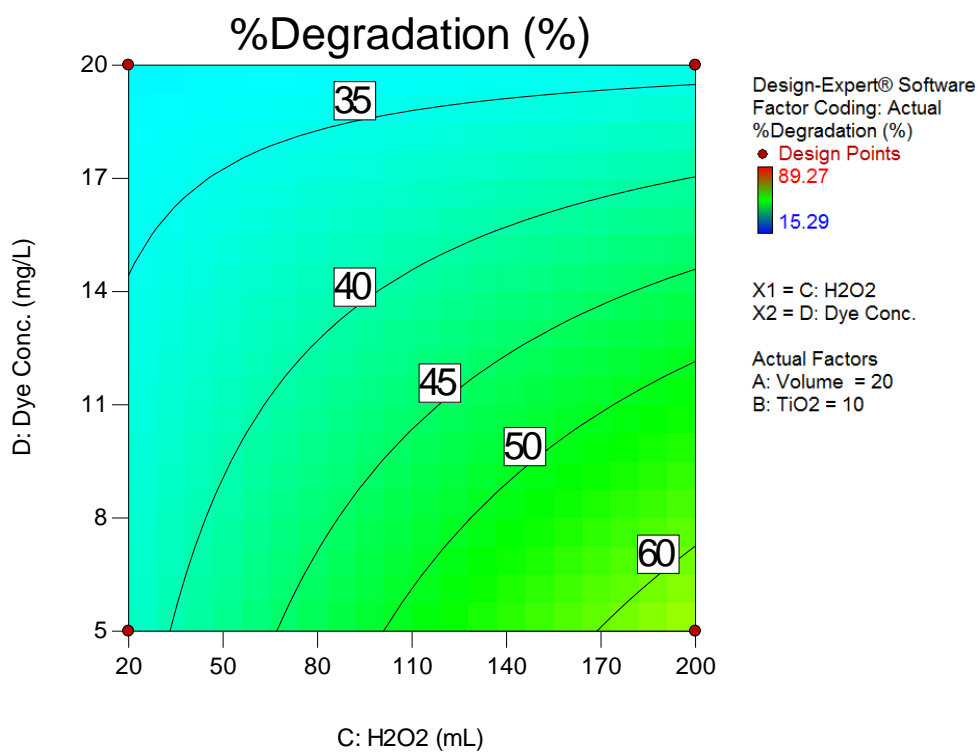
Figure 5.7: CD interaction on the % degradation with volume and TiO_2 set at 20 L and 10 g respectively

5.8 Effect of TiO₂ on k_Freeman-Tukey

The TiO_2 parameter, **B**, was the only model term that was forced into the model. This means that even though it showed a P-value higher than 0.05, the term had to be included and analysed as it was one of the major parameters in this study. Design-Expert® allows the user to eliminate (error) or include (force) a term into the model even if the term may have been statistically included or excluded due to the relative percentage contribution in to the main response.

Figure **5.8** (a) and (b) shows k_Freeman-Tukey as a function of volume with (a) volume set on 5 L, H_2O_2 set on 20 mL, and IDC set on 5 mg/L; and (b) volume set on 20 L, H_2O_2 set on 20 mL, and IDC set on 5 mg/L.

a)   *b)*
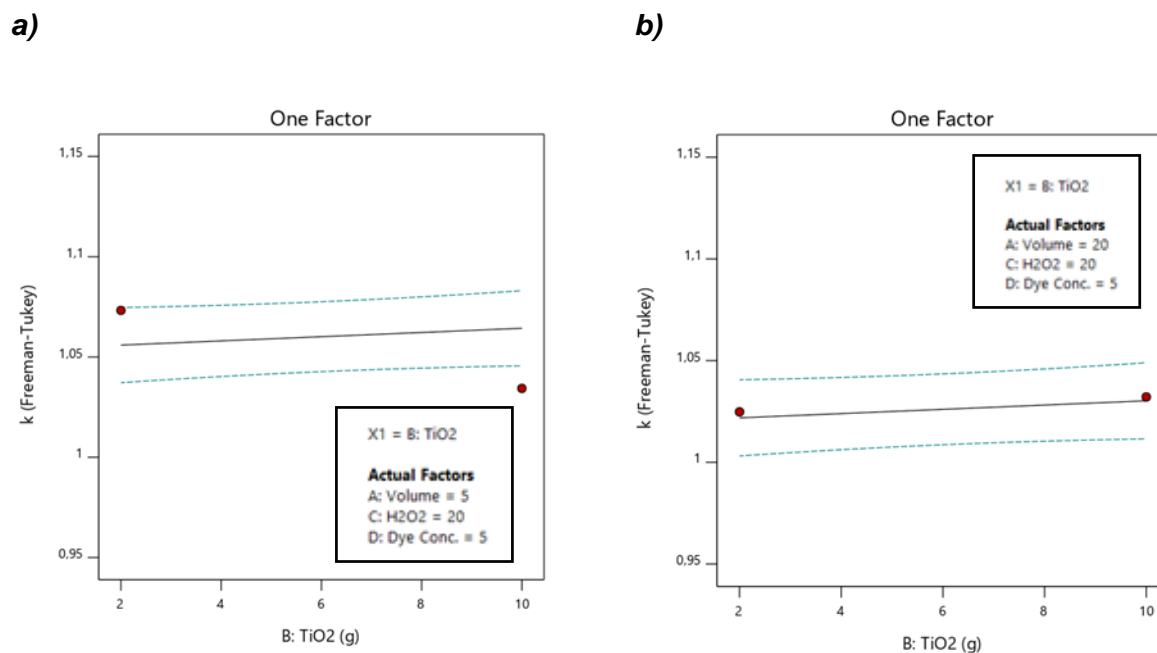
Figure 5.8: TiO_2 as a function of k_Freeman-Tukey, a) volume set on 5 L, H_2O_2 set on 20 mL and IDC set on 5 mg/L b) volume set on 20 L, H_2O_2 set on 20 mL and IDC set on 5 mg/L

Figure **5.8** a) and b) shows an increase in volume from 5 L to 20 L while keeping IDC and H_2O_2 constant at 5 mg/L and 20 mL respectively. The main observation is that an increase in TiO_2 will improve the reaction rate constant. The adjustment of volume in Figure **5.8** shows that that an increase in volume will decrease the reaction rate constant. The drop that brought about this change decreased the reaction rate constant from a change of 1.055 to 1.064 to a change of 1.021 to 1.032. Furthermore, when H_2O_2 is increased from 20 mL to 200 mL it improves the volume impact, as can be seen in Figure 5.8 b) and figure 5.9 a); this adjustment improves the k_Freeman-Tukey from a change of 1.021 to 1.032 to a change of 1.046 to 1.054.

a)   *b)*
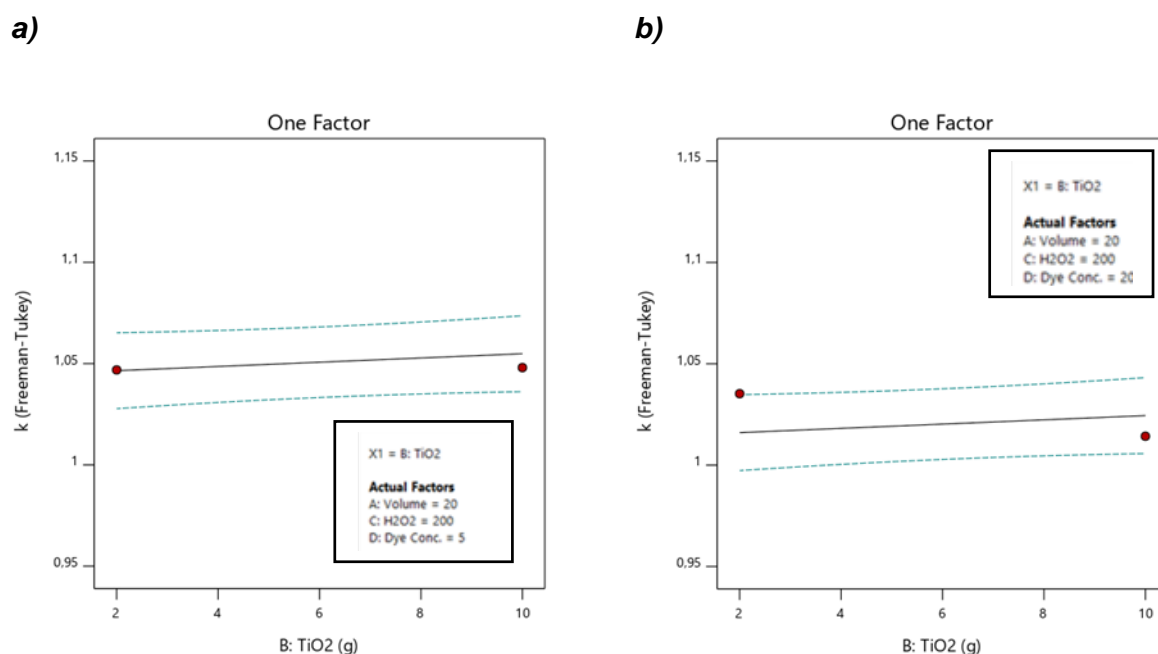
Figure 5.9: TiO_2 as a function of k_Freeman-Tukey, a) volume set on 20 L, H_2O_2 set on 200 mL and IDC set on 5 mg/L b) volume set on 20 L, H_2O_2 set on 200 mL and IDC set on 20 mg/L

Adjusting the IDC from 5 mg/L to 20 mg/L introduced a negative effect which decreased the reaction rate constant from a change of 1.046 to 1.054 to a change of 1.016 to 1.024.

As expected, the increase in TiO_2 was found to increase the reaction rate constant under all adjustments. The increase in the mass of TiO_2 was at all times found to have a positive slope. This is in agreement with literature that states that the increase in catalyst mass will result in an increase in the number of active sites available in the system, although each and every volume has a limiting value (Chen & Ray, 1998).

5.9 Effect of interaction term between Volume and H_2O_2 (AC) on k_ Freeman-Tukey

The interaction between volume and H_2O_2 was shown to be significant, with a Prob>F value of 0.0684. The significant terms in the model were selected automatically using a backward, forward and stepwise model selection method. Through this method, Equation *5.5* was obtained, while a similar model resulted when a manual model selection was obtained. Therefore the model is of high confidence as it was selected through using two different methods. It is important to note that *AC* as an interaction is beyond the recommended Prob>F value of 0.05 as it is reported to be 0.0684; however, the model was hierarchically selected and the individual parameters *A* and *C* were found to be significant with Prob>F values of 0.0001 and 0.0072 respectively.

Figure *5.10* shows the contour lines for the percentage degradation as a function of H_2O_2 and volume. The parameter settings in this case are 2 g and 5 mg/L for TiO_2 and IDC respectively.

Observation on the behavior of the *AC* parameter is that the k_Freeman-Tukey constant rapidly increases with an increase in volume, when the parameters are set to; TiO_2 set at 2 g and IDC set at 5 mg/L. Under these conditions, a high FreemanTukey constant is obtained at 5 L and 200 mL of H_2O_2, while this behavior changes as the volume is adjusted to 20 L and also drops significantly when H_2O_2 is reduced to 20 mL. It can be observed in Figure *5.10* that the contour

lines representing the k_Freeman–Tukey constant bend towards opposite directions on the high levels of the *A* and *C* parameters, and are found to be straight in the center. This highlights the fact that the effects become nonlinear towards maximum parameters. The results found in Figure *5.10* and Figure *5.11* appear to be duplicates, even though the TiO_2 parameter has been changed from 2 g to 10 g, which implies that the TiO_2, *B*, parameter is effect is low in this interaction term.
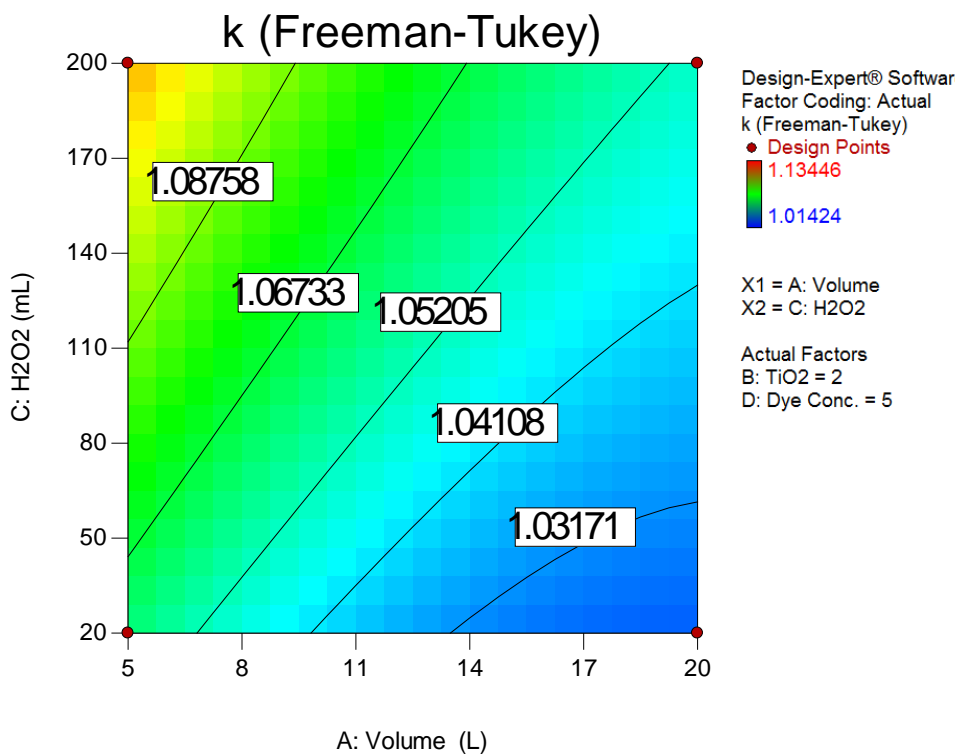
Figure 5.10: Volume and H_2O_2 parameter effect on k_freeman-Tukey constant, with IDC set at 5 mg/L and TiO_2 set at 2 g
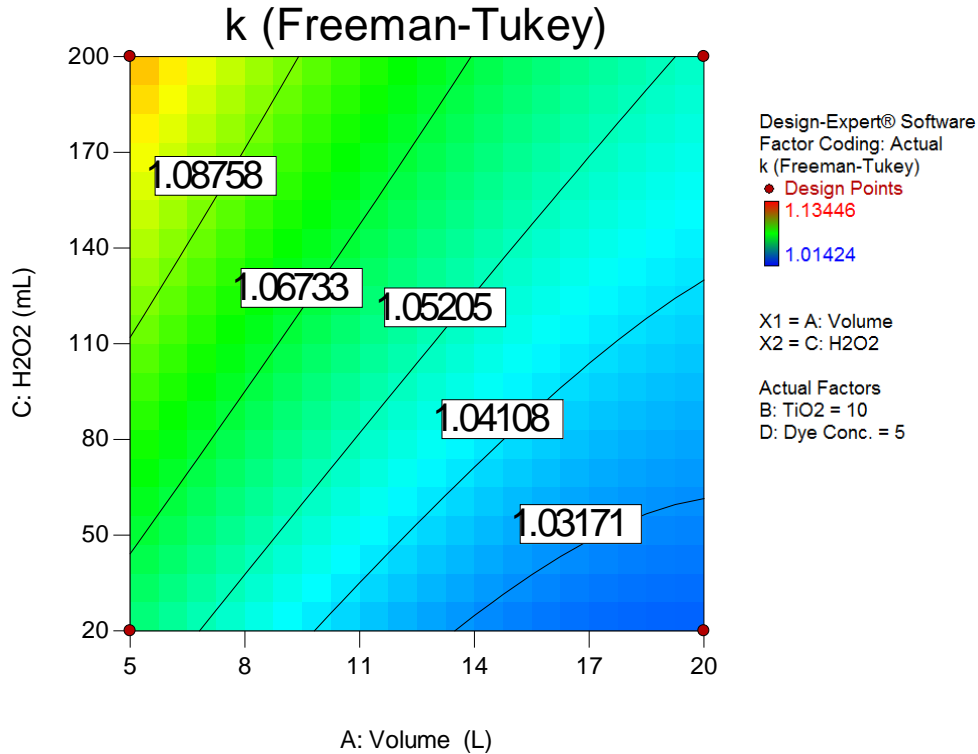
Figure 5.11: Volume and H_2O_2 parameter effect on k_Freeman-Tukey constant, with IDC set at 5 mg/L and TiO_2 set at 10 g

When the IDC term is increased from 5 mg/L to 20 mg/L the kinetic behavior changes. It was found that the H_2O_2 dosage required begins to decrease beyond volumes higher than 16 L while the H_2O_2 required increases with the increase in volume in the region between 5 L and 8 L. It is also evident that a k_Freeman-Tukey constant of 1.0291 can be obtained by a H_2O_2 dosage of 90 mL to 200 mL for volumes higher than 16 L and this relationship is nonlinear as shown in Figure *5.12*. Volumes between 5 L and 8 L can be treated in a linear relationship by a H_2O_2 dosage ranging from 20 mL to 200mL for a resulting k_Freeman-Tukey of 1.0673. Above 14 L the response becomes non-linear.
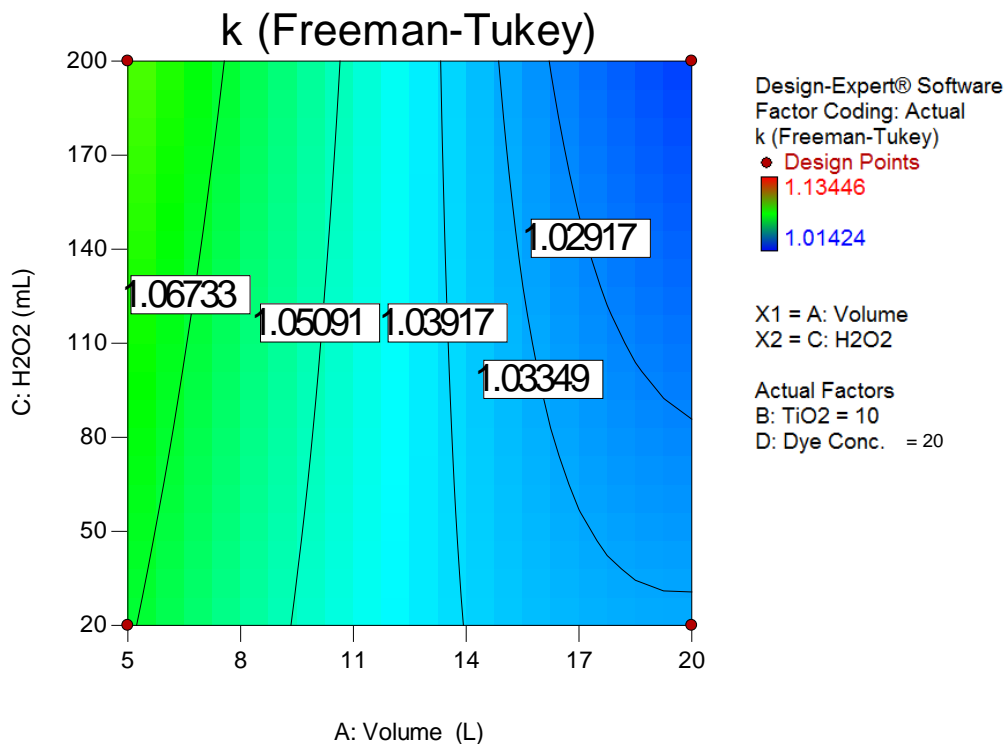
Figure 5.12: Volume and H_2O_2 parameter effect on k_Freeman-Tukey constant, with IDC set at 20 mg/L and TiO_2 set at 10

It can be anticipated that the reaction rates will improve with the increase in H_2O_2 dosage due to the fact that the addition of H_2O_2 inhibits the electron-hole recombination by acting as an alternative electron acceptor to oxygen, this can also be due to the fact that H_2O_2 can split photocatalytically to produce a hydroxyl radial directly (Daneshvar et al., 2003).

5.10 Effect of interaction term between H_2O_2 and IDC (CD) on the k, Freeman-Tukey

The interaction between H_2O_2 and IDC was shown to be the most significant interaction term, in the order of significance as it was reported to have a Prob>F value of 0.0180. As opposed to the **AC** term which was included on hierarchical bases, the **CD** term is significant directly as it is found to be well below the recommended p-value (0.05). The **CD** interaction also appears to be the only pair that is a common significant pair among the studied responses.

Figure **5.13** and Figure **5.14** present the contour lines for the k_Freeman-Tukey as a function of H_2O_2 and initial dye concentration, with TiO_2 and volume being the variable parameters.

In this interaction term, H_2O_2 also appeared to be having an essential role, as it is observed in Figure **5.13** that the highest k_Freeman-Tukey constant is obtained at the higher H_2O_2 level (200 mL). The relationship that was observed at volume of 5 L and TiO_2 of 2 g was a nonlinear relationship across as opposed to the **AC** interaction which showed linearity at low volumes and nonlinearity at high volumes. Figure **5.13** showed that H_2O_2 dosages above 170 mL to 200 mL can deliver a k_Freeman-Tukey of 1.103 when the IDC was set anywhere below 10 mg/L. The obtainable k_Freeman-Tukey increased as the H_2O_2 dosage increased. When the volume was increased from 5 L to 20 L the kinetic behavior changed towards a lower region of k-Freeman-Tukey and was nonlinear as shown in Figure **5.14**. The surface response behavior shown in Figure **5.14** could be assumed to be showing that a plateau level has been reached interms of kinetic behavior. This can be justified by the quenching effect that sets in when H_2O_2 becomes in excess as reported by (Behnajady et al., 2007). The explanation of the decrease in reaction rate as the initial dye concentration increase was due to the fact that the more organic substances there in the system, there more the organic substances would be absorbed onto the surface of the catalyst and therefore the generation of OH• will reduce, causing the catalyst to provide fewer

active sites. Further, the high dye concentrations also act as an obstruction to photons and the absorption of photons by catalyst decreased which consequently affected the reaction rate (Behnajady et al., 2007).

The individual effects of A^2, A, C and D will not be dealt with independently as their influences are already depicted in the interaction terms AC and DC.
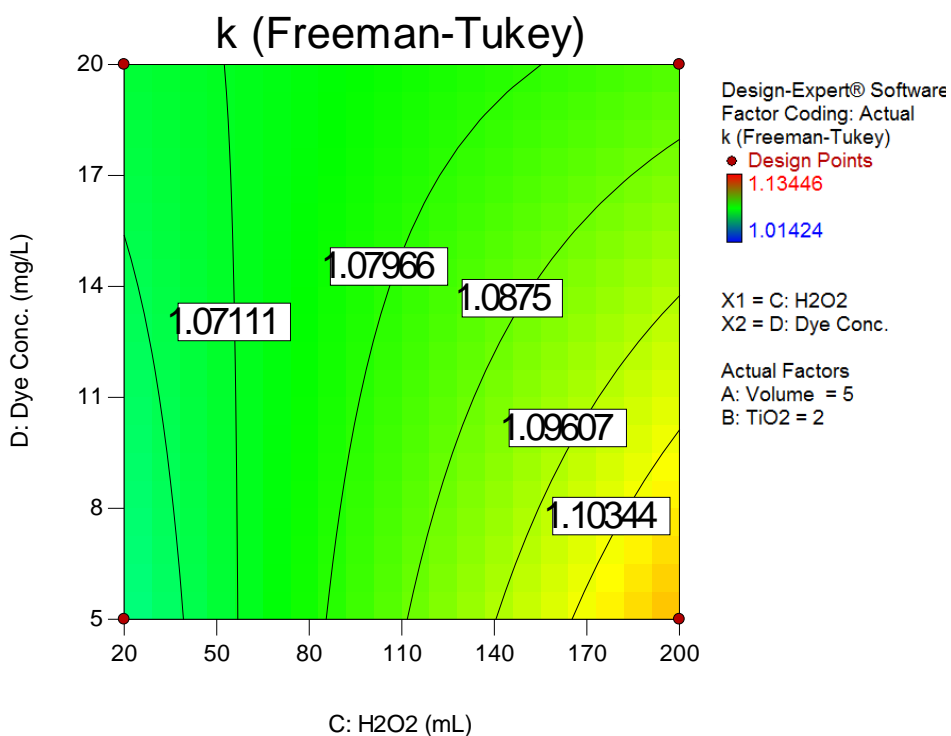
Figure 5.13: H_2O_2 and IDC interaction parameter effect on k_Freeman-Tukey constant, with volume set at 5 L and TiO_2 set at 2 g
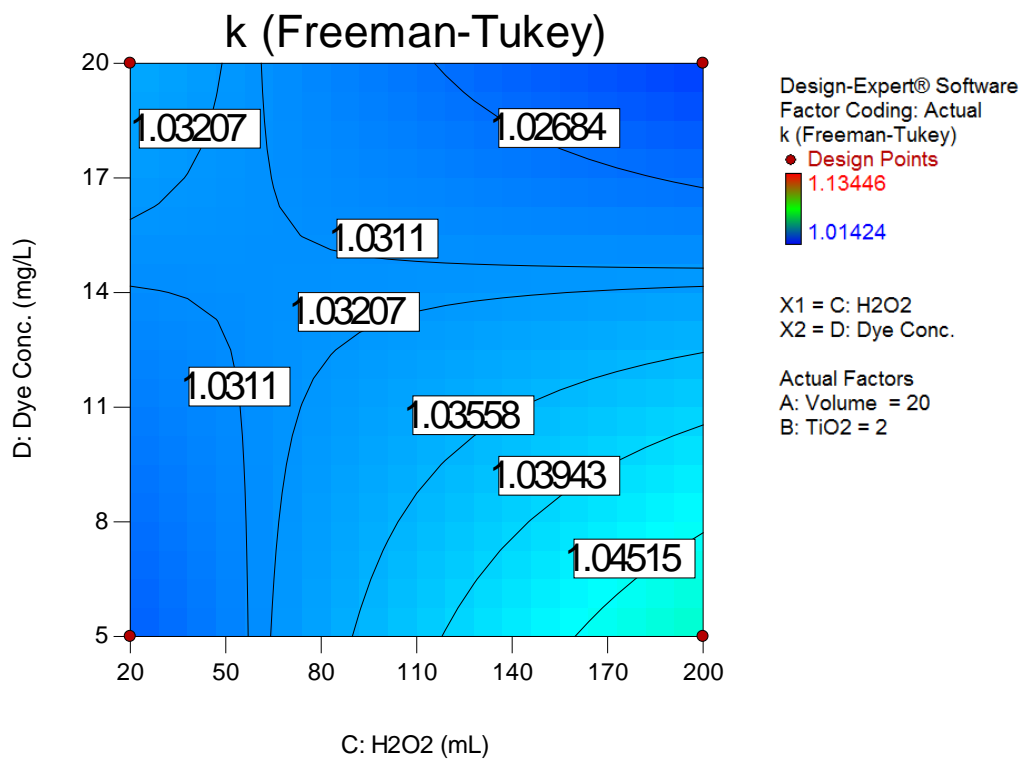
Figure 5.14: H_2O_2 and IDC interaction parameter effect on k_Freeman-Tukey constant, with volume set at 5 L and TiO_2 set at 2 g

5.11 Optimisation and validation of MO degradation Model

This section entails the optimisation of the volume term and the responces using the internal optimisation features of Dx 10, subsequnet to that an external validation of the model was conducted using the solver tool from Microsoft Excel. Under the optimisation node the software allows the user to optimise the parameter of the choice by either selecting maximise, minimise or keep in range. In this case the volume term and the responses were set to maximise and the IDC, H_2O_2 and TiO_2 were kept in range. The software then provides numerous solutions (97 solutions were obtained in this case) according to the optimisation crateria and based on the desirability ratio (≤ 1) the optimum solution can be selected. The desirability should be as close to 1 as possible.

Table 5.4: Optimisation solutions

Solution	Volume (L)	TiO_2 (g)	H_2O_2 (mL)	IDC (mg/L)	Desirability ratio
1	20	10	200	5	0.66
2	19.99	9.96	199.9	5	0.66
3	19.75	9.99	200	5	0.66
4	19.99	9.98	199.3	5	0.66
97	18.06	9.97	24.08	19.18	0.43

Table *5.4* shows solution 1 to 4 and solution 97, solutions 5 to 96 have not been shown in this table, this also table shows that the desirabiltiy values of solutions 1 to 4 are the same.The desirabilty decreases as the solutions go high ending at the desirability of 0.43 of solution 97. In this case solution 1 was the selected solution based on the fact that the suggested parameters were easy to measure in the lab, even though they did not differ much numerically.

The % degradation found in this solution was 64.6% and the k_Freeman-Tukey was 1.0507, which would be 0.0022 min^{-1} when reverted to the actual reaction rate constant through Equation **5.2**. These results would be achieved by a volume of 20 L; TiO$_2$ dosage of 10 g; H$_2$O$_2$ dosage of 200 mL and an initial dye concentration of 5 mg/L. These optimum operating conditions were run in the laboratory 3 times and the mean was taken into account, the mean of these conditions yielded a degradation percentage of 67.07% and a k_Freeman-Tukey of 1.0452 and that is 0.0020 in terms of actual reaction rate constant. This can be confirmed on the confirmation report as seen in Table **5.5**:

Table 5.5: A confirmation report as obtained from DX 10

Response	Mean	Median1	Std Dev	n	SE Pred	95% PI Low	Data Mean	95% PI High
	Predicted	Predicted						
k	0.0024	0.0024				0.0009	0.0042	0.0059
% Degradation	64.62	64.62	14.86	3	11.74	40.39	67.07	88.85
k_Freeman-Tukey	1.0507	1.0507	0.0152	3	0.012	1.03	1.0666	1.08

The mean of the confirmation experiment showed 67.07% degradation and 1.06 k_Freeman-Tukey which is better than what the model suggested, this indicates that the model is accurate and suitable, this is also confirmed by the fact that the data mean lies between the values of 95% PI low and 95% PI high as seen in Table **5.5**. Subsequant to the optimization and a succesful confirmation experiment a model validation was carried our externally using the solver tool from Microsoft Excel. The model was further validated by running tests in the laboratory under varied conditions within constraints of the model and compare it with the predicted results for a degradation percentage of 80% and 50%. The corresponding parameters **B**, **C**, and **D** were

guessed by iteration and recorded next to their corresponding parameter **A** as shown Table **5.6** and Table **5.7**. The parameters that were predicted by iteration were then used to determine the response % degradation (model) and it was expected to guess 80% and 50% depending on the set yield. The same conditions were tested practically in the laboratory to determine % degradation (experimental) and further plotted as shown in Figure **5.15** and Figure **5.16**. It can be observed from Figure **5.15** and Figure **5.16** that the model validation was successful.

Table 5.6: Raw data for 80% degradation model validation

Y	80%					
A	B	C	D			
Volume(L)	TiO_2(g)	H_2O_2(mL)	IDC(mg/L)	Δ	% degradation (model)	% degradation (experimental)
5	5	122	5	-1.3E-05	80.53	80
7.5	5.4	157	5	0	79.99	82
10	6	193	5	6.3E-06	79.97	80
12.5	9	200	5	0	80.49	80
20	10	200	5	-16.465	63.53	60
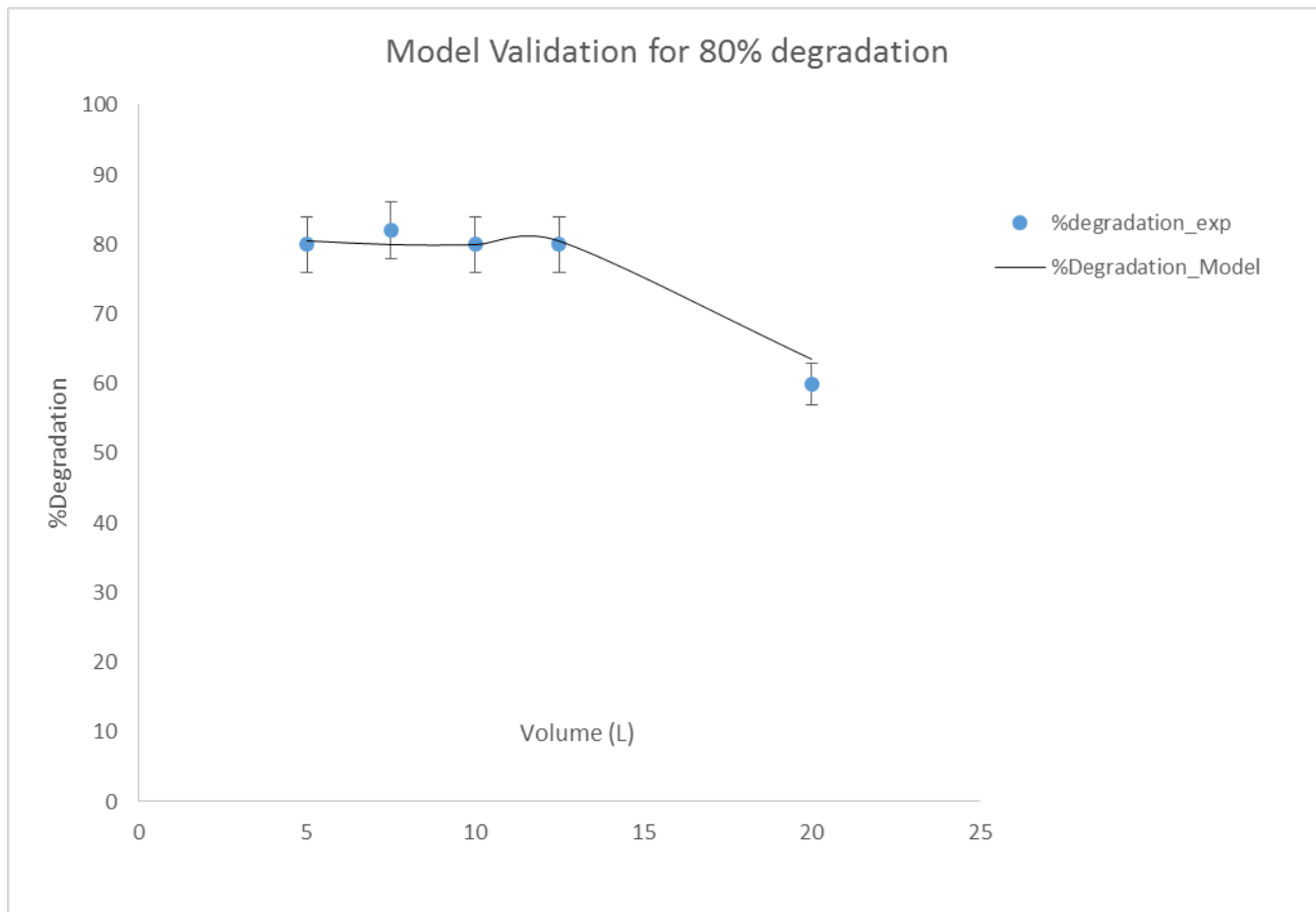
Figure 5.15: Model validation for 80% degradation

Table 5.7: Raw data for 50% degradation model validation

Y					50%	
A	B	C	D			
Volume (L)	TiO$_2$(g)	H$_2$O$_2$(mL)	IDC(mg/L)	Δ	% degradation (model)	% degradation (experimental)
5	2	200	20	5	57.17	57
7.5	2	199	19	2.90E-08	52.80	53
10	2	200	16	0	52.34	52
12.5	2	200	13	6.30E-06	51.87	52
20	3	200	5	1.89E-05	50.45	50
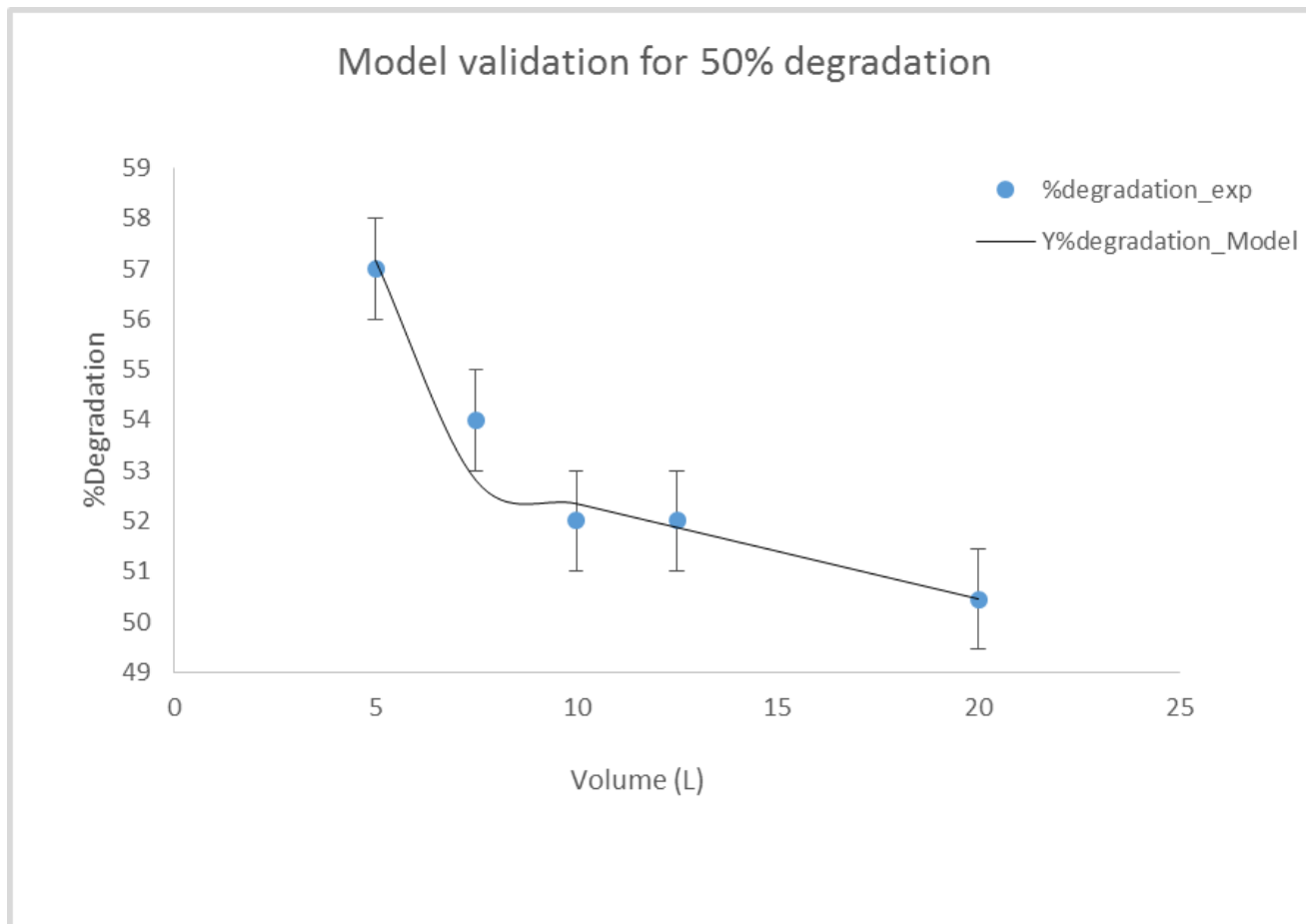
Figure 5.16: Model validation for 50% degradation

Table *5.6* and Table *5.7* show the raw data of the model validation. The iterated values of IDC for

the 80% validation are in agreement with the findings in this study, namely that the lower the IDC,

the higher the % degradation. It can also be noted that the lower volumes were recorded to have

a high yield in terms of % degradation.

5.12 Conclusion

The statistical experimentation method eliminates the limitations of classical empirical factor-by-factor methods, and in this study has been proved to be a powerful tool for investigating interaction terms and optimisation of the degradation of MO by UV/TiO_2 in a CRBPR system. The high correspondence of the model showed that a first-order polynomial and a second-order polynomial model for % degradation and reaction rate constant could be successfully used to optimise and investigate interaction terms. The results predicted by the model (64.6%) were in good agreement with the experimental data (67.07%), which confirms the reliability of the methodology used. Furthermore, the results showed a common most influential term for both responses, namely **CD** (H_2O_2, initial dye concentration). The results also showed that the individual factor **B** (TiO_2) had a significant impact on the % degradation, while it had no influence at all on the reaction rate constant. Factors that showed high impact on the reaction rate constants (**AC**, **CD**) appeared to be less impactful as the volume was increased. However, the dynamics were not necessarily similar to that of the % degradation, where the **CD** interaction remained valid across the experimented volume range. For individual parameters, the increase in TiO_2 showed a positive impact on the % degradation while the increase in volume showed a negative impact. This applied to both high and low levels of initial dye concentrations. On both responses, the H_2O_2 parameter showed the level of plateau, which is in agreement with the literature. The model validation that was carried out to test the accuracy and the capability of the obtained regression equations to pre-estimate specific parameters was highly successful, and also appears to maintain its level of accuracy between a yield of 50% and 80% degradation.

Chapter 6 – Conclusion and recommendations

This study investigated and obtained scale-up models for prototype photocatalytic reactor for the treatment of textile effluent. This was due to the fact that numerous authors reporting groundbreaking work on a beaker scale while there was a gap in the representation of the knowledge in a bench, pilot and industrial scale (Linsebigler et al., 1995; Pierre, 2013; Schneider et al., 2016; Chowdhury et al., 2015). Wang et al. (2013b) stated that the operating parameters optimised in the laboratory scale often suffer a mismatch in an actual scenario. Reactor modeling is essential for the application of heterogeneous photocatalysis on an industrial scale (Satuf et al., 2007). This, therefore, necessitated that a photocatalytic reactor is designed on a pilot scale and address the dynamics of the photocatalytic parameters, especially the volume parameter which is not adequately addressed in literature. Due to the complexities of the photocatalysis reaction, it was proposed that a statistical engineering approach is employed and a CCD from Stat-Ease® (Design Expert V 10.0.7) tool pack was used, not only to study the significant terms during scale-up but also how these significant terms interact with one another and to develop and predictable scalable model that can be used to estimate operating conditions beforehand.

6.1 Results summary

This section presents the summary of the results.

6.1.1 Reactor design results summary

The 20 L reactor in this work was designed to operate under isothermal conditions, monochromatic light (no mixture of different light sources was employed), no dead zones, steady-state flow rate conditions, efficient and uniform radiation profiles, and constant physical properties. Various reactor configurations were considered and the geometry of choice was the annular

shape. It can also be supported theoretically that using annular geometry, under assumptions of constant transport flow properties, monochromatic light, and an incompressible flow, the system will respect the law of conservation of mass (Schneider et al., 2016; Cassano et al., 1967). The lamp configuration also took into account the radiation balance to ensure constant radiation flux through the reacting medium. The reactor was designed as a jacketed vessel with an interior acting as a cooling chamber and lamp space and lid serving as a lamp holder and cooling water feed line holder. The reacting fluid reacted on the outer shell which was 19.0 mm in thickness. The total height of the reactor was 453 mm with a width of 180 mm. The outer tube had a total thickness of 3.0 mm and the inner tube an inner diameter of 150.0 mm.

6.1.2 Operating parameter effects on chosen responses (k and % degradation)

A systematic experimental design layout was conducted using the Stat-Ease® experimental tool pack with 4 factors and 2 levels. The design layout yielded 30 runs including central point and star points. The quantities of H_2O_2 and TiO_2 were established, as well as the impact of the parameters on the responses k (which was transformed to k_Freeman-Tukey due to the fact that the reaction rate constant response range was greater than 10) and % degradation. The obtained and analysed k_Freeman-Tukey constant response was reverted to reaction rate constant during the post-analysis stage. The parameters of interest were volume (L) ranging from 5 to 20 L; TiO_2 (g) ranging from 2 to 10 g; H_2O_2 (mL) ranging from 20 to 200 mL; and IDC (mg/L) ranging from 5 to 20 mg/L. The individual effects of various parameters were analysed through the F-test and further confirmed by the automatic model selection to ensure significance. The possible interactions were also selected in the same manner. It was found that there was an interaction term **CD** (H_2O_2 and initial dye concentration) and that this interaction term was inversely proportional to both responses. The maximum % degradation (80%) was obtained under the conditions of the IDC range 5 to 8 mg/L and H_2O_2 of range $\geq$ 160 mL dosage, and the optimum

reaction rate constant was 0.0093 and was obtained at H_2O_2 dosage $\geq$ 160 mL and IDC of ranges between 5 to 12 mg/L.

The goodness of fit of the obtained regression models was validated by a high R^2 coefficient. The model F-values were found to be 13.07 and 10.67 for k_Freeman-Tukey and % degradation respectively. This implies that there is only a 0.01% chance that an F-value this large could be due to noise. A ratio of adequate precision greater than 4 implies that the model can be used to navigate the design space, while the adequate precision found for responses was 12.74. The predicted R-squared of 0.61 was found to be in reasonable agreement with the adjusted R-squared of 0.71, where the difference was observed to be less than 0.2. The lack-of-fit F-value is found to be 2.53 and is not significant, which implies that the lack of fit is not significant relative to pure error. For individual impacts, it was found that TiO_2 dosage had no influence on the reaction rate constant, whilst it showed a Probability >F value of 0.0266 for the % degradation. Two correlations were developed to predict the % degradation as well as the reaction rate constant as a function of process parameters as shown in Equation *5.3* and Equation *5.5*.

The most influential parameters found in this study are shown in Table *6.1*, the H_2O_2 and initial dye concentration interaction was found to be the common interaction between the two responses were inversely proportional to the volume parameter.

Table 6.1: Process parameters and interaction that affect the % degradation and k(freeman-Tukey)

Responses	**A** Volume (L)	**B** TiO$_2$ dosage (g)	**C** H$_2$O$_2$ dosage (mL)	**D** IDC (mg/L)	**AC**	**CD**
% degradation	✓	✓	✓	✓	−	✓
k$_{Freeman-Tukey}$	✓	F	✓	✓	H	✓
✓ significant, − insignificant, F Forced and H hierarchically selected (Cassano et al., 1967)						

A correlation for the determination of the percentage degradation as a function of volume, catalyst, initial dye concentration and oxidizer was derived from the factorial trial results, uniquely addressing the effect of volume which is conspicuous in its absence in literature as:

$$Y_{(\% \, deg)} = 66.75 - 2.52A + 1.94B + 0.19C - 0.133D - 0.00955CD$$

6.2 Conclusion

A continuous recirculating batch photoreactor system was designed and constructed. The resulting heterogeneous photocatalytic system was stable during start-up, operation, and shutdown. The critical issue addressed was that the reactive area was kept uniform across all volumes being studied in comparison with traditional batch systems. Furthermore, the light transport was also controlled and kept uniform through this design, which enabled the investigation of the relationship and interactions of the operating parameters as a functions of volume.

From the factorial trial it was found that the optimum H_2O_2 dosage for the studied volume range was above 160 mL. The TiO_2 dosage was found to have no impact on k. The optimum TiO_2 found on the % degradation response was 10 g when the volume was 5 L and H_2O_2 set at 20 mL, and the IDC in the ranges less than 10 mg/L.

6.3 Contributions and recommendations for future research

This work contributes to understanding interaction of parameters, especially the volume parameter as it is very seldom reported in literature. The work also further confirmed that there is no linearity in the scale-up of photocatalysis. Furthermore, it showed that scale-up methodology can be made possible through the empirical experimental methodology using the design of experiments approach. A correlation for the prediction of % degradation based on process parameters are now available for scaling between 5 L and 20 L for the first time.

Recommendations for future work can include but is not limited to:

- Extend the work to treat higher volumes.

- Development of a system to immobilise the TiO_2 particles, so that the post catalyst separation step can be eliminated.

- Inclusion of automated pH adjustment system to investigate the effect of pH on percentage degradation of Azo dyes.

- A systematic study of the use of dilution ratios of treated effluent/fresh effluent which will lower IDC and treatment time.

References

Aleboyeh, A., Daneshvar, N. & Kasiri, M.B. 2008. Optimization of CI Acid Red 14 azo dye removal by electrocoagulation batch process with response surface methodology. *Chemical Engineering and Processing: Process Intensification*, 47(5): 827–832.

Allen, N.S. ed. 2010. *Photochemistry and photophysics of polymer materials*. Hoboken, N.J: J. Wiley.

Alrousan, D.M.A., Polo-López, M.I., Dunlop, P.S.M., Fernández-Ibáñez, P. & Byrne, J.A. 2012. Solar photocatalytic disinfection of water with immobilised titanium dioxide in re-circulating flow CPC reactors. *Applied Catalysis B: Environmental*, 128: 126–134.

Augugliaro, V., Baiocchi, C., Prevot, A.B., García-López, E., Loddo, V., Malato, S., Marcí, G., Palmisano, L., Pazzi, M. & Pramauro, E. 2002. Azo-dyes photocatalytic degradation in aqueous suspension of TiO_2 under solar irradiation. *Chemosphere*, 49(10): 1223–1230.

Bahadir, K. & Rauf, M.. 2008. Responce surface methodology (RSM) of photoinduced decoloration of toludine blue. *Chemical Engineering Journal*, 136: 25–30.

Bandala, E.R., Arancibia-Bulnes, C.A., Orozco, S.L. & Estrada, C.A. 2004. Solar photoreactors comparison based on oxalic acid photocatalytic degradation. *Solar Energy*, 77(5): 503–512.

Behnajady, M.., Modirsha, N., Daneshvar, N. & Rabbani, M. 2007. Photocatalytic degradation of an azo dye in a tubular continos-flow photoreactor with immobilized TiO_2 on glass plates.pdf. , 127: 167–176.

Bignozzi, C.A. & Alexander, B.D. eds. 2011. *Photocatalysis*. Berlin: Springer.

Box, G.E.P. & Draper, N.R. 2007. *Response surfaces, mixtures, and ridge analyses*. 2nd ed. Hoboken, N.J: John Wiley.

Braham, R.J. & Harris, A.T. 2009. Review of major design and scale-up considerations for solar photocatalytic reactors. *Industrial & Engineering Chemistry Research*, 48(19): 8890–8905.

Brockbank, S.A., Russon, J.L., Giles, N.F., Rowley, R.L. & Wilding, W.V. 2013. Infinite dilution activity coefficients and Henry's law constants of compounds in water using the inert gas stripping method. *Fluid Phase Equilibria*, 348: 45–51.

Camera-Roda, G., Santarelli, F. & Martin, C.A. 2005. Design of photocatalytic reactors made easy by considering the photons as immaterial reactants. *Solar Energy*, 79(4): 343–352.

Cassano, A.E., Silveston, P.L. & Smith, J.M. 1967. Photochemical reaction engineering. *Industrial & Engineering Chemistry*, 59(1): 18–38.

Chen, D. & Ray, A.K. 1998. Photodegradation kinetics of 4-nitrophenol in TiO_2 suspension. *Water Research*, 32(11): 3223–3234.

Cho, I.-H. & Zoh, K.-D. 2007. Photocatalytic degradation of azo dye (Reactive Red 120) in TiO_2/UV system: Optimization and modeling using a response surface methodology (RSM) based on the central composite design. *Dyes and Pigments*, 75(3): 533–543.

Chowdhury, M., Ntiribinyange, M., Nyamayaro, K. & Fester, V. 2015. Photocatalytic activities of ultra-small β-FeOOH and TiO_2 heterojunction structure under simulated solar irradiation. *Materials Research Bulletin*, 68: 133–141.

Cornell, J.A. 1990. *How to Apply Response Surface Methodology*. ASQC.

Daneshvar, N., Salari, D. & Khataee, A.R. 2003. Photocatalytic degradation of azo dye acid red 14 in water: investigation of the effect of operational parameters. *Journal of Photochemistry and Photobiology A: Chemistry*, 157(1): 111–116.

Dijkstra, Panneman, Winkelman J.G.M & Kelly J.J. 2002. Dijkstra, M.F.J - Modeling the photocatalytic degradation of a formic acid in a reactor with immobilised catalyst..pdf. www.elsevier.com/locate/ces.

Elliott, L.D., Knowles, J.P., Koovits, P.J., Maskill, K.G., Ralph, M.J., Lejeune, G., Edwards, L.J., Robinson, R.I., Clemens, I.R., Cox, B., Pascoe, D.D., Koch, G., Eberle, M., Berry, M.B. & Booker-Milburn, K.I. 2014. Batch versus Flow Photochemistry: A Revealing Comparison of Yield and Productivity. *Chemistry - A European Journal*, 20: 15226–15232.

Fernandez-Ibañez, P., Malato, S. & Enea, O. 1999. Photoelectrochemical reactors for the solar decontamination of water. *Catalysis Today*: 11.

Fogler, H.S. 2006. *Elements of chemical reaction engineering*. 4th ed., 3.printing. Upper Saddle River, NJ: Pearson Education International/Prentice Hall PTR.

Freeman, M.F. & Tukey, J.W. 1950. Transformations Related to the Angular and the Square Root. *The Annals of Mathematical Statistics*, 21(4): 607–611.

Hayek. 2016. What is the result of using a catalyst in a chemical reaction? | Socratic. *Socratic.org*. https://socratic.org/questions/what-is-the-result-of-using-a-catalyst-in-a-chemical-reaction 3 September 2018.

Kaneco, S., Rahman, M.A., Suzuki, T., Katsumata, H. & Ohta, K. 2004. Optimization of solar photocatalytic degradation conditions of bisphenol A in water using titanium dioxide. *Journal of Photochemistry and Photobiology A: Chemistry*, 163(3): 419–424.

Kanki, T., Hamasaki, S., Sano, N., Toyoda, A. & Hirano, K. 2005. Water purification in a fluidized bed photocatalytic reactor using TiO_2-coated ceramic particles. *Chemical Engineering Journal*, 108(1–2): 155–160.

Khuri, A.I. ed. 2006. *Response surface methodology and related topics*. Hacenksack, N.J: World Scientific.

Kobayakawa, K., Sato, C., Sato, Y. & Fujishima, A. 1998. Continuous-flow photoreactor packed with titanium dioxide immobilized on large silica gel beads to decompose oxalic acid in excess water. *Journal of Photochemistry and Photobiology A: Chemistry*, 118(1): 65–69.

Kommineni, S., Zoeckler, J., Stocking, A., Liang, P.S., Flores, A., Rodriguez, R., Browne, T., Roberts, P.R. & Brown, A. 2000. 3.0 Advanced Oxidation Processes. *TREATMENT Technologies for Removal of Methyl Tertiary Butyl Ether (MTBE) from Drinking Water: Air Stripping, Advanced Oxidation Process, Granular Activated Carbon, Synthetic Resin Sorbents. National Water Research Institute, Second Edition, 410f*: 109–208.

Konstantinou, I.K. & Albanis, T.A. 2004. TiO_2-assisted photocatalytic degradation of azo dyes in aqueous solution: kinetic and mechanistic investigations: A review. *Applied Catalysis B: Environmental*, 49(1): 1–14.

Li Puma, G., Toepfer, B. & Gora, A. 2007. Photocatalytic oxidation of multicomponent systems of herbicides: Scale-up of laboratory kinetics rate data to plant scale. *Catalysis Today*, 124(3–4): 124–132.

Linsebigler, A.L., Lu, G. & Yates, J.T. 1995. Photocatalysis on TiO_2 Surfaces: Principles, Mechanisms, and Selected Results. *Chemical Reviews*, 95(3): 735–758.

Liu, H.-L. & Chiou, Y.-R. 2005. Optimal decolourization efficiency of Reactive Red 239 by UV/TiO 2 photocatalytic process coupled with response surface methodology. *Chemical Engineering Journal*, 112(1): 173–179.

Marugan, J., Van Grieken, R., Cassano, A.E. & Alfano, O.M. 2009. Scaling-up of slurry reactors for the photocatalytic oxidation of cyanide with TiO_2 and silica-supported TiO_2 suspensions. *Catalysis Today*, 144(1): 87–93.

Maskill, K.G., Knowles, J.P., Elliott, L.D., Alder, R.W.& Booker-Milburn, K.I. 2013. Complexity from Simplicity: Tricyclic Aziridines from the Rearrangement of Pyrroles by Batch and Flow Photochemistry. *Angewandte Chemie International Edition*, 52(5): 1499–1502.

Mehos, M., Turchi, C., Pacheco, J., Boegel, A.J., Merrill, T. & Stanley, R. 1992. *Pilot-scale study of the solar detoxification of VOC-contaminated groundwater*. National Renewable Energy Lab., Golden, CO (United States). http://www.nrel.gov/docs/legosti/old/4981.pdf 14 July 2017.

Missen, R.W., Mims, C.A. & Saville, B.A. 1999. *Introduction to chemical reaction engineering and kinetics*. New York, NY: Wiley.

Montgomery, D.C. 1997. *Design and analysis of experiments*. Hoboken, N.J: Wiley.

Motegh, M., van Ommen, J.R., Appel, P.W. & Kreutzer, M.T. 2014. Scale-Up Study of a Multiphase Photocatalytic Reactor Degradation of Cyanide in Water over TiO_2. *Environmental science & technology*, 48(3): 1574–1581.

Myers, R.H., Montgomery, D.C. & Anderson-Cook, C.M. 2009. *Response surface methodology: process and product optimization using designed experiments*. 3rd ed. Hoboken, N.J: Wiley.

Oyama, T., Aoshima, A., Horikoshi, S., Hidaka, H., Zhao, J. & Serpone, N. 2004. Solar photocatalysis, photodegradation of a commercial detergent in aqueous TiO_2 dispersions under sunlight irradiation. *Solar Energy*: 8.

Pelayo, P.J.V. 2014. *Scale-Up Methodology for Bench-Scale Slurry Photocatalytic Reactors Using Combined Irradiation and Kinetic Modelling.* University of Western Ontario.

Pierre, P. 2013. *Photocatalysis and water purification.*

Puma, G.L. & Yue, P.L. 2001. The modeling of a fountain photocatalytic reactor with a parabolic profile. *Chemical engineering science*, 56(2): 721–726.

Rajamanickam, D. & Shanthi, M. 2016. Photocatalytic degradation of an organic pollutant by zinc oxide – solar process. *Arabian Journal of Chemistry*, 9: S1858–S1868.

Ray, A.K. & Beenackers, A.A. 1998. Development of a new photocatalytic reactor for water purification. *Catalysis today*, 40(1): 73–83.

Ryan, T.P. 2007. *Modern experimental design.* Hoboken, N.J: Wiley-Interscience.

Satuf, M.L., Brandi, R.J., Cassano, A.E. & Alfano, O.M. 2007. Scaling-up of slurry reactors for the photocatalytic degradation of 4-chlorophenol. *Catalysis Today*, 129(1): 110–117.

Says, D.A. 2009. Borosilicate Glass - Properties of Borosilicate Glass (Pyrex/Duran) by Goodfellow Ceramic & Glass Division. *AZoM.com*. https://www.azom.com/article.aspx?ArticleID=4765 15 February 2018.

Schneider, J., Bahnemann, D., Ye, J., Puma, G.L. & Dionysiou, D.D. 2016. *Photocatalysis: Fundamentals and Perspectives.* Royal Society of Chemistry.

Sheikh, M.U.D., Naikoo, G.A., Thomas, M., Bano, M. & Khan, F. 2016. Solar-assisted photocatalytic reduction of methyl orange azo dye over porous TiO_2 nanostructures. *New Journal of Chemistry*, 40(6): 5483–5494.

Sichel, C. & Tello, J. 2007. Effect of UV solar intensity and dose on the photocatalytic disinfection of bacteria and fungi. *Catalysis Today*: 9.

Soltani, R.D.C., Rezaee, A., Khataee, A.R. & Safari, M. 2014. Photocatalytic process by immobilized carbon black/ZnO nanocomposite for dye removal from aqueous medium: Optimization by response surface methodology. *Journal of Industrial and Engineering Chemistry*, 20(4): 1861–1868.

Thind, P.S., Kumari, D. & John, S. 2017. TiO_2/H_2O_2 mediated UV photocatalysis of Chlorpyrifos: Optimization of process parameters using response surface methodology. *Journal of Environmental Chemical Engineering*.

Thu, H.B., KARKMAZ, M., PUZENAT, E., GUILLARD, C. & HERRMANN, J.-M. 2005. From the fundamentals of photocatalysis to its applications in environment protection and in solar purification of water in arid countries. : 13.

Timothy, N. 2017. *Photochemical Processes In Continuous-flow Reactors: From Engineering Principles to Chemical Applications.* World Scientific.

Toh, C.H. 2007. *Response Surface Methodology.* Universiti Teknologi Malaysia.

Turton, R.A., Bailie, R.C., Whiting, W.B., Shaeiwitz, J.A. & Bhattacharyya, D. 2012. *Analysis, Synthesis and Design of Chemical Processes.* Prentice Hall.

Valadés-Pelayo, P.., Guayaquil Sosa, F., Serrano, B. & de Lasa, H. 2015. Eight-lamp externally irradiated bench-scale photocatalytic reactor (scale-up and perfomance prediction).pdf. *Chemical Engineering Journal*, 282: 142–151.

Wang, C., Liu, H. & Qu, Y. 2013. TiO_2-based photocatalytic process for purification of polluted water: bridging fundamentals to applications. *Journal of Nanomaterials*, 2013: 1.

Wielopolski, M. 2010. *Testing molecular wires: A photophysical and Quantum Chemical Assay*. Springer Science & Business Media.

Willumstad, T.P., Haze, O., Mak, X.Y., Lam, T.Y., Wang, Y.-P. & Danheiser, R.L. 2013. Batch and Flow Photochemical Benzannulations Based on the Reaction of Ynamides and Diazo Ketones. Application to the Synthesis of Polycyclic Aromatic and Heteroaromatic Compounds. *The Journal of Organic Chemistry*, 78: 11450–11469.

Wu, C.-H., Chang, H.-W. & Chern, J.-M. 2006. Basic dye decomposition kinetics in a photocatalytic slurry reactor. *Journal of hazardous materials*, 137(1): 336–343.

Xu, H.-Y., Liu, W.-C., Shi, J., Zhao, H. & Qi, S.-Y. 2014. Photocatalytic discoloration of Methyl Orange by anatase/schorl composite: optimization using response surface method. *Environmental Science and Pollution Research*, 21(2): 1582–1591.

Zar, J.H. 2010. *Biostatistical Analysis*. Hoboken, N.J:Prentice Hall.

Appendices

Appendix 1: Time-concentration curves raw data

A 1: Time-Concentration curve raw data

Run#14

Run#15

Run#16

Run#17

Run#18

Run#19

Run#20

Run#21

Run#22

Run#23

Run#24

Run#25

Run#26

Run#27

Run #28

Run#29

Run #30
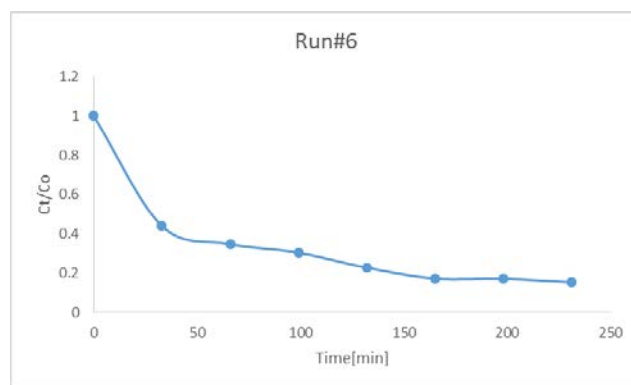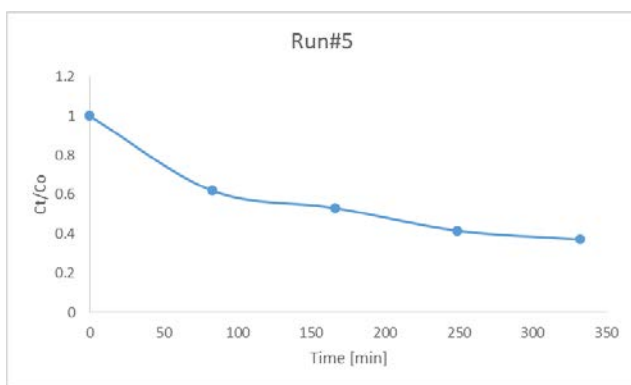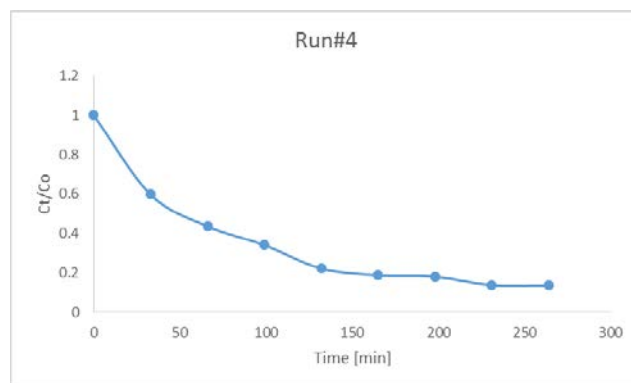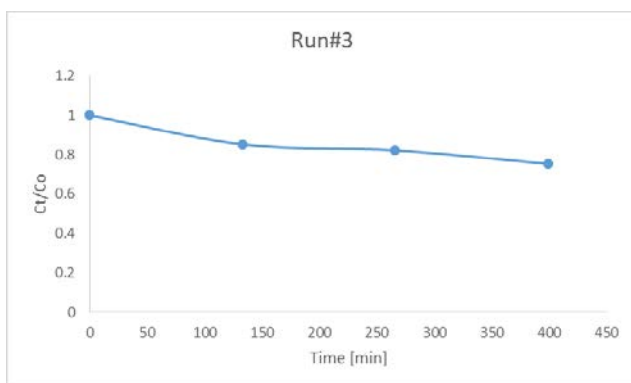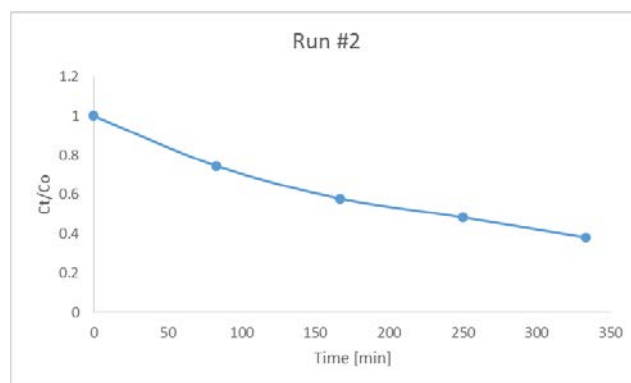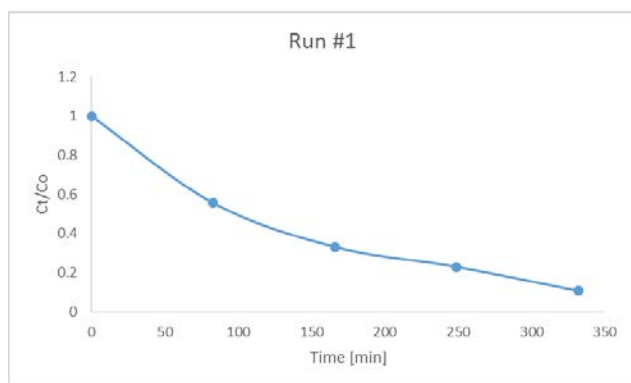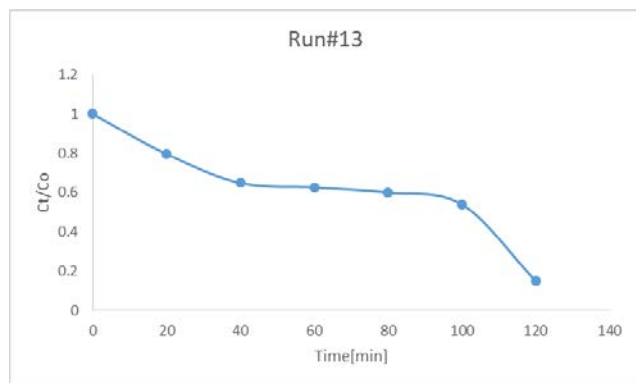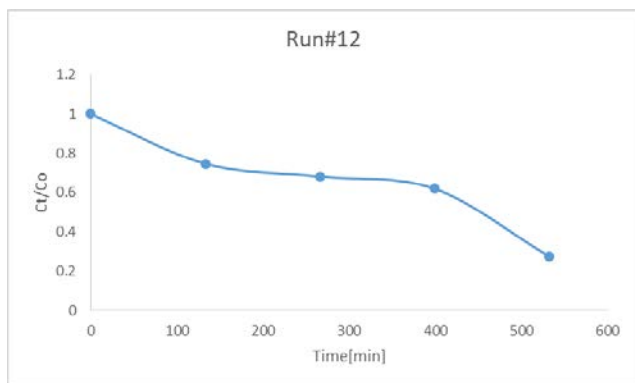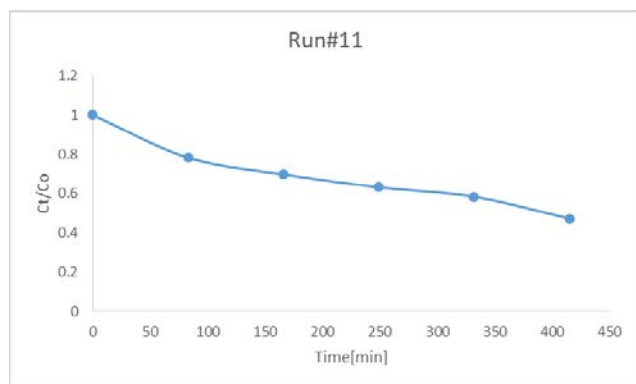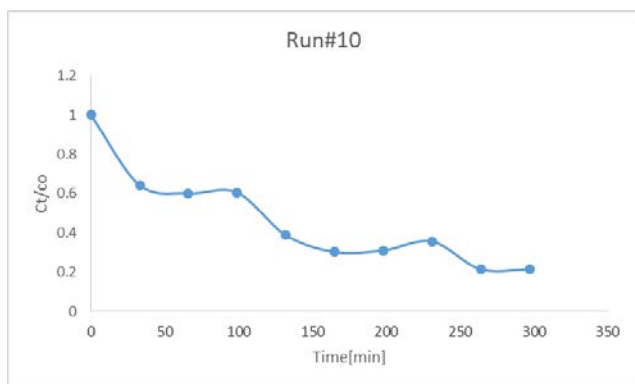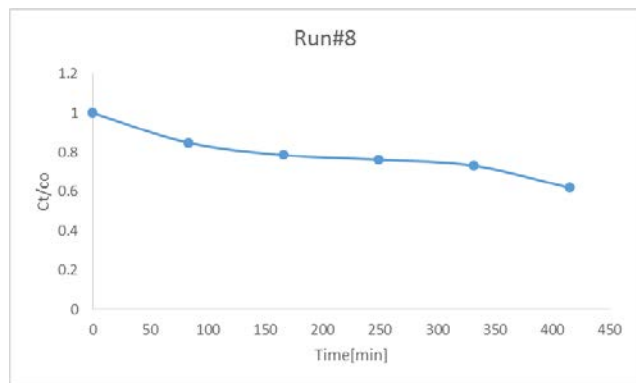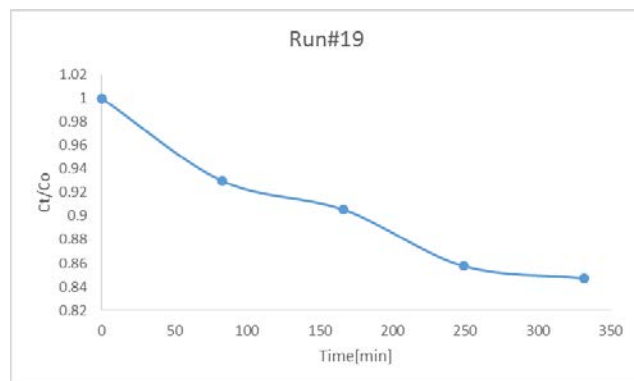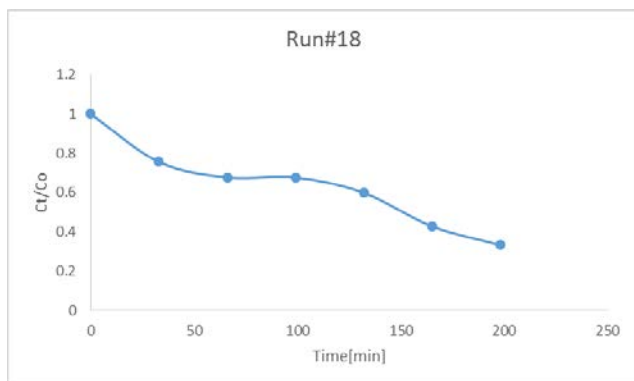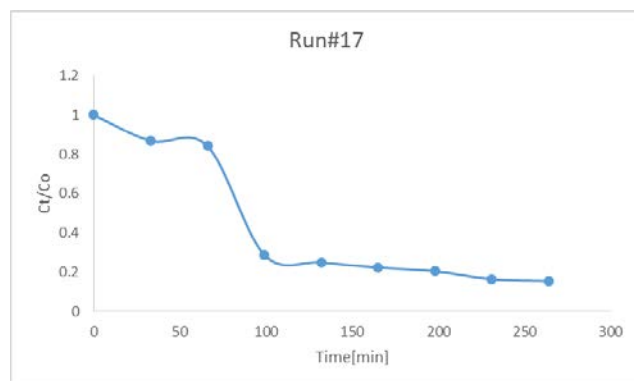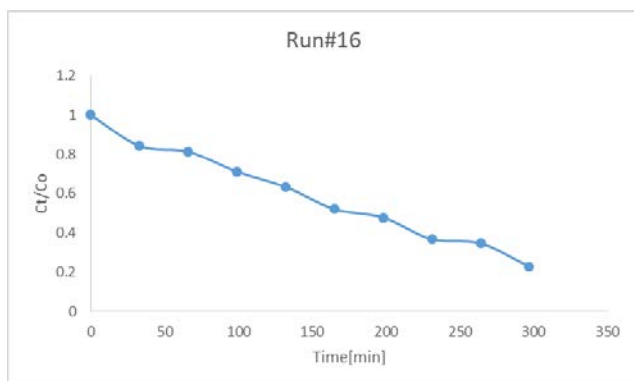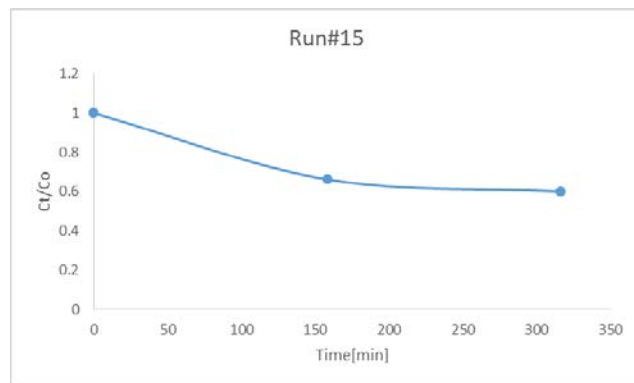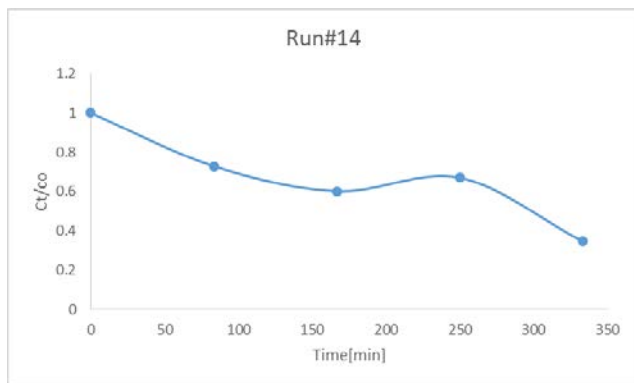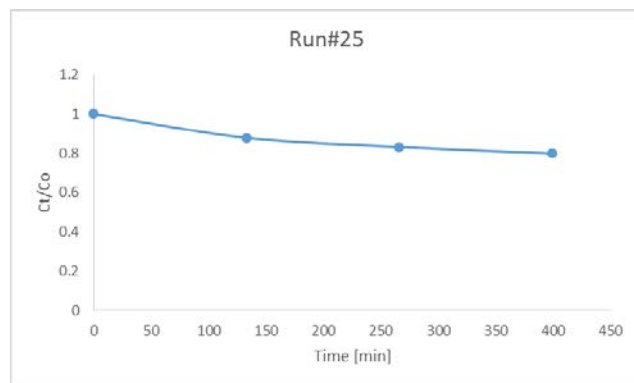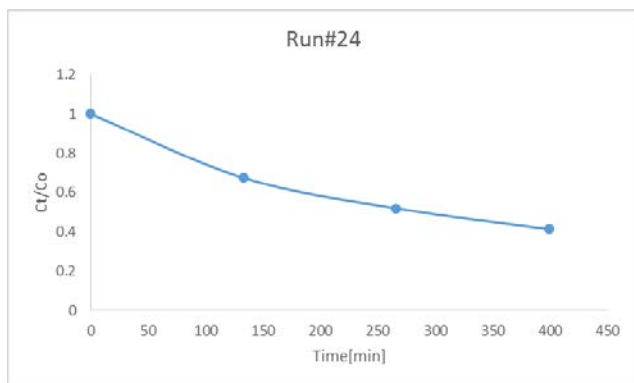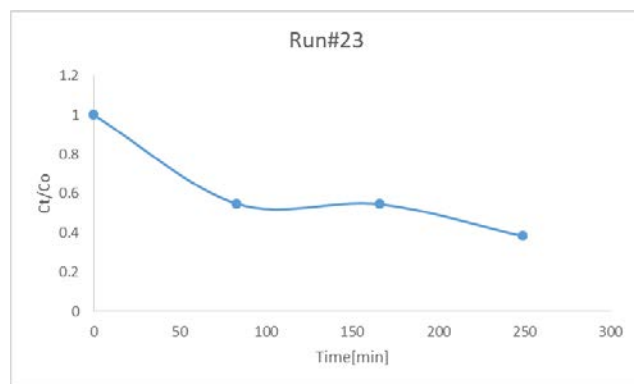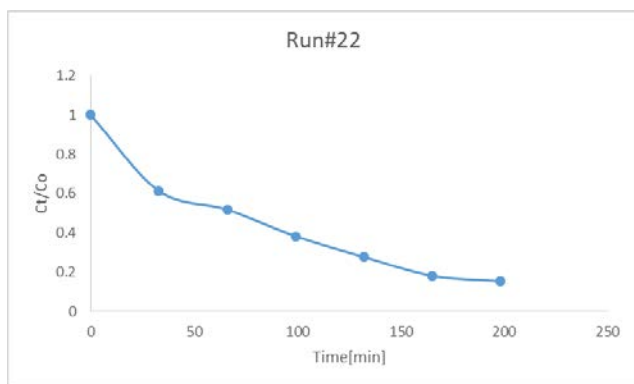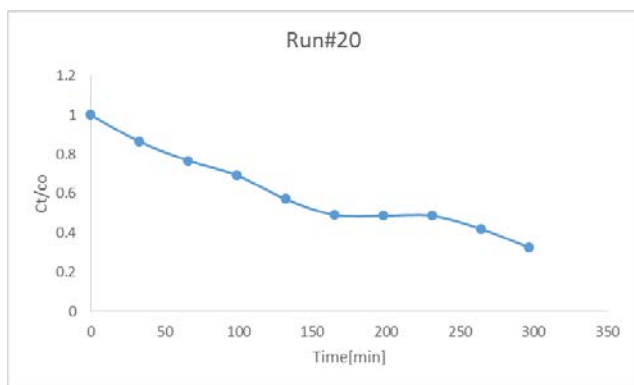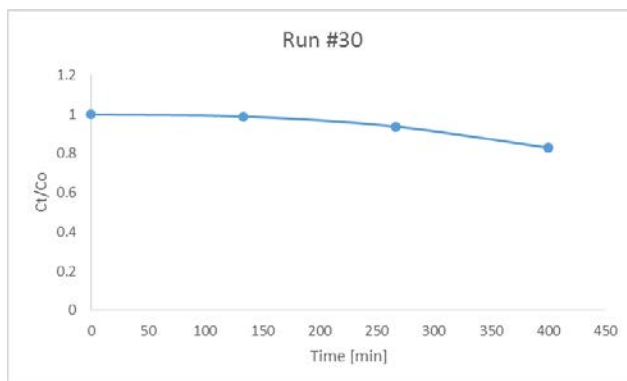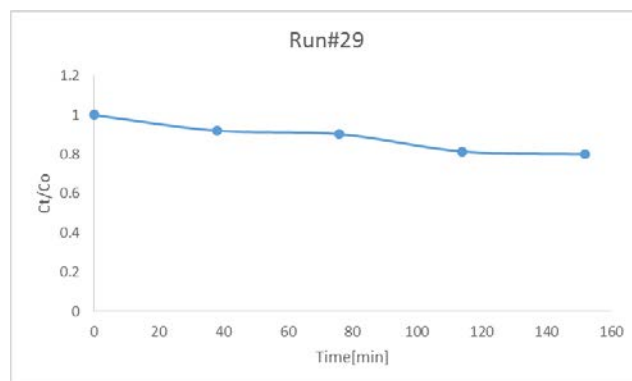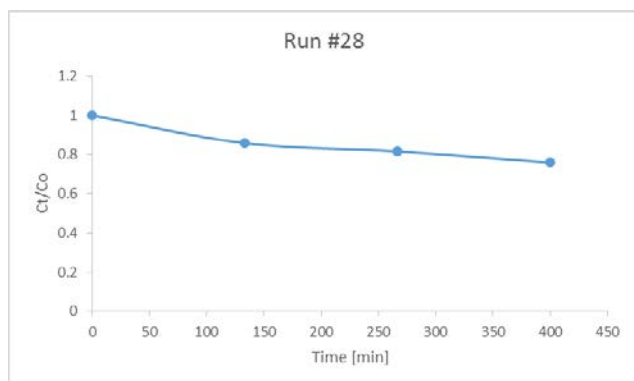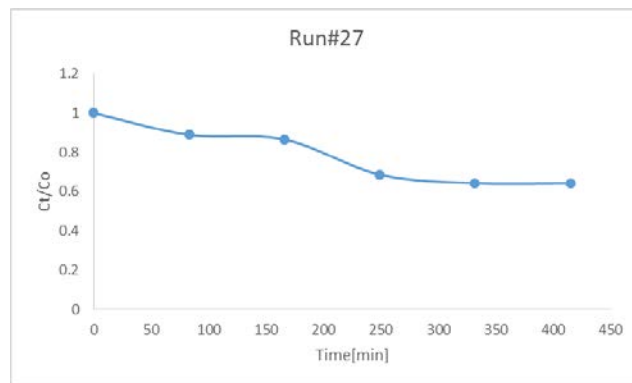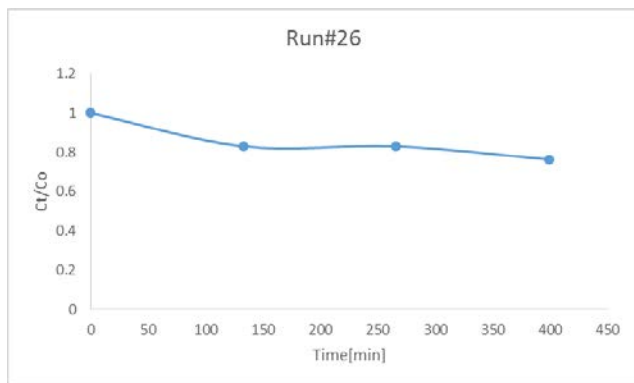
Appendix 2: % degradation raw data

Warning: The Cubic model is aliased.

Fit Summary

A 2: Response 2 % degradation

Source	Sequential p-value	Lack of Fit p-value	Adjusted R²	Predicted R²	
Linear	**< 0.0001**	**0,4742**	**0,5949**	**0,4952**	**Suggested**
2FI	0,3374	0,4968	0,6156	0,4191	
Quadratic	0,5371	0,4541	0,5997	0,1446	
Cubic	0,2123	0,8437	0,7265	0,1261	Aliased

A 3: Sequential Model Sum of Squares [Type I]

Source	Sum of Squares	df	Mean Square	F-value	p-value	
Mean vs Total	86149,14	1	86149,14			
Linear vs Mean	**11113,94**	**4**	**2778,49**	**11,65**	**< 0.0001**	**Suggested**
2FI vs Linear	1662,76	6	277,13	1,22	0,3374	
Quadratic vs 2FI	765,31	4	191,33	0,8116	0,5371	
Cubic vs Quadratic	2408,60	8	301,08	1,87	0,2123	Aliased
Residual	1127,51	7	161,07			
Total	1,032E+05	30	3440,91			

Select the highest order polynomial where the additional terms are significant and the model is not aliased.

A 4: Model Summary Statistics

Source	Std. Dev.	R²	Adjusted R²	Predicted R²	PRESS	
Linear	**15,45**	**0,6508**	**0,5949**	**0,4952**	**8620,63**	**Suggested**
2FI	15,05	0,7481	0,6156	0,4191	9921,26	
Quadratic	15,35	0,7929	0,5997	0,1446	14608,98	
Cubic	12,69	0,9340	0,7265	0,1261	14925,25	Aliased

Focus on the model maximizing the Adjusted R² and the Predicted R².

A 5: Lack of Fit Tests

Source	Sum of Squares	df	Mean Square	F-value	p-value	
Linear	**4910,76**	**20**	**245,54**	**1,17**	**0,4742**	**Suggested**
2FI	3248,01	14	232,00	1,10	0,4968	
Quadratic	2482,69	10	248,27	1,18	0,4541	
Cubic	74,09	2	37,05	0,1758	0,8437	Aliased
Pure Error	1053,41	5	210,68			

The selected model should have insignificant lack-of-fit.

ANOVA for Reduced 2FI model

A 6: Response 2: % degradation

Source	Sum of Squares	df	Mean Square	F-value	p-value	
Model	11779,33	5	2355,87	10,67	< 0.0001	significant
A-Volume	7308,45	1	7308,45	33,10	< 0.0001	
B-TiO_2	1231,82	1	1231,82	5,58	0,0266	
C-H_2O_2	955,82	1	955,82	4,33	0,0483	
D-Dye Conc.	1617,85	1	1617,85	7,33	0,0123	
CD	665,38	1	665,38	3,01	0,0954	
Residual	5298,80	24	220,78			
Lack of Fit	4245,38	19	223,44	1,06	0,5239	not significant
Pure Error	1053,41	5	210,68			

Cor Total	17078,12	29				

Factor coding is Coded.
Sum of squares is Type III - Partial

The Model F-value of 10,67 implies the model is significant. There is only a 0,01% chance that an F-value this large could occur due to noise.

P-values less than 0,0500 indicate model terms are significant. In this case A, B, C, D are significant model terms. Values greater than 0.1000 indicate the model terms are not significant. If there are many insignificant model terms (not counting those required to support hierarchy), model reduction may improve your model.

The Lack of Fit F-value of 1,06 implies the Lack of Fit is not significant relative to the pure error. There is a 52,39% chance that a Lack of Fit F-value this large could occur due to noise. Non-significant lack of fit is good -- we want the model to fit.

A 7: Fit Statistics

Std. Dev.	14,86	R²	0,6897
Mean	53,59	Adjusted R²	0,6251
C.V. %	27,73	Predicted R²	0,5268
		Adeq Precision	12,7449

The Predicted R² of 0,5268 is in reasonable agreement with the Adjusted R² of 0,6251; i.e. the difference is less than 0.2.

Adeq Precision measures the signal to noise ratio. A ratio greater than 4 is desirable. Your ratio of 12,745 indicates an adequate signal. This model can be used to navigate the design space.

A 8: Coefficients in Terms of Coded Factors

Factor	Coefficient Estimate	df	Standard Error	95% CI Low	95% CI High	VIF
Intercept	53,59	1	2,71	47,99	59,19	
A-Volume	-18,88	1	3,28	-25,65	-12,11	1,0000
B-TiO$_2$	7,75	1	3,28	0,9785	14,52	1,0000
C-H$_2$O$_2$	6,83	1	3,28	0,0551	13,60	1,0000
D-Dye Conc.	-8,88	1	3,28	-15,66	-2,11	1,0000
CD	-6,45	1	3,71	-14,12	1,22	1,0000

The coefficient estimate represents the expected change in response per unit change in factor value when all remaining factors are held constant. The intercept in an orthogonal design is the overall average response of all the runs. The coefficients are adjustments around that average based on the factor settings. When the factors are orthogonal the VIFs are 1; VIFs greater than 1 indicate multi-colinearity, the higher the VIF the more severe the correlation of factors. As a rough rule, VIFs less than 10 are tolerable.

Final Equation in Terms of Coded Factors

% degradation	=
+53,59	
-18,88	A
+7,75	B
+6,83	C
-8,88	D
-6,45	CD

The equation in terms of coded factors can be used to make predictions about the response for given levels of each factor. By default, the high levels of the factors are coded as +1 and the low levels are coded as -1. The coded equation is useful for identifying the relative impact of the factors by comparing the factor coefficients.

Final Equation in Terms of Actual Factors

% degradation	=
+66,75328	
-2,51753	Volume
+1,93793	TiO_2
+0,195291	H_2O_2
-0,133580	Dye Conc.
-0,009554	H_2O_2 * Dye Conc.

The equation in terms of actual factors can be used to make predictions about the response for given levels of each factor. Here, the levels should be specified in the original units for each factor. This equation should not be used to determine the relative impact of each factor because the coefficients are scaled to accommodate the units of each factor and the intercept is not at the centre of the design space.

Appendix 3: k_Freeman-Tukey raw data

Warning: The Cubic model is aliased.

Fit Summary

A 9: Response 3: k (Freeman-Tukey)

Source	Sequential p-value	Lack of Fit p-value	Adjusted R²	Predicted R²	
Linear	**< 0.0001**	**0,0750**	**0,5871**	**0,4526**	**Suggested**
2FI	0,2063	0,0904	0,6378	0,1481	
Quadratic	0,3583	0,0883	0,6511	0,0028	
Cubic	0,0141	0,9580	0,9056	0,9254	Aliased

A 10: Sequential Model Sum of Squares [Type I]

Source	Sum of Squares	df	Mean Square	F-value	p-value	
Mean vs Total	33,34	1	33,34			
Linear vs Mean	**0,0151**	**4**	**0,0038**	**11,31**	**< 0.0001**	**Suggested**
2FI vs Linear	0,0028	6	0,0005	1,58	0,2063	
Quadratic vs 2FI	0,0013	4	0,0003	1,18	0,3583	
Cubic vs Quadratic	0,0037	8	0,0005	6,06	0,0141	Aliased
Residual	0,0005	7	0,0001			
Total	33,36	30	1,11			

Select the highest order polynomial where the additional terms are significant and the model is not aliased.

A 11: Model Summary Statistics

Source	Std. Dev.	R²	Adjusted R²	Predicted R²	PRESS	
Linear	**0,0183**	**0,6440**	**0,5871**	**0,4526**	**0,0128**	**Suggested**
2FI	0,0171	0,7627	0,6378	0,1481	0,0200	
Quadratic	0,0168	0,8196	0,6511	0,0028	0,0234	
Cubic	0,0087	0,9772	0,9056	0,9254	0,0018	Aliased

Focus on the model maximizing the **Adjusted R²** and the **Predicted R²**.

A 12: Lack of Fit Tests

Source	Sum of Squares	df	Mean Square	F-value	p-value	
Linear	**0,0078**	**20**	**0,0004**	**3,72**	**0,0750**	**Suggested**
2FI	0,0050	14	0,0004	3,43	0,0904	
Quadratic	0,0037	10	0,0004	3,53	0,0883	
Cubic	9,106E-06	2	4,553E-06	0,0433	0,9580	Aliased
Pure Error	0,0005	5	0,0001			

The selected model should have insignificant lack-of-fit.

ANOVA for Reduced Quadratic model

A 13: Response 3: k (Freeman-Tukey)

Source	Sum of Squares	df	Mean Square	F-value	p-value	
Model	0,0185	7	0,0026	11,73	< 0.0001	significant
A-Volume	0,0121	1	0,0121	53,74	< 0.0001	
B-TiO$_2$	0,0004	1	0,0004	1,60	0,2191	
C-H$_2$O$_2$	0,0020	1	0,0020	8,92	0,0068	
D-Dye Conc.	0,0006	1	0,0006	2,79	0,1092	
AC	0,0008	1	0,0008	3,75	0,0657	
CD	0,0015	1	0,0015	6,65	0,0171	
A²	0,0010	1	0,0010	4,65	0,0423	
Residual	0,0050	22	0,0002			
Lack of Fit	0,0044	17	0,0003	2,48	0,1600	not significant
Pure Error	0,0005	5	0,0001			
Cor Total	0,0235	29				

Factor coding is Coded.

Sum of squares is Type III - Partial

The Model F-value of 11,73 implies the model is significant. There is only a 0,01% chance that an F-value this large could occur due to noise.

P-values less than 0,0500 indicate model terms are significant. In this case A, C, CD, A² are significant model terms. Values greater than 0.1000 indicate the model terms are not significant. If there are many insignificant model terms (not counting those required to support hierarchy), model reduction may improve your model.

The Lack of Fit F-value of 2,48 implies the Lack of Fit is not significant relative to the pure error. There is a 16,00% chance that a Lack of Fit F-value this large could occur due to noise. Non-significant lack of fit is good -- we want the model to fit.

A 14: Fit Statistics

Std. Dev.	0,0150	**R²**	0,7887
Mean	1,05	**Adjusted R²**	0,7214
C.V. %	1,42	**Predicted R²**	0,5705
		Adeq Precision	13,1534

The Predicted R² of 0,5705 is in reasonable agreement with the Adjusted R² of 0,7214; i.e. the difference is less than 0.2.

Adeq Precision measures the signal to noise ratio. A ratio greater than 4 is desirable. Your ratio of 13,153 indicates an adequate signal. This model can be used to navigate the design space.

A 15: Coefficients in Terms of Coded Factors

Factor	Coefficient Estimate	df	Standard Error	95% CI Low	95% CI High	VIF
Intercept	1,05	1	0,0040	1,04	1,06	
A-Volume	-0,0243	1	0,0033	-0,0312	-0,0174	1,0000
B-TiO_2	0,0042	1	0,0033	-0,0027	0,0111	1,0000
C-H_2O_2	0,0099	1	0,0033	0,0030	0,0168	1,0000
D-Dye Conc.	-0,0055	1	0,0033	-0,0124	0,0013	1,0000
AC	-0,0073	1	0,0038	-0,0151	0,0005	1,0000
CD	-0,0097	1	0,0038	-0,0175	-0,0019	1,0000
A²	0,0093	1	0,0043	0,0004	0,0182	1,0000

The coefficient estimate represents the expected change in response per unit change in factor value when all remaining factors are held constant. The intercept in an orthogonal design is the overall average response of all the runs. The coefficients are adjustments around that average based on the factor settings. When the factors are orthogonal the VIFs are 1; VIFs greater than 1 indicate multi-colinearity, the higher the VIF the more severe the correlation of factors. As a rough rule, VIFs less than 10 are tolerable.

Final Equation in Terms of Coded Factors

k (Freeman-Tukey)	=
+1,05	
-0,0243	A
+0,0042	B
+0,0099	C
-0,0055	D
-0,0073	AC
-0,0097	CD
+0,0093	A²

The equation in terms of coded factors can be used to make predictions about the response for given levels of each factor. By default, the high levels of the factors are coded as +1 and the low levels are coded as -1. The coded equation is useful for identifying the relative impact of the factors by comparing the factor coefficients.

Final Equation in Terms of Actual Factors

k (Freeman-Tukey)	=
+1,07047	
-0,006190	Volume
+0,001049	TiO_2
+0,000424	H_2O_2
+0,000840	Dye Conc.
-0,000011	Volume * H_2O_2
-0,000014	H_2O_2 * Dye Conc.
+0,000165	Volume ^{2}

The equation in terms of actual factors can be used to make predictions about the response for given levels of each factor. Here, the levels should be specified in the original units for each factor. This equation should not be used to determine the relative impact of each factor because the coefficients are scaled to accommodate the units of each factor and the intercept is not at the centre of the design space.